

Effects of Chitosan Oligosaccharide and Probiotics on Chronic Kidney Disease Rats



Mr. Weerapat Anegkamol

A Dissertation Submitted in Partial Fulfillment of the Requirements
for the Degree of Doctor of Philosophy in Medical Biochemistry

Department of Biochemistry

FACULTY OF MEDICINE

Chulalongkorn University

Academic Year 2022

Copyright of Chulalongkorn University

ผลของโคโคซาน โอลิโกแซคคาไรด์และโปรไบโอติกส์ต่อหนูที่มีภาวะไตวายเรื้อรัง



วิทยานิพนธ์นี้เป็นส่วนหนึ่งของการศึกษาตามหลักสูตรปริญญาวิทยาศาสตรดุษฎีบัณฑิต
สาขาวิชาชีวเคมีทางการแพทย์ ภาควิชาชีวเคมี
คณะแพทยศาสตร์ จุฬาลงกรณ์มหาวิทยาลัย
ปีการศึกษา 2565
ลิขสิทธิ์ของจุฬาลงกรณ์มหาวิทยาลัย

Thesis Title	Effects of Chitosan Oligosaccharide and Probiotics on Chronic Kidney Disease Rats
By	Mr. Weerapat Anegkamol
Field of Study	Medical Biochemistry
Thesis Advisor	Associate Professor THASINAS DISSAYABUTRA, M.D. Ph.D.
Thesis Co Advisor	NATTHAYA CHUAYPEN, Ph.D. Associate Professor ASADA LEELAHAVANICHKUL, M.D. Ph.D.

Accepted by the FACULTY OF MEDICINE, Chulalongkorn University in
Partial Fulfillment of the Requirement for the Doctor of Philosophy

..... Dean of the FACULTY OF
MEDICINE
(Associate Professor CHANCHAI SITTIPUNT, M.D.)

DISSERTATION COMMITTEE

..... Chairman
(Lecturer Sawanee Sutheeworapong, Ph.D.)
..... Thesis Advisor
(Associate Professor THASINAS DISSAYABUTRA,
M.D. Ph.D.)
..... Thesis Co-Advisor
(NATTHAYA CHUAYPEN, Ph.D.)
..... Thesis Co-Advisor
(Associate Professor ASADA LEELAHAVANICHKUL,
M.D. Ph.D.)
..... Examiner
(Professor Sittisak Honsawek, Ph.D. M.D.)
..... Examiner
(Associate Professor KANITHA PATARAKUL, Ph.D.
M.D.)
..... Examiner
(Lecturer TANITTHA CHATSUWAN, Ph.D.)

วีรพัฒน์ เอนกกมล : ผลของไคโตซานโอลิโกแซคคาไรด์และโพรไบโอติกส์ต่อหนูที่มีภาวะไตวายเรื้อรัง. (Effects of Chitosan Oligosaccharide and Probiotics on Chronic Kidney Disease Rats) อ.ที่ปรึกษาหลัก : รศ. ดร. นพ.ฐิติณัฐ คิชยบุตร, อ.ที่ปรึกษาร่วม : ดร.ณัฐธยาน์ ช่วยเพ็ญ, รศ. ดร. นพ.อัมฤกษ์ ลิพหวนิชกุล

ผู้ป่วยโรคไตเรื้อรังที่มีอัตราการกรองของเสียลดลง จะเกิดความคิดผิดปกติในการทำงานของเนื้อเยื่อหลายระบบ อันเป็นผลจากการคั่งของสารพิษในร่างกาย ปัจจัยที่ส่งเสริมการคั่งของสารพิษในร่างกายปัจจัยหนึ่ง คือ การสูญเสียสมดุลของจุลชีพในลำไส้ ซึ่งทำให้ร่างกายสร้างสารพิษในลำไส้เพิ่มมากขึ้น และทำให้เกิดภาวะลำไส้รั่ว เพิ่มการดูดซึมสารพิษเข้าสู่ร่างกาย ฟอสเฟตเป็นสารที่เพิ่มการดูดซึมผ่านช่องว่างระหว่างเซลล์ และการดูดซึมเพิ่มมากขึ้นในผู้ป่วยโรคไตเรื้อรังที่มีภาวะลำไส้รั่ว เกิดเป็นภาวะฟอสเฟตในเลือดสูง ทำให้เกิดระดับฮอร์โมนพาราไทรอยด์สูง เกิดความผิดปกติของแร่ธาตุในกระดูกและเกิดโรคกระดูกผุตามมา ในการศึกษาครั้งนี้ผู้วิจัยได้ศึกษาผลของการเสริมโอลิโกแซคคาไรด์และโพรไบโอติกส์ต่อการเปลี่ยนแปลงระดับฟอสเฟตและฮอร์โมนพาราไทรอยด์ในเลือด รวมถึงการเปลี่ยนแปลงของกระดูก และประชากรเชื้อจุลชีพในลำไส้ ในเซลล์ทดลองและในหนูที่เป็นโรคไตเรื้อรัง โดยเลือกโอลิโกแซคคาไรด์สามชนิด ได้แก่ไคโตซานโอลิโกแซคคาไรด์ อินูลิน และรีชีสแทนต์ มอลโตเด็กซ์ทริน และจุลชีพในกลุ่ม แลคโตบาซิลลัส และ บิฟิโดแบคทีเรียม ที่ถูกสกัดออกมาจากอุจจาระของผู้เข้าร่วมงานวิจัยสุขภาพดี และมีประสิทธิภาพในการเพิ่มค่าความต้านทานไฟฟ้าผ่านเยื่อหุ้มลำไส้และการลดการอักเสบในเซลล์ชนิด Caco-2 เพื่อนำไปทดสอบในหนูที่เป็นโรคไตเรื้อรัง ในรูปของโพรไบโอติกและซินไบโอติก ผลการศึกษาพบว่า โพรไบโอติก อินูลินและรีชีสแทนต์ มอลโตเด็กซ์ทริน มีประสิทธิภาพในการเพิ่มค่าความต้านทานไฟฟ้าผ่านเยื่อหุ้มลำไส้ที่ถูกกระตุ้นการอักเสบ และ เชื้อ **Lactobacillus salivarius** สายพันธุ์ LBR2-28 กับ **Bifidobacterium longum** สายพันธุ์ BFS3-09 มีประสิทธิภาพในการเพิ่มค่าความต้านทานไฟฟ้าผ่านเยื่อหุ้มลำไส้สูงและลดการอักเสบในเซลล์ทดลองเมื่อนำมาทดสอบในสัตว์ทดลอง พบว่า ซินไบโอติกชนิดที่ 1 ซึ่งประกอบไปด้วยไคโตซานโอลิโกแซคคาไรด์ อินูลิน เชื้อทั้งสองชนิดดังกล่าว มีประสิทธิภาพสูงสุดในการลดฟอสเฟตและพาราไทรอยด์ในเลือด อย่างไรก็ตาม ไม่พบความแตกต่างระหว่างความหนาแน่นของมวลกระดูกของหนูในกลุ่มใด ๆ

กล่าวโดยสรุป ซินไบโอติกชนิดที่ 1 น่าจะมีประโยชน์ในการบรรเทาภาวะฟอสเฟตและฮอร์โมนพาราไทรอยด์ในเลือดสูง ที่พบในโรคไตเรื้อรังได้อย่างมีประสิทธิภาพ และช่วยลดความไม่สมดุลของเชื้อจุลชีพในลำไส้ ซึ่งน่าจะช่วยลดการสร้างและการดูดซึมสารพิษเข้าสู่ร่างกายได้เช่นกัน การศึกษาขั้นถัดไปจะดำเนินการผลิตซินไบโอติกต้นแบบเพื่อทดสอบในหนูโรคไตเรื้อรัง และในผู้ป่วยโรคไตเรื้อรังต่อไป

สาขาวิชา ชีวเคมีทางการแพทย์
ปีการศึกษา 2565

ลายมือชื่อนิติกร
ลายมือชื่อ อ.ที่ปรึกษาหลัก
ลายมือชื่อ อ.ที่ปรึกษาร่วม
ลายมือชื่อ อ.ที่ปรึกษาร่วม

6174767730 : MAJOR MEDICAL BIOCHEMISTRY

KEYWORD Chronic kidney disease, Probiotics, Chitosan Oligosaccharide,

D: Hyperphosphatemia, Mineral and Bone Disorder, Gut microbiota

Weerapat Anegkamol : Effects of Chitosan Oligosaccharide and Probiotics on Chronic Kidney Disease Rats. Advisor: Assoc. Prof. THASINAS DISSAYABUTRA, M.D. Ph.D. Co-advisor: NATTHAYA CHUAYPEN, Ph.D., Assoc. Prof. ASADA LEELAHAVANICHKUL, M.D. Ph.D.

Chronic kidney disease (CKD) patients suffer from the accumulation of toxic substances in their blood due to the loss of kidney function, which results in hyperphosphatemia. This condition contributes to hyperparathyroidism, leading to the development of chronic kidney disease-related mineral bone disorder (CKD-MBD). Additionally, CKD patients experience changes in their gut microbiota, disrupting epithelial tight junctions and allowing excessive absorption of dietary phosphate. In this study, we aimed to investigate the effects of various oligosaccharides and probiotics on the gut microbiota, intestinal barrier, hyperphosphatemia, and hyperparathyroidism in CKD rats. We isolated *Lactobacillus* and *Bifidobacterium* strains from healthy participants and tested their ability to enhance transepithelial electrical resistance and reduce inflammation in Caco-2 cells, to determine their suitability as probiotics. Moreover, we evaluated the impact of oligosaccharides, including chitosan oligosaccharide (COS), inulin, and maltodextrin, on Caco-2 cells in terms of non-toxic concentration, enhancement of transepithelial electrical resistance, and expression of tight junction genes.

Subsequently, all the selected oligosaccharides and probiotics were administered to CKD rats induced by intraperitoneal injection of cisplatin. Following 12 weeks of oral treatment with a combination of COS, inulin, ***Lactobacillus salivarius*** LBR2-28, and ***Bifidobacterium longum*** BFS3-09, we observed a slight alteration in gut microbiota diversity and an increase in the relative abundance of beneficial bacteria in the rat intestine. Furthermore, this treatment promoted intestinal barrier function and led to a reduction in hyperphosphatemia and hyperparathyroidism, although no significant change in bone density was observed. Our findings indicate that this treatment approach has the potential to ameliorate hyperparathyroidism in CKD-MBD, highlighting its therapeutic implications in managing the associated complications.

Field of Study: Medical Biochemistry

Student's Signature

.....

Academic 2022

Advisor's Signature

Year:

.....

Co-advisor's Signature

.....

Co-advisor's Signature

.....

ACKNOWLEDGEMENTS

This research work would not have been accomplished without Assoc.Prof.Dr. Thasinas Dissayabutra, who initiated the idea of the concept and experimental works, Lecturer Dr. Natthaya Chuaypen for her support in molecular techniques which is immensely valuable, Assoc.Prof.Dr. Asada Leelahavanichkul for help and support in animal experiments, Prof. Mana Taweewisit for his support in the pathophysiological examination, and Assit.Prof.Dr. Maroot Kaewwongse for his advice in animal administration. I would like to extend my gratitude to Mr. Peerapat Visitchanakun, Dr. Asada's student, for all his help and advice through the experimental works. I would like to thank Tawatchai Chumponsuk and Tanyaporn Keratibumrunpong of Metabolic Disease in Gastrointestinal and Urinary System Research Unit, lab scientists for their support in microbiology, molecular biology, and cell culture experiments. I also thank members of the 724 lab, Center of Excellence in Hepatitis and Liver Cancer for their support and advice on laboratory instruments, chemicals, and techniques. I would like to thank my family members for their support from the beginning and my sister, Raveewan, for her financial support through this difficult period of time.

I would like to acknowledge the Department of Biochemistry, Faculty of Medicine, Chulalongkorn University for the five-semester tuition fee support, the Faculty of Medicine, Chulalongkorn University for two-year monthly financial support, and Rachadapiseksompode Fund (GA65/33), Fundamental Fund, and Thailand Research Fund (RSA280077) for the research grant.

Weerapat Anegkamol

TABLE OF CONTENTS

	Page
.....	iii
ABSTRACT (THAI)	iii
.....	iv
ABSTRACT (ENGLISH).....	iv
ACKNOWLEDGEMENTS.....	v
TABLE OF CONTENTS	vi
LIST OF TABLES.....	x
LIST OF FIGURES	xiii
Chapter I Introduction.....	1
Chapter II Literature Reviews	5
2.1 Chronic kidney disease.....	5
2.1.1. Definition and stages.....	5
2.1.2. Clinical importance	6
2.1.3. Complication	7
2.2 Phosphate homeostasis	7
2.2.1. Intestinal phosphate absorption.....	8
2.2.2. Tight junction proteins and gut barrier integrity	11
2.2.3. Renal phosphate reabsorption	14
2.2.4. Phosphate regulation factors	15
a. Vitamin D	15
b. Parathyroid hormone	17
c. Fibroblast growth factor 23	22

2.2.5. Hyperphosphatemia, hyperparathyroidism, and metabolic bone disease	25
2.3 Gut microbiota in chronic kidney disease	26
2.3.1. Gut microbiota.....	26
2.3.2. Gut dysbiosis	29
2.3.3. Chronic kidney disease and microbiota changes	30
2.3.4. Probiotics.....	30
2.3.5. Prebiotics.....	32
2.4 Measurement of diversity of intestinal bacteria	34
2.5 Alpha and Beta Diversity	34
Chapter III Materials and Methods.....	38
3.1 <i>In vitro</i> study.....	38
3.1.1. Cell culture	38
3.1.2. MTT-cell viability assay	38
3.1.3. Transepithelial electrical resistance (TEER).....	39
3.1.4. Gene expression of tight junction proteins	40
3.1.5. Bacterial isolation, screening, and identification	41
3.1.6. Prebiotics preliminary test.....	44
3.1.7. Treatment preparation	45
3.2 <i>In vivo</i> study	46
3.2.1. Animal preparation and CKD induction	46
3.2.2. Blood, feces, and organ collection	48
3.2.3. Gene expression of tight junction protein	49

3.2.4. Serum calcium-phosphate profiling	49
3.2.5. Histopathological evaluation.....	49
3.2.6. Intestinal microbiota analysis.....	50
3.2.7. Statistical analysis	51
3.2.8. Ethical consideration	51
Chapter 4 Results.....	52
4.1 Isolation and screening of bacteria.....	52
4.2 Prebiotic.....	56
4.2.1. MTT cell viability assay.....	56
4.2.2. TEER.....	57
4.2.3. Gene expression of tight junction proteins	58
4.3 Animal experiments	58
4.3.1. Body weight	58
4.3.2. Serum creatinine.....	59
4.3.3. Serum phosphate	61
4.3.1. Parathyroid hormone.....	62
4.3.2. Urine phosphate and calcium excretion rate	63
4.3.3. Gene expression of tight junction proteins	65
4.3.4. Histopathological examination	65
4.3.5. Correlation test.....	79
4.3.6. Fecal Microbiota Analysis	79
Chapter 5 Discussion.....	109
5.1 Screening of probiotic candidates	109

5.2 <i>In vitro</i> study on prebiotics.....	109
5.3 Animal experiments	112
Chapter 6 Conclusion	120
REFERENCES	121
VITA.....	137



LIST OF TABLES

	Page
Table 1. Risk factors of chronic kidney disease.....	6
Table 2. Factors that alter renal regulation of phosphate	15
Table 3. Dose of prebiotics in animal experiment	45
Table 4. Groups in animal experiment	48
Table 5. %TEER compared to control in Caco-2 cells treated by candidate bacterial colonies.....	54
Table 6. Bacterial identification results from 16S rRNA gene sequence The percentage relatives to the PBS control.....	55
Table 7 Summary of the sample frequency.....	81
Table 8 Relative abundance of the bacterial Phyla in Control group (median \pm IQR)	87
Table 9 Relative abundance of the bacterial Phyla in CKD group (median \pm IQR).....	88
Table 10 Relative abundance of the bacterial Phyla in COS group (median \pm IQR).....	89
Table 11 Relative abundance of the bacterial Phyla in Inulin group (median \pm IQR)	90
Table 12 Relative abundance of the bacterial Phyla in Maltodextrin group (median \pm IQR)	91
Table 13 Relative abundance of the bacterial Phyla in L. casei group (median \pm IQR)	92
Table 14 Relative abundance of the bacterial Phyla in Synbiotic1 group (median \pm IQR)	93

Table 15 Relative abundance of the bacterial Phyla in Synbiotic2 group (median \pm IQR)	94
Table 16. Top 20 of relative abundance (%) from week 12 of the bacterial Genera in Control group (median \pm IQR) showing on week 0 and week 12.	98
Table 17. Top 20 of relative abundance (%) from week 12 of the bacterial Genera in CKD group (median \pm IQR) showing on week 0 and week 12.	99
Table 18. Top 20 of relative abundance (%) from week 12 of the bacterial Genera in COS group (median \pm IQR) showing on week 0 and week 12.	100
Table 19. Top 20 of relative abundance (%) from week 12 of the bacterial Genera in Inulin group (median \pm IQR) showing on week 0 and week 12.	101
Table 20. Top 20 of relative abundance (%) from week 12 of the bacterial Genera in Maltodextrin group (median \pm IQR) showing on week 0 and week 12.	102
Table 21. Top 20 of relative abundance (%) from week 12 of the bacterial Genera in L. casei group (median \pm IQR) showing on week 0 and week 12.	103
Table 22. Top 20 of relative abundance (%) from week 12 of the bacterial Genera in Synbiotic 1 group (median \pm IQR) showing on week 0 and week 12.	104
Table 23. Top 20 of relative abundance (%) from week 12 of the bacterial Genera in Synbiotics 2 group (median \pm IQR) showing on week 0 and week 12.	105

Table 24. Median and IQR of the difference of relative abundance between week 12 and week 0 in synbiotic 1 group.....106

Table 25. Median and IQR of the difference of relative abundance between week 12 and week 0 in synbiotic 2 group.....107



LIST OF FIGURES

	Page
Figure 1. Histopathological characteristics of chronic kidney disease in glomeruli and interstitium of kidney cortex	6
Figure 2. Systemic balance in adult humans	8
Figure 3 Intestinal absorption of phosphate.	10
Figure 4. Tight junctions protein between intestinal epithelial cells:	12
Figure 5. TEER measurement setup.....	13
Figure 6. Proximal tubular epithelium phosphate transport.....	14
Figure 7. Vitamin D metabolism.....	16
Figure 8. Signal transduction of vitamin D	16
Figure 9. Calcium sensing receptor on parathyroid cell	18
Figure 10. Relationship between blood calcium and PTH.....	18
Figure 11. PTH1R signaling pathways	19
Figure 12. Osteoclastogenesis stimulation	20
Figure 13. Mechanism of PTH-induced phosphate excretion in proximal convoluted tubule	21
Figure 14. Organs response to PTH	22
Figure 15. Signaling pathways of FGF23 in various organs.....	22
Figure 16. FGF23 action on FGFR and Klotho in the parathyroid cells	23
Figure 17. FGFR/klotho complex formation	24
Figure 18. The systemic regulation of phosphate	24
Figure 19. Microbial physiological impact on host	28
Figure 20. Microbial physiological impact on host	31

Figure 21. Bifidobacterium spp. (A) and Lactobacillus spp. (B)	32
Figure 22. Chitosan oligosaccharide	33
Figure 23. Multidetecation microplate reader.....	39
Figure 24. Epithelial Voltohmmeter.....	40
Figure 25. PCR primers sequence for RT-qPCR and product sizes; A. GAPDH, B. Claudin-1, C. Occludin, and D. Zonula occludens (149-151).	40
Figure 26. Specific PCR primer sequence. A: Specific primers for Lactobacilli, B: Universal bacteria primers (154).....	43
Figure 27. Specific PCR primers sequence. A: Specific primers for Bifidobacterium, B: Universal bacteria primers (153).	43
Figure 28. Media screened bacterial colonies	52
Figure 29. Shape and catalase screened bacterial colonies	53
Figure 30. MTT cell viability of Caco-2 cells treated by various concentrations of prebiotics.....	56
Figure 31. %TEER compared to control of Caco-2 cells treated by prebiotics.....	57
Figure 32. Expression of tight junction mRNA in Caco-2 cells treated by prebiotics.....	58
Figure 33. Weight of the rats.....	59
Figure 34. Serum creatinine	60
Figure 35. Serum phosphate.....	61
Figure 36. Serum phosphate changes	62
Figure 37. Serum parathyroid hormone	63
Figure 38. Urine phosphate and calcium excretion rate.....	64
Figure 39. RNA expression of tight junction protein in jejunum	65

Figure 40. H&E-stained kidney section demonstrating glomeruli and tubules.	66
Figure 41. Trabecular bone stained with H&E of Control group:	67
Figure 42. Trabecular bone stained with H&E of CKD group: ..	67
Figure 43. Trabecular bone stained with H&E of COS group: ...	68
Figure 44. Trabecular bone stained with H&E of Inulin group: ..	68
Figure 45. Trabecular bone stained with H&E of Maltodextrin group:	68
Figure 46. Trabecular bone stained with H&E of L. casei group:	69
Figure 47. Trabecular bone stained with H&E of Synbiotic 1 group:	69
Figure 48. Trabecular bone stained with H&E of Synbiotic 2 group:	69
Figure 49. Immunohistochemical staining of the jejunum with anti-ZO-1 antibody of Control group:	70
Figure 50. Immunohistochemical staining of the jejunum with anti-ZO-1 antibody of CKD group:	71
Figure 51. Immunohistochemical staining of the jejunum with anti-ZO-1 antibody of COS group:	72
Figure 52. Immunohistochemical staining of the jejunum with anti-ZO-1 antibody of Inulin group:	73
Figure 53. Immunohistochemical staining of the jejunum with anti-ZO-1 antibody of Maltodextrin group:	74
Figure 54. Immunohistochemical staining of the jejunum with anti-ZO-1 antibody of L. casei group:	75

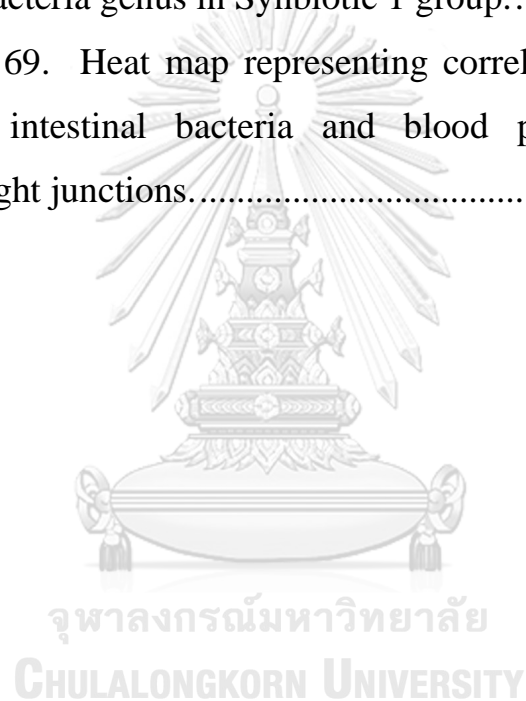
Figure 55. Immunohistochemical staining of the jejunum with anti-ZO-1 antibody of Synbiotic 1 group:.....	76
Figure 56. Immunohistochemical staining of the jejunum with anti-ZO-1 antibody of Synbiotic 2 group:.....	77
Figure 57. Median and IQR of the staining positive area score of the anti-ZO-1 antibody on rats jejunum.	78
Figure 58. Alpha rarefaction	80
Figure 59. Histogram of the frequency per sample.....	81
Figure 60. Shannon index of all groups comparing pre-treatment and post-treatment is represented in median and interquartile range.....	82
Figure 61. Shannon index of each groups comparing pre-treatment and post-treatment is represented in median and interquartile range.....	83
Figure 62. Shannon index of pre-treatment and post treatment comparing all groups are represented in median and interquartile range.	83
Figure 63. Pielou's evenness of all groups comparing pre-treatment and post-treatment is represented in median and interquartile range.....	84
Figure 64. Pielou's evenness of each groups comparing pre-treatment and post-treatment is represented in median and interquartile range.....	85
Figure 65. Pielou's evenness of pre-treatment and post treatment comparing all groups. Pielou's evenness of all groups at week 0 were significantly different (Kruskal-Wallis test: p-value = 0.009). The difference was not significant at week 12 (Kruskal-Wallis test: p-value = 0.1985).....	85

Figure 66. Firmicutes to Bacteroidota ratio of all groups comparing pre-treatment and post-treatment is represented in median and interquartile range.96

Figure 67. Firmicutes to Bacteroidota ratio of each groups comparing pre-treatment and post-treatment is represented in median and interquartile range.96

Figure 68. Proportion of the significant change in relative abundance of bacteria genus in Synbiotic 1 group.107

Figure 69. Heat map representing correlation between relative abundance of intestinal bacteria and blood parameters and RNA expression of tight junctions.108



Chapter I

Introduction

Chronic kidney disease (CKD) is a disease presenting with decreased glomerular filtration rate (GFR) as a result of any abnormalities of renal structure and function (1). It was reported by Jha *et al.* (2013) that the global prevalence of CKD is estimated at 8 to 16 % (2). Moreover, the mortality caused by CKD gradually increased from 937.7 to 1,234.9 thousand individuals per year over a decade, from 2005 to 2015 (3), and was accounted for 3.10% of mortality caused by all non-communicable diseases in 2015. When the patients develop chronic renal disease, in which the GFR is less than 60 mL/min/1.73 m², they fail to sufficiently excrete water and toxic substances via urine. In addition, when GFR is lower than 15 mL/min/1.73 m², called end-stage renal disease (ESRD), it is considered that urinary excretion of water and waste products are lethally inadequate, and patients must depend on renal replacement therapy or renal transplant for survival (4).

CKD patients suffer from the retention of toxic substances in their blood. The toxic substances in the body of the patients originate from the metabolites of body cells and, interestingly, intestinal bacteria. Even though most of the existing bacteria in the gastrointestinal tract are commensal, some of them involve in the production of endotoxins (5, 6). Phosphate is one of the most abundant compounds found in the body and diet and is considered a uremic toxin since CKD patients fail to eliminate the excessive phosphate from the body. This results in a high level of phosphate in the blood, hyperphosphatemia, and contributes to parathyroid hormone (PTH) elevation (secondary hyperparathyroidism) and calcitriol insufficiency, which develops renal osteodystrophy (7). Not only the toxic substances that leak into the bloodstream but in CKD patients, phosphate absorption through paracellular transport also promotes the severity of chronic kidney disease-metabolic bone disease (CKD-MBD).

CKD patients had an alteration of the intestinal microbiota, bacteria that colonized the gastrointestinal tract, which may contribute to the disruption of epithelial tight junction and could lead to translocation of endotoxins through the intestinal barrier (8). However, some intestinal bacteria play an important role in preventing the absorption of toxic substances from the intestine to the bloodstream by promoting the expression of tight junction proteins of the intestinal epithelial cell and increase intestinal barrier integrity (9). In order to alleviate the progression and complications of CKD, including CKD-MBD, it could be suggested that normalization of the gut bacterial community is a potential treatment (10).

The composition and function of the intestinal microbiome in humans are influenced by diet. Some complex carbohydrates, especially indigestive polysaccharides and oligosaccharides are metabolized by these intestinal bacteria and used to promote their growth (11, 12). These carbohydrates, known as prebiotics, selectively stimulate the growth of the health-associated bacteria, for example, fructooligosaccharide (FOS), galactooligosaccharide (GOS), and inulin (13). However, each bacterial family prefers the different types of prebiotics for their growth promotion. A systemic review and meta-analysis reported beneficial outcomes of prebiotics and probiotics treatments, including elevation of residual renal function, decreasing serum inflammatory cytokines, increasing anti-inflammatory cytokines, and a reduction of serum urea concentration (14, 15). In addition, chitosan oligosaccharide (COS), a degradation product of chitosan/chitin, is a carbohydrate substance that has been interested and widely studied for a decade (16). Many studies revealed the role of COS in the increased expression of tight junction protein in an intestinal epithelial cell, reducing paracellular transport of toxic substances through intestinal epithelium, and reducing the loss of the epithelial barrier integrity by inflammation (17-19).

Even though the intestinal microbiota modulated the intestinal barrier integrity (20), the effects of the biotics and phosphate absorption in CKD have not been well established. We hypothesized that COS would promote the tight junction of intestinal epithelial cells in the CKD rat model and reduce the absorption of phosphate, which may ameliorate the CKD-MBD.

Research questions

Do the supplement of COS and other commercial oligosaccharides ameliorate hyperphosphatemia and MBD in CKD rats?

Do the supplement of probiotic-potential bacteria ameliorate hyperphosphatemia and MBD in CKD rats?

Does the supplement alter gut microbiomes in CKD rats?



Main Objectives

To investigate the effects of oligosaccharides supplementation on hyperphosphatemia and MBD in CKD rats

To investigate the effects of probiotics supplementation on hyperphosphatemia and MBD in CKD rats

Minor objectives

To investigate the effects of oligosaccharides and probiotics supplementation on a tight junction in inflammatory-induced Caco-2 cell

To investigate the effects of oligosaccharides and probiotics supplementation on renal pathology, function and uremic toxin levels in CKD rats

To investigate the effects of oligosaccharides and probiotics supplementation on the alteration of intestinal microbiota in CKD rats

Hypotheses

The supplement of COS and other commercial oligosaccharides ameliorate hyperphosphatemia and MBD in CKD rats.

The supplement of probiotic-potential bacteria ameliorate hyperphosphatemia and MBD in CKD rats.

The supplement alters gut microbiomes in CKD rats.

Chapter II

Literature Reviews

2.1 Chronic kidney disease

2.1.1. Definition and stages

Chronic kidney disease (CKD) is a disease that involves progressive and irreversible dysfunction and changes in the structure of the kidneys, which contributes to a higher risk of other clinical complications and mortality (21). The decreasing glomerular filtration rate and leakage of plasma proteins into urine are the presentation of glomerular damage in CKD patients. However, CKD is also pathologically characterized by glomerulosclerosis, interstitial fibrosis, loss of filtration slit and foot process of podocytes, tubular atrophy, loss of peritubular capillaries, and inflammation, as shown in Figure 1.

CKD is categorized according to the glomerular filtration rate (CKD stage 1 to 5) and albuminuria (A1 to A3). The most severe stage of CKD, a kidney failure (CKD stage 5), is reached when the GFR drops below $15 \text{ mL} \cdot \text{min}^{-1} \cdot 1.73 \text{ m}^{-2}$ (22).

The common causes of CKD are diabetes mellitus and hypertension. However, several risk factors were found to associates with the occurrence of chronic kidney disease, as described in Table 1 (23).

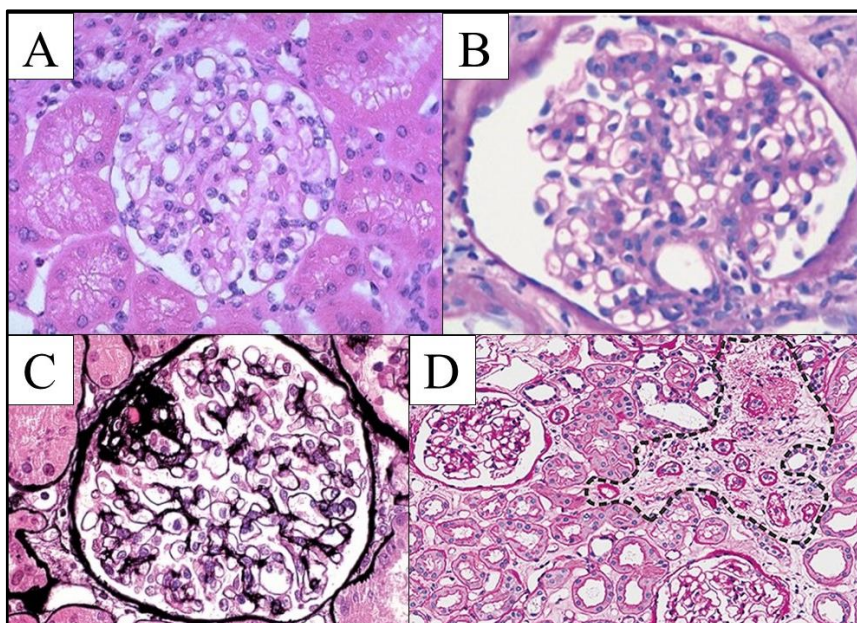


Figure 1. Histopathological characteristics of chronic kidney disease in glomeruli and interstitium of kidney cortex

A) Normal glomerulus, B) Mesangial hypercellularity (Robert I., 2014)(24), C) Focal segmental glomerulosclerosis (Agati D., et al., 2011) (25), D) Fibrosis with tubular atrophy (black dashed outline) (Denic A., et al., 2017) (26).

Table 1. Risk factors of chronic kidney disease

Risk factor	Characteristics of higher risk
Genetic component	Uromodulin mutation (27) APOL1 mutation (28)
Family history	CKD found in a family member (29)
Ethnicity	African American is higher than Caucasian American (30, 31)
Age	Elderly population (32)
Obesity	Overweight (33) and high waist-to-hip ratio (34)
Smoking	Smoking > 20 cigarettes per day (35)
Acute kidney injury	Adult with a history of kidney injury (36)
Nephrotoxins	Taking > 1000 pills of acetaminophen in a lifetime (37)
Hypertension	Having a higher risk with a higher stage of hypertension (38)
Diabetes mellitus	Diabetic patients (39)

2.1.2. Clinical importance

During the early stage of CKD, the patients are usually asymptomatic. Once the disease advances to a late stage, decreased renal function contributes to the

retention of fluid and electrolytes, as well as the accumulation of toxic substances, called uremic toxins, in the blood. The end-stage renal disease (ESRD) patients who could not sufficiently eliminate the uremic toxin, can survive by depending on lifetime renal replacement therapy (RRT) including, hemodialysis, peritoneal dialysis and kidney transplantation. Generally, the progression of CKD can be attenuated by modifying the patients' lifestyle and diet. However, there is no standard medical treatment that directly alleviates uremic toxin in the blood of CKD patients. (22).

2.1.3. Complication

Kidney is a vital organ that regulates the homeostasis of the body. The impaired function of the kidney contributes to the metabolic disorders involving the imbalance of numerous substances in the body. The impaired ammonium excretion and inadequate bicarbonate production typically lead to acid accumulation in the body fluid, acidosis, and damaging more tissues and organs (40-42). CKD increases the risk of several complications in the patients, including cardiovascular diseases, metabolic acidosis, anemia, mineral and bone disorder (MBD), hyperkalemia, hyperphosphatemia, and hyperparathyroidism.

2.2 Phosphate homeostasis

Phosphate is an essential molecule in an organism. It participates in several vital molecules in the cell as a part of the cell membrane, genetic material, and energy molecules. The inorganic phosphate (Pi) also plays a critical role in bone mineralization and mineral metabolism. Phosphate cycle in the body is regulated by many organs (Figure 2). Pi is supplied to the body by intestinal absorption from the diet and excreted by the kidneys. The phosphate in the body is eliminated through urination and defecation. The extracellular Pi pool is body fluid that may transfer into soft tissue Pi pool (presenting in the form of phospholipids, phosphoproteins, nucleic acids, and nucleotides) or skeletal system. Hence, Pi imbalance, such as hypophosphatemia due to over-excretion of urinary phosphate, may contribute to the impaired bone mineralization according to the interdependence of calcium and Pi in the rate of bone matrix, as hydroxyapatite formation (43-45).

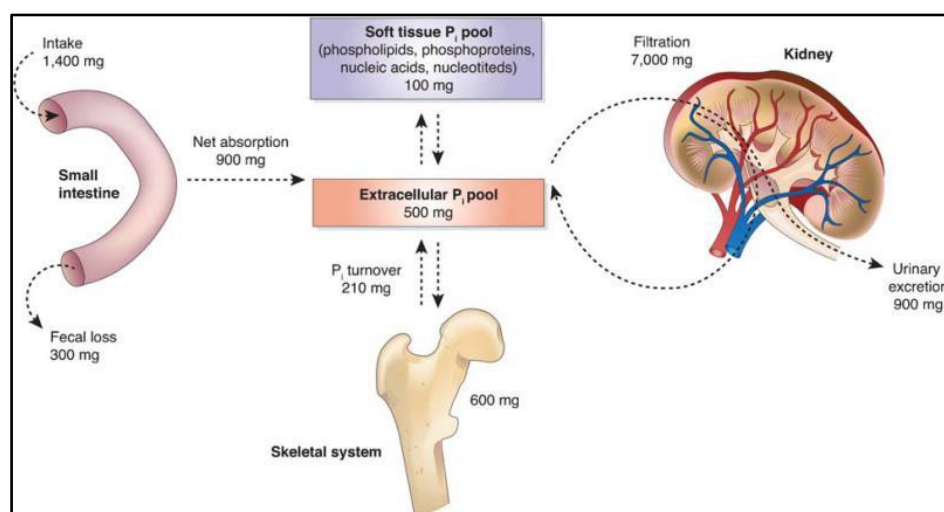


Figure 2. Systemic balance in adult humans (Kiehl and Ghishan, 2008) (45)

2.2.1. Intestinal phosphate absorption

Phosphate is generally found in many types of food as it is part of nucleic acid. Phosphate-containing additives such as phosphoric acid, sodium phosphate, and sodium polyphosphate are found in many processed food and beverage products. Dietary phosphate is absorbed through transepithelial transportation via sodium-dependent phosphate transport protein 2B (NaPi-IIb), which belongs to the type II family of transporters and presents in the ileal brush border (46). A study in a NaPi-IIb gene knockout mouse model demonstrated that the sodium-dependent Pi transport protein abolished mice had increased phosphate in feces but decreased phosphate in urine, suggesting decreased intestinal phosphate absorption (47). This shows the importance of the transporter in dietary phosphate absorption. The transporters on intestinal epithelial cells that mediate the transcellular absorption of phosphate are shown in Figure 3A. Transcellular phosphate absorption by NaPi-IIb is secondary active depending on the gradient creating by sodium-potassium ATPase (NaK ATPase) on the basolateral membrane. Recently, the intracellular phosphate efflux on the basolateral membrane is not clearly described (48). Pi in the blood plasma is freely filtrated into the glomeruli.

Nevertheless, transepithelial Pi absorption is not the only contribution in the total Pi absorption in the intestine. According to the difference in the concentration of

Pi between blood (0.75-1.45 mM) and intestinal lumen (0.5-17.5 mM depending on dietary Pi load) (49), Pi absorption occurs via paracellular transport. It was found in the study on adenine-induced-CKD mice that NaPi-IIb knockout mice had slightly lower blood phosphate than the wild type mice (50). The similar results were also reported in the study of the effects of NaPi-IIb gene deletion on acute intestinal absorption conducted by Sabbagh *et al.* (2009) (47). Furthermore, NaPi-IIb inhibitor, ASP3325, failed to reduce Pi level in the blood of hyperphosphatemic ESRD patients in a clinical trial (51). This result showed that even though the transcellular transport is inhibited, the intestinal absorption rate of the phosphate is unaffected (48) Knopfel *et al.* (2019) demonstrated in NaPi-IIb-knockout mice that flux measurement of phosphate from apical to the basolateral side of intestinal epithelial tissue was not different in wild type and knockout mice. Moreover, no difference was detected in the duodenum, jejunum, ileum, and colon of the mice (52). Hence, the authors proposed that there is an alternative route of intestinal phosphate absorption, which plays an important role in intestinal phosphate absorption. (48).

Recent studies reviewed that phosphate influx occurs at the paracellular region (Figure 3B). The important factors that determine the rate of the intestinal paracellular Pi absorption are the concentration gradient across the epithelial tissue, electrical gradient, and the integrity of the tight junction (53).

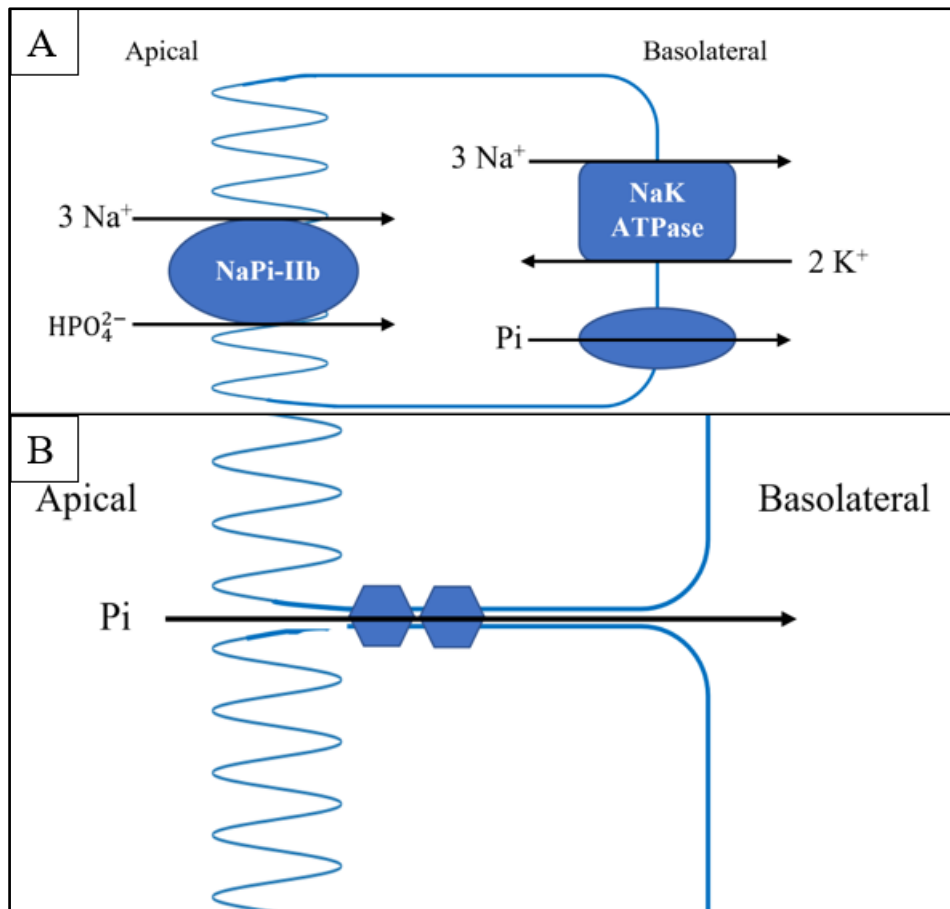


Figure 3 Intestinal absorption of phosphate.

A: Transcellular intestinal phosphate absorption, B: Paracellular intestinal phosphate absorption. (Modified from Saurette M. and Alexander R., 2019) (48)

King *et. al.* (2018) observed that tenapanor (sodium proton exchanger inhibitor) effectively reduces paracellular phosphate absorption while preserving transcellular absorption. They also noted a significant increase in transepithelial electrical resistance, which serves as an indicator of intestinal epithelial integrity. Furthermore, several studies have reported similar findings by suppressing the expression of sodium hydrogen exchanger 3 contributes to the observed increase in transepithelial resistance due to the retention of intracellular positive ion (proton). These findings suggest that the enhanced transepithelial resistance facilitates paracellular phosphate absorption (54). Recently, the tenapanor has been tested by phase 3 clinical trial conducted by Block *et. al.* (2021) to reduce the elevated serum phosphate in hyperphosphatemia patients and submitted as a new drug application to US FDA by Ardelyx, Inc. According to the findings, the administration of tenapanor

at doses of 3 mg, 10 mg, and 30 mg resulted in a significant reduction in serum phosphate levels after 8 weeks, dose independently. This suggests that tenapanor has the ability to inhibit proton excretion into the gut lumen, leading to an increase in the electrical gradient and an increase in transepithelial electrical resistance (TEER) values. The observed increase in TEER contributes to a reduction in paracellular transport of phosphate and ultimately leads to a decrease in serum phosphate level. These results support the notion that tenapanor's mechanism of action involves the modulation of proton excretion and the subsequent impact on TEER, resulting in the regulation of phosphate transport and serum phosphate levels (55).

It could be suggested that the amelioration of hyperphosphatemia and hyperparathyroidism may succeed by limiting paracellular phosphate absorption. In the present study, we aimed to suppress paracellular phosphate transport by promoting tight junction protein by probiotics.

2.2.2. Tight junction proteins and gut barrier integrity

Epithelial cells are connected to the adjacent cells by three types of epithelial cell junctions, tight junctions, adherent junctions, and desmosomes. Tight junctions are necessary for sealing the intercellular spaces and provide a monolayer intestinal epithelial barrier that regulates the transportation of luminal fluid into the basolateral side where the diffusion of the substances takes place, intracellular transport. The intestinal epithelial cells and tight junction proteins are illustrated by Figure 4 (56). The tight junctions are the intercellular protein complex that composes of the transmembrane protein, including claudins, occludin, and zonula occludens. The protein complex is connected to intracellular actin via a protein complex of zona occludens (ZO-1 and ZO-2). The junctional adhesion molecules (JAMs) are the transmembrane receptor found at tight junctions. They may bind with each other or other types of adhesion molecules such as integrin (57, 58).

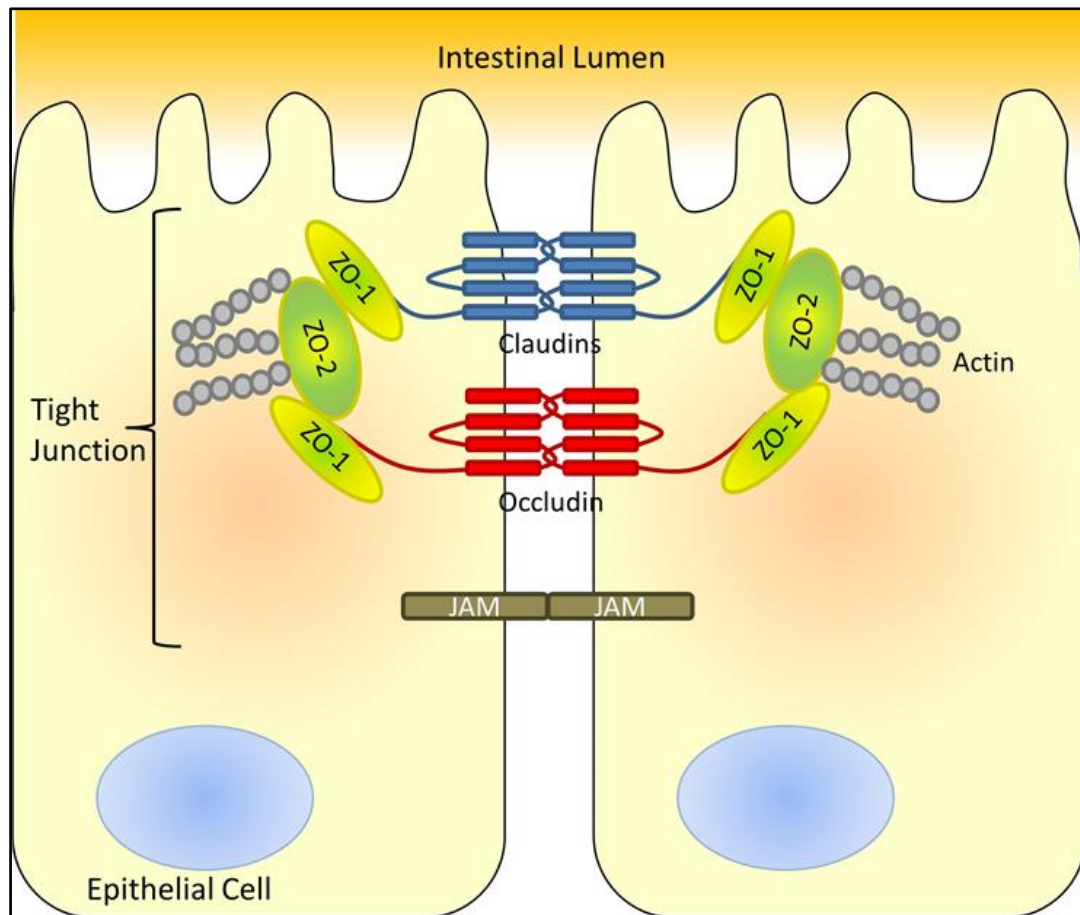


Figure 4. Tight junctions protein between intestinal epithelial cells: JAM, junctional adhesion molecule; ZO, zona occludens (Collin et al., 2017) (56).

The luminal charged substances of 0.4 nm diameter may be passively permeable through the tight junctions and are regulated by claudin (59). In contrast, the uncharged soluble molecules enter the basolateral side by the leakage through large pores created by the inconsistency of the tight junction transmembrane proteins (60). The increased permeability of intestinal epithelium plays an important role in the susceptibility to gastrointestinal diseases such as irritable bowel disease (IBD) and celiac disease (61). The barrier function of the tight junction depends on the transmembrane adhesion proteins, including claudins. The barrier function can be determined by transepithelial electrical resistance (TEER). When the TEER is relatively low, it indicates low integrity of the intestinal epithelium, termed by “leaky gut” (62).

TEER measurement is an *in vitro* experiment for the evaluation of tight junction integrity. The technique is carried out in a cell culture model of an epithelial

monolayer. It is used in many cell types that are commercially available. The electrical resistance, measured in ohms, quantitatively represents the barrier integrity of a cellular monolayer. The electrodes are put into the apical side and basolateral side of the monolayer that cultured in a transwell cell culture plate, as shown in Figure 5. The total electrical resistance (R_{total}) between both sides is calculated by the summation of the cell layer resistance (R_{TEER}), culture medium resistance (R_{M}), semipermeable membrane insert resistance (R_{I}), and the electrode medium interface resistance (R_{EMI}). Then, TEER ($\text{TEER}_{\text{reported}}$) value is calculated as the multiply between the cell-specific resistance (R_{tissue}) and the area of a semipermeable membrane and generally reported in a unit of $\Omega \cdot \text{cm}^2$ (cell-specific resistance (R_{tissue}) is the difference between total electrical resistance (R_{total}) and the blank resistance (R_{blank}) (63). The low TEER value indicates the high permeability of the electrolytes from the apical side to the basolateral side of the cell.

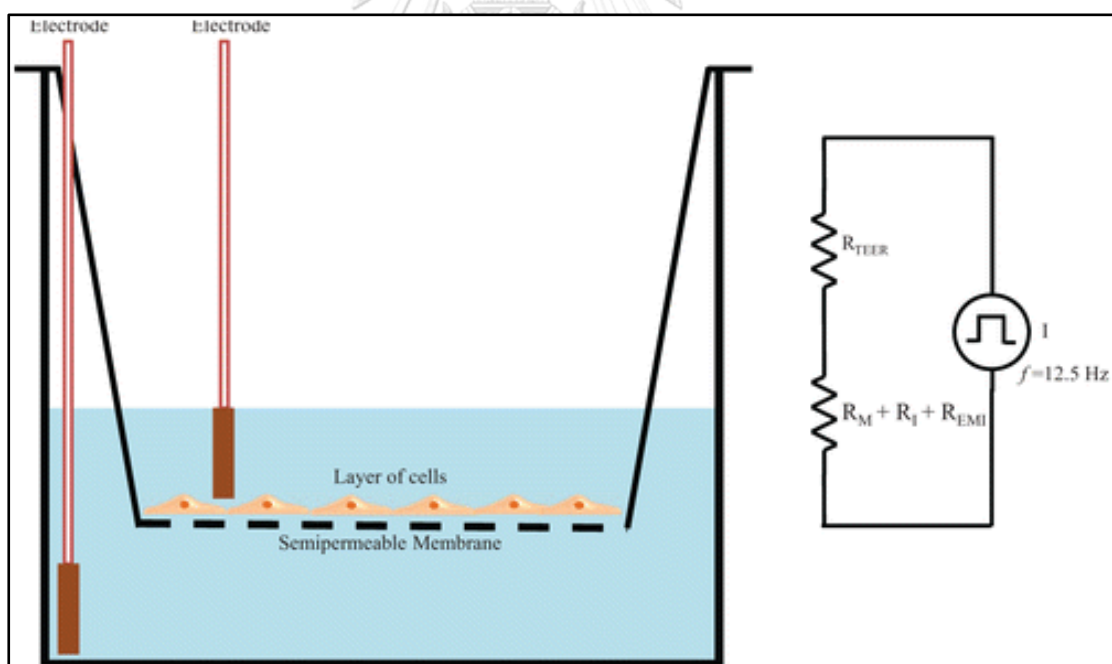


Figure 5. TEER measurement setup (Srinivasan B. et al., 2015) (63)

2.2.3. Renal phosphate reabsorption

Kidney is the key organ in phosphate homeostasis. The phosphate of 3,700 to 6,100 mg is filtered by glomeruli every day in an adult human. Only 600 to 1,500 mg of phosphate is excreted in the urine per day, which is only 15-25% of the daily filtered load. To maintain the blood phosphate level, 85% of phosphate is reabsorbed in the proximal convoluted tubule by sodium-dependent phosphate transport protein 2A, 2C (NaPi-IIa, NaPi-IIc, and Pi-T II), as shown in Figure 6 (64, 65). The other parts of the tubule play a minor role in the regulation, and the transporter involved has not been clearly identified (66).

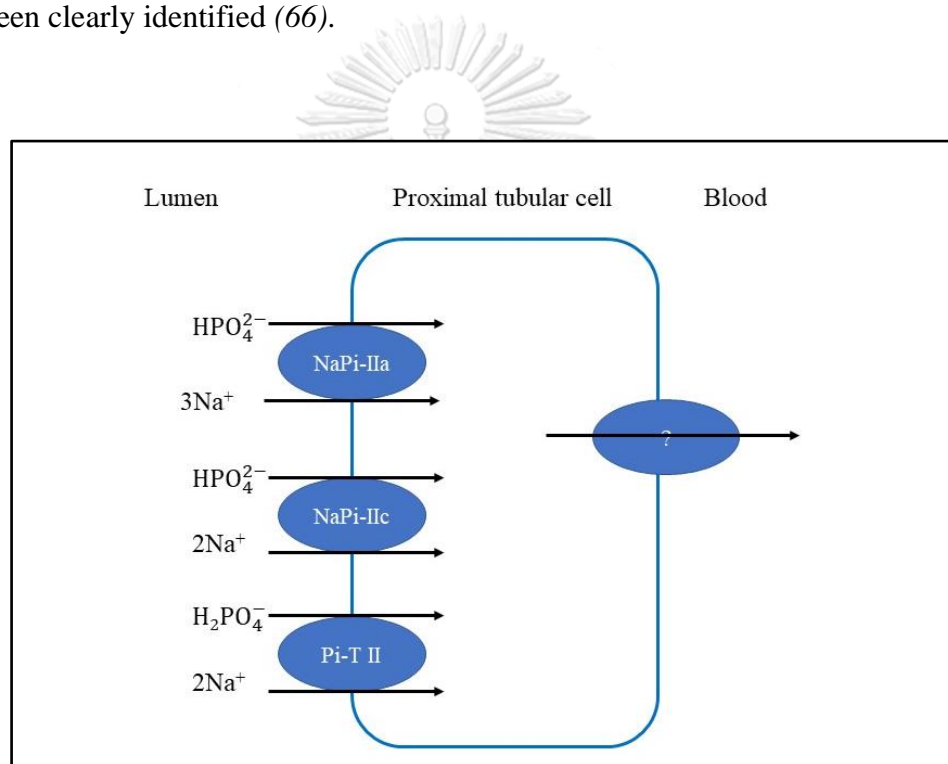


Figure 6. Proximal tubular epithelium phosphate transport.
(Modified from Curthoys N. and Moe O., 2014)(67)

The renal phosphate reabsorption depends on the abundance of the sodium-dependent phosphate transport protein on the luminal side of the tubule. The abundance is controlled by hormonal regulation. The factors that alter the phosphate regulation by kidneys by renal reabsorption are summarized in Table 2.

Table 2. Factors that alter renal regulation of phosphate (Blaine J. et al., 2015) (68)

Increase phosphate reabsorption	Decrease phosphate reabsorption
Low-phosphate diet	PTH
1,25 dihydroxyvitamin D3	FGF23
Thyroid hormone	High-phosphate diet
	Metabolic acidosis
	Potassium deficiency
	Glucocorticoid
	Dopamine
	Hypertension
	Estrogen

2.2.4. Phosphate regulation factors

The phosphate homeostasis is strictly maintained by a collective compartment including hormones and regulatory factors such as active vitamin D, parathyroid hormone (PTH), and phosphatonins (FGF-23, sFRP-4, MEPE) (69). Calcium and phosphate are loaded into the serum via the stimulation of bone demineralization and enhanced intestinal absorption that is mediated by vitamin D (70). It also reduces renal phosphate excretion by decreasing the expression of the type IIa sodium-dependent phosphate cotransporter (NaPi-IIa) in the proximal tubule of nephrons which are regulated by PTH and FGF23 hormone (66).

a. Vitamin D

Vitamin D is a lipid-soluble vitamin responsible for the intestinal absorption of calcium, magnesium, and phosphate. The important form of vitamin D in the human is vitamin D3 (calcitriol) (71). Vitamin D precursor is synthesized from epidermal adipose tissue by ultraviolet exposure and received from food. The activation of vitamin D occurs by hydroxylation enzymes in the liver and kidneys. In the liver, cholecalciferol is converted to 25-hydroxycholecalciferol by vitamin D-25-hydroxylase (25(OH)D3). Then, 25(OH)D3 in the blood circulation is converted into 1,25 dihydroxycholecalciferol (1,25 dihydroxyvitamin D3) or calcitriol, a biologically active form of vitamin D, by 25(OH)D3-1 α -hydroxylase in the kidneys. The transportation of vitamin D and its metabolites in blood circulation is facilitated by

vitamin D binding protein (DBP). Vitamin D has a major role in the regulation of calcium and phosphate and the promotion of bone growth and remodeling. The function of active vitamin D is deactivated by the hydroxylation by vitamin D3 24 α -hydroxylase into secalciferol and calcitriol, respectively (Figure 7).

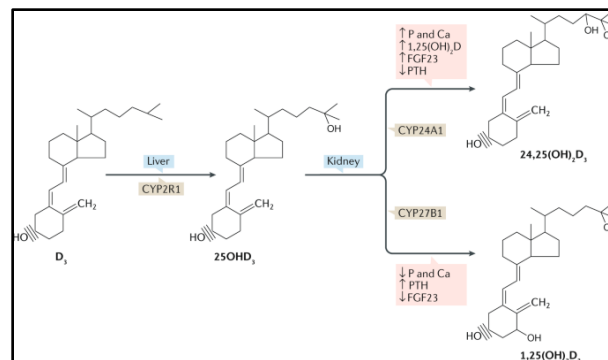


Figure 7. Vitamin D metabolism
(Bikle D. and Christakos S., 2020)(72)

Calcitriol has an essential role in calcium homeostasis and metabolism. It is transported through the phospholipid bilayer of the plasma membrane of the target cells and binds to the vitamin D receptor (VDR) in the cytoplasm. The activated receptor enters the nucleus of the target cells and activates the transcription of its target genes with the activation of vitamin D response elements (VDRE), as shown in Figure 8 (73).

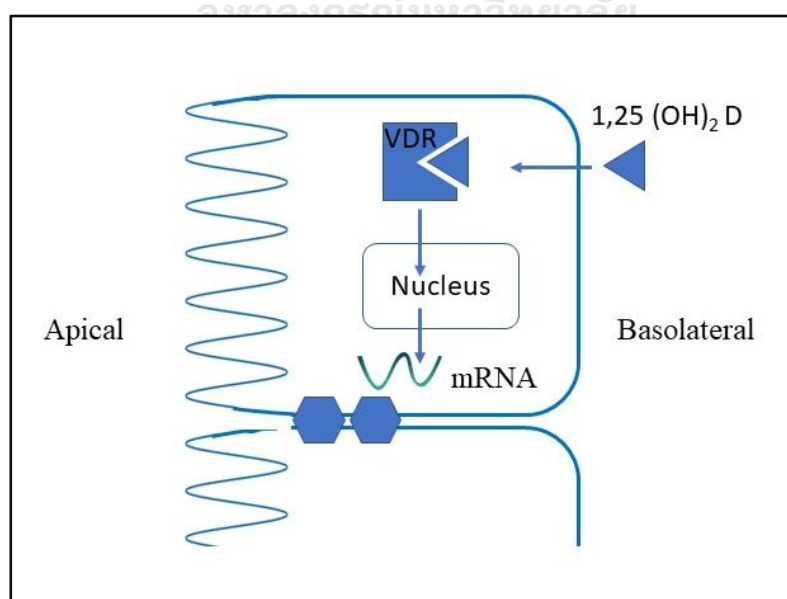


Figure 8. Signal transduction of vitamin D

The intestinal absorption of calcium increases responding to calcitriol by increasing the expression of calcium transport proteins, epithelial calcium channel TRPV6 (Transient Receptor Potential Vanilloid subfamily member 6), and calcium-binding protein (CaBP, calbindin). Calcitriol also functions as a negative regulator of PTH. The binding between VDR and its ligand on parathyroid cells down-regulates PTH gene expression and up-regulates VDRs and calcium-sensing receptors (CaSR) (74). Blood calcium and phosphate levels are maintained by calcitriol. The function of osteoblast responses to calcitriol at multiple levels. The receptor activator of the NF- κ B ligand of osteoblast is induced by calcitriol to regulate phosphate homeostasis by increasing FGF23. It also stimulates mesenchymal stem cell differentiation to osteoblast lineage and inhibits adipocytogenesis through the Wnt pathway (75).

b. Parathyroid hormone

Parathyroid hormone (PTH) is secreted from the chief cell of the parathyroid gland in response to serum calcium, phosphate, FGF23, and 1,25-dihydroxyvitamin D3 (calcitriol). It is the key hormone to regulate the serum calcium balance. PTH plays a role in the regulation of serum calcium, serum phosphate, and vitamin D synthesis via two major organs, including bones, and kidneys (76). Calcium concentration in blood is detected by the calcium-sensing receptor (CaSR), a class C G-protein coupling receptor, in the parathyroid cells (77). Activation of CaSR leads to the activation of phospholipase C (PLC), resulting in an increasing cytosolic calcium concentration that triggers mitogen-activated protein kinase (MAPK) signaling cascade and inhibition of vesicle fusion and exocytosis of parathyroid hormone, resulting in the suppression of parathyroid hormone release (Figure 9). Only a tiny elevation of serum calcium contributes to the dramatic decline of serum PTH, as shown in Figure 10.

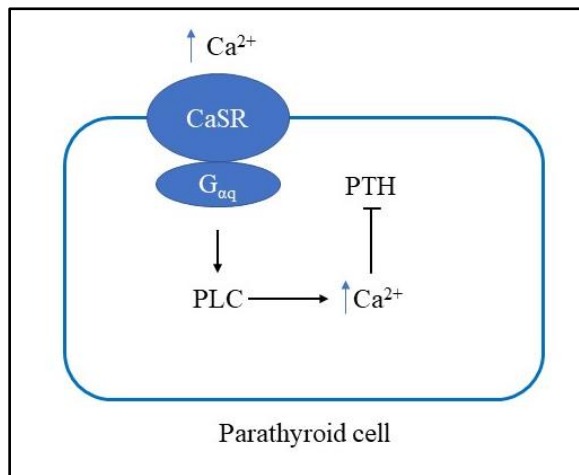


Figure 9. Calcium sensing receptor on parathyroid cell (modified from Bouchet T. and Henley J., 2005) (78)

Moreover, the spontaneous increase of both serum calcium and phosphate enhances the aggregation between calcium and phosphate in the blood and leads to the formation of calcium phosphate complex which contributes to vascular calcification (79).

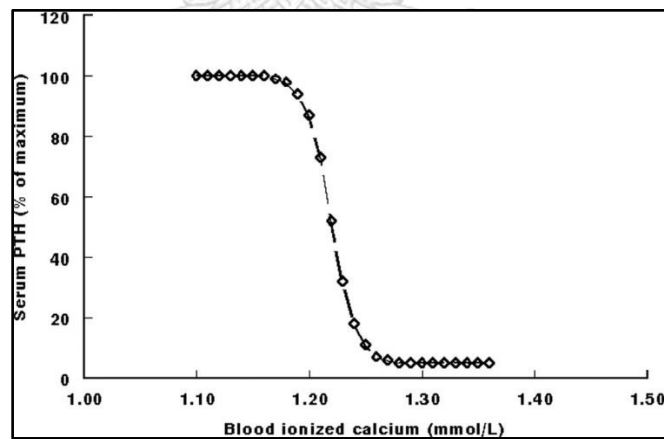


Figure 10. Relationship between blood calcium and PTH (Chen A. and Goodman G., 2004) (80)

PTH targets parathyroid hormone/parathyroid hormone-related peptide receptor (parathyroid hormone 1 receptor, PTH1R) on the cell membrane of the target organs, including bones and kidneys. Activation of PTH1R, a G protein-coupling receptor, triggers adenylate cyclase and phospholipase C signaling cascades (Figure 11).

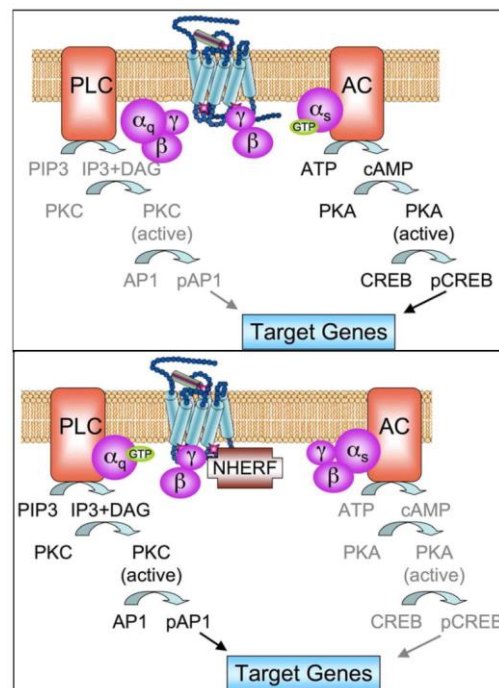


Figure 11. PTH1R signaling pathways (Datta S. and Abou-Samra B., 2009) (81)

Hydroxyapatite, $\text{Ca}_{10}(\text{PO}_4)_6(\text{OH})_2$, is the largest reservoir of calcium and phosphate in the body. Osteoblast (mineralizing cell), osteoclast (demineralizing cell), and osteocyte are the cells that responsible for production, maintenance, and remodeling (degradation and biosynthesis of bone). PTH plays an essential role in bone resorption by stimulation of osteoclastogenesis, the differentiation of the precursor cells into osteoclasts through the pathway of RANKL (receptor activator of nuclear factor kappa-B ligand) stimulation on the osteoblast and osteoprotegerin inhibition (Figure 12) (82, 83). The osteoclasts degrade hydroxyapatite and release calcium and phosphate into the blood.

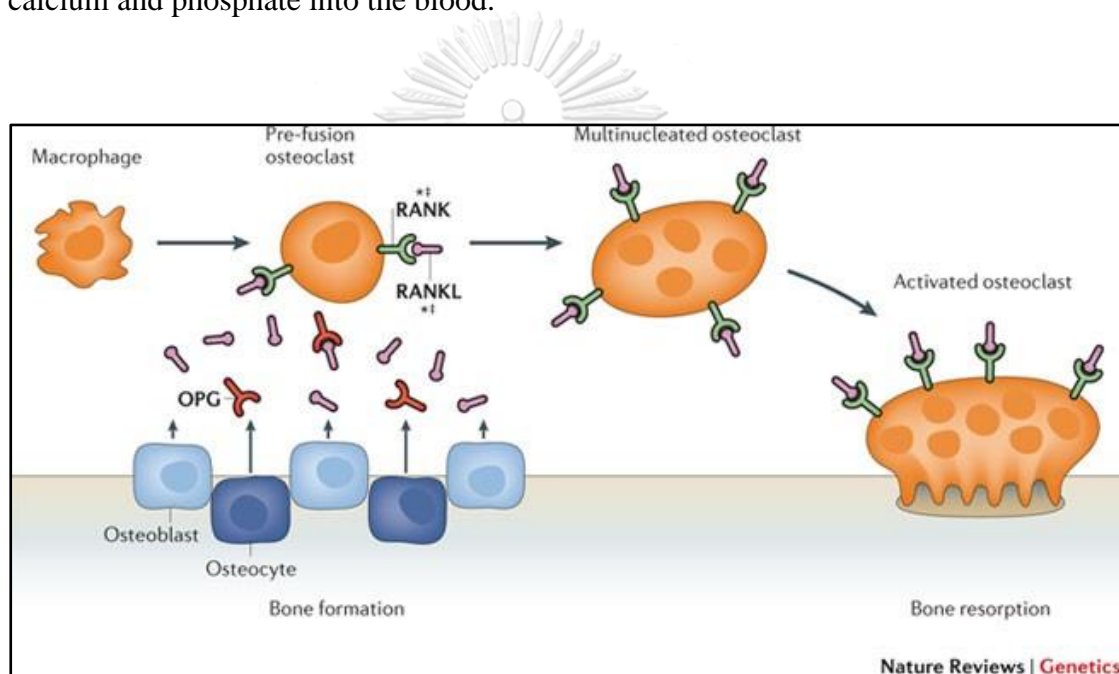


Figure 12. Osteoclastogenesis stimulation
(Richards J. et al., 2012) (84)

Approximately 250 mmol of calcium ions are filtered from the glomerulus into the Bowman's capsule every day. However, only five mmol per day is excreted in the urine. About 98% of the calcium in the glomerular filtrate is reabsorbed throughout the tubule of nephrons (68). The reabsorption of calcium ions influenced by PTH occurs only in the distal convoluted tubules by activating specific ion channels, such as TRPV5 (85). PTH also increases phosphate urine excretion by regulating sodium-dependent phosphate transporter via protein kinase A (PKA) and protein kinase C (PKC). In the absence of PTH, NaPi-IIa on the apical side of the renal tubule reabsorbs phosphate from the glomerular filtrate into the cell. When

PTH1R is activated by the presence of PTH, the signaling cascades are triggered to reduce phosphate reabsorption by the internalization of NaPi-IIa and to break down its mRNA (Figure 13) (68).

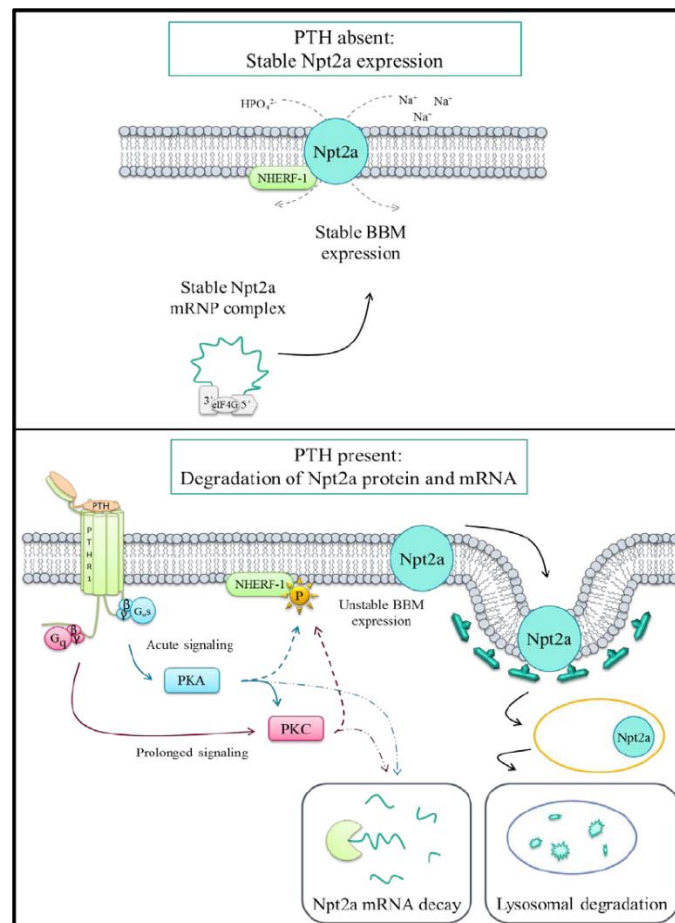


Figure 13. Mechanism of PTH-induced phosphate excretion in proximal convoluted tubule (Murray R. et al., 2015) (86)

Calcium absorption by the intestine is not directly controlled by PTH. However, PTH regulates 25-hydroxy vitamin D₃ 1-alpha-hydroxylase enzyme, which stimulates the conversion of 25-hydroxy vitamin D into 1,25-dihydroxy vitamin D (active vitamin D, calcitriol) by the kidney. The active vitamin D up-regulates the production of calbindin, a calcium binding protein, in the intestine, which increases intestinal calcium absorption (85, 87). Moreover, the active vitamin D also stimulates transcellular phosphate absorption via the stimulation of NaPi-IIb expression and

function (88). The overall PTH actions on its target organs are summarized in Figure 14.

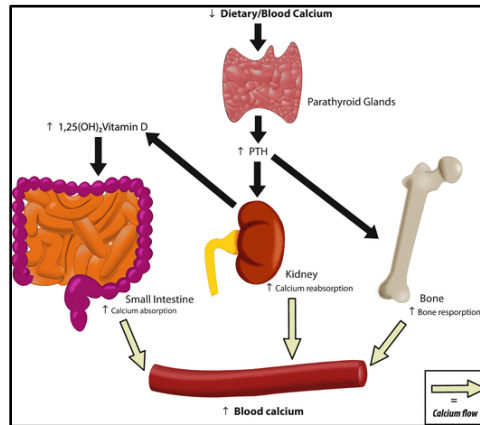


Figure 14. Organs response to PTH (Gaffney-Stormberg E. et al., 2017) (73)

c. Fibroblast growth factor 23

The elevated serum phosphate induces fibroblast growth factor 23 (FGF23) secretion by osteoblasts and osteocytes in bones. FGF23 secreted into blood circulation acts on various organs, including kidneys, parathyroid, heart, and bone. Signaling pathways in each organ and their responses to FGF23 are summarized in Figure 15.

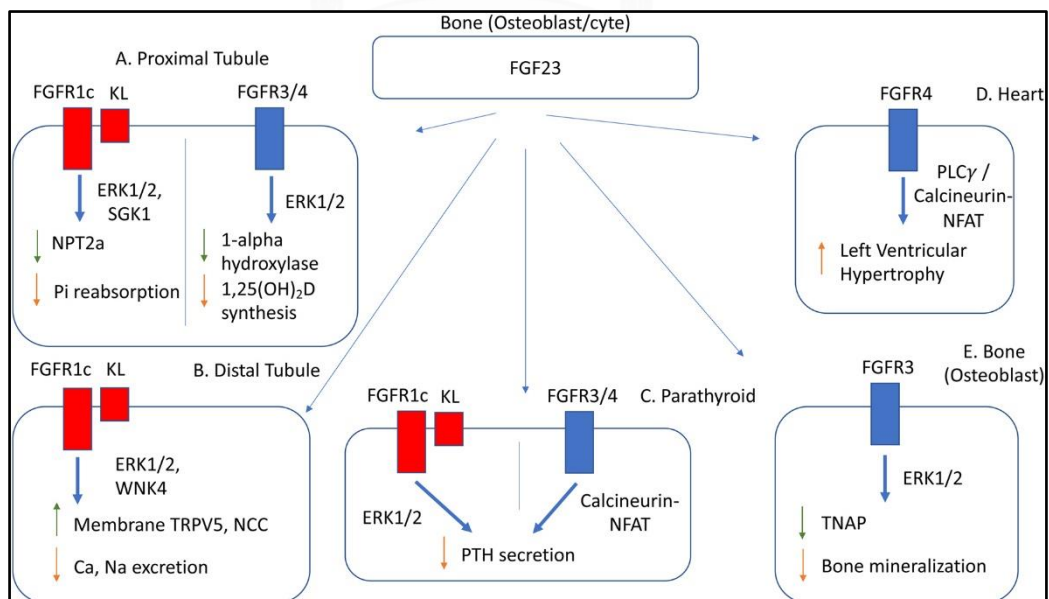


Figure 15. Signaling pathways of FGF23 in various organs (Ho B. and Bergwitz C., 2021) (89)

FGF23 binds to its receptor (FGFR) on the target organs, including kidneys and parathyroid glands, and triggers the signaling pathway involving in phosphate homeostasis. FGF23 activates the calcineurin pathway via FGFR and mitogen-activated protein kinase (MAPK) pathway via FGFR/Klotho complex. Both pathways inhibit the secretion of PTH from parathyroid cells (Figure 16).

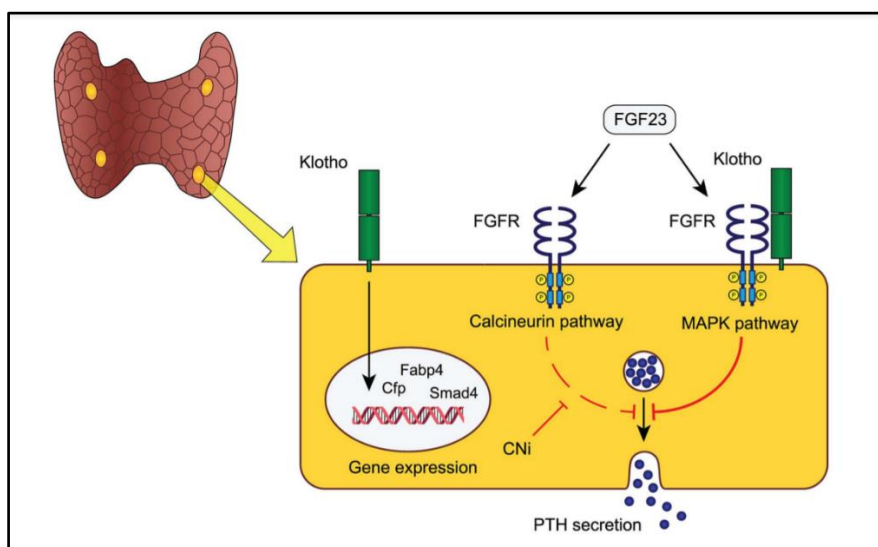


Figure 16. FGF23 action on FGFR and Klotho in the parathyroid cells (Olauson H. et al., 2013) (90)

The Klotho protein is a transmembrane protein function as the obligate co-receptor for FGF23. However, protease enzymes can convert the membrane-bound klotho into blood circulation. In humans, klotho is encoded by the KL gene. The schematic structure of the FGFR/klotho complex is shown in Figure 17. The KL2 domain of klotho has an extended arm (termed by receptor binding area, RBA) that binds the D3 domain of FGFR1c, creating a groove that fits their ligand FGF23. Interestingly, a collection of studies found that the complex of FGF23, FGFR, and klotho requires heparan sulfate to activate the tyrosine kinase of FGFR1c (91).

FGF23 reduces phosphate reabsorption by increasing renal phosphate clearance in the proximal tubule of the nephrons through the degradation of NaPi-IIa/NHERF-1 (sodium-proton exchanger regulatory factor) complex by phosphorylation of NHERF-1 membrane anchoring protein (92). The secretion of

FGF23 is promoted by both PTH and active vitamin D and suppressed by negative feedback regulation.

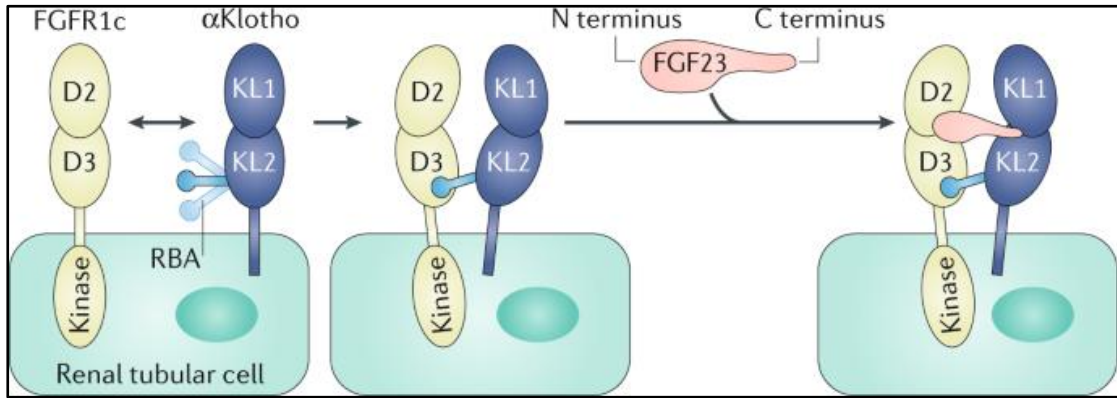


Figure 17. FGFR/klotho complex formation (Koru-o M.,2019) (91)

A study in the NaPi-IIb gene knockout mouse model revealed that the decreased urinary phosphate excretion correlated with reduced levels of the FGF23 in the blood and the elevated protein expression of the renal phosphate transporter NaPi-IIa. It suggested that the absence of intestinal NaPi-IIb triggers physiological mechanisms of the kidneys to stabilize phosphate homeostasis (47). The systemic regulation diagram of phosphate by FGF23, PTH, and vitamin D is shown in Figure 18.

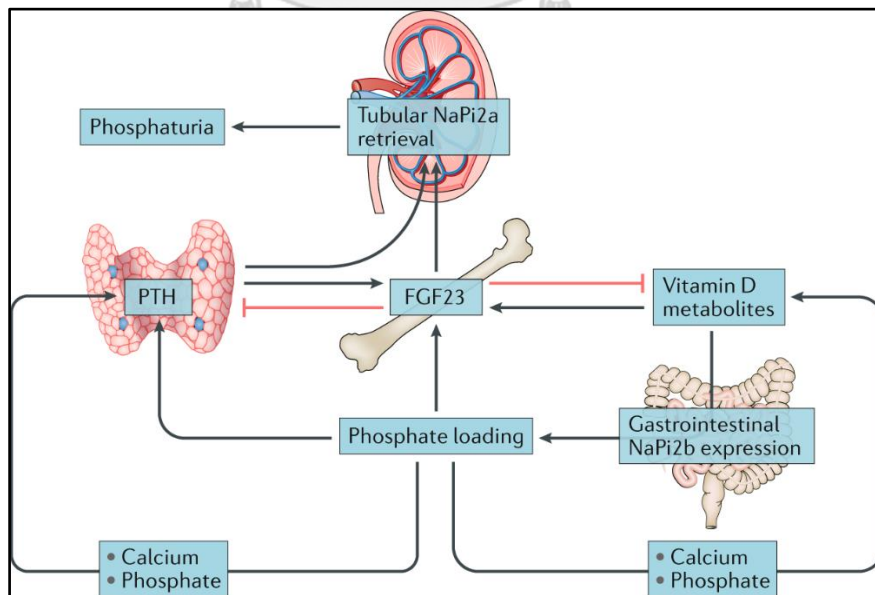


Figure 18. The systemic regulation of phosphate (Vervloet M., 2019)(93)

2.2.5. Hyperphosphatemia, hyperparathyroidism, and metabolic bone disease

The impaired renal function in CKD patients contributes to the reduced glomerular filtration rate and renal phosphate excretion. Accumulated serum phosphate promotes a series of physiological responses, including PTH secretion, osteoclast activation, and increasing bone resorption, which further increases serum phosphate levels. The progressive elevation of serum PTH responding to the hyperphosphatemia is called secondary hyperparathyroidism. As the bone continuously demineralized according to hyperparathyroidism in CKD patients, results in metabolic bone disease (MBD). MBD is a common complication of CKD that leads to pathologic fracture and systemic vascular calcification, and cardiovascular mortality in CKD patients.

Clinical investigations reveal the association of dietary phosphate and premature aging, vascular calcification, cardiovascular mortality, risk of kidney failure, and bone disorders (94, 95). The National Kidney Foundation Kidney Disease Outcomes Quality Initiative (KDIGO) guideline suggested that the patients are recommended for dietary phosphate restriction and hypophosphatemic agents (96). However, restriction of dietary phosphate intake is difficult to comply with. High amount of inorganic phosphate (P_i) is usually found in processed foods and soft drinks, while other organic phosphates are naturally found in most types of food (97). High content of daily dietary phosphate intake is expected to induce a high concentration gradient in the intestinal lumen, enhancing both transcellular and paracellular absorption across the intestinal epithelium. Decreasing intestinal phosphate absorption is expected to help restrict serum phosphate loading. It was believed that inhibition of NaPi-IIb would correct hyperphosphatemia in CKD. However, the effect of inhibition is still controversially discussed. Larsson *et al.* (2018) reported a clinical trial that the NaPi-IIb inhibitor failed to reduce serum phosphate in end-stage renal disease (ESRD) patients (51). Therefore, the regulation of paracellular permeability is considered a solution for reducing intestinal phosphate absorption.

The intestinal tight junction and barrier function were reported to be disrupted by uremic toxins (including ammonia, urea, and uric acid) both in the cell line and mouse model (98, 99). Disruption of this barrier function underlies the importance of the correction of leaky gut in amelioration of hyperphosphatemia in CKD patients.

2.3 Gut microbiota in chronic kidney disease

2.3.1. Gut microbiota

Gut microbiota refers to the populations of microorganisms that colonize in the human gastrointestinal tract. The collection of these microorganisms is ingested together with diet and is known to strengthen the intestinal epithelial integrity of the host (100). The compositions of microbiota vary along the gastrointestinal tract. Acidic condition in the stomach and duodenum causes the lower abundance of the gut flora than those in jejunum/ileum and the large intestine. In contrast, the highest bacterial density is found in the colon (approximately 10^{12} colony-forming units per mL) (101). More than 2000 species of bacteria were identified from human feces. They were classified into 12 phyla which four major phyla are *Firmicutes*, *Bacteroidetes*, *Actinobacteria*, and *Proteobacteria* and 386 species among them were found to be strictly anaerobic (102). More than 90% of relative abundance (percent composition relative to the total abundance of the gut microbes) belongs to *Bacteroidetes* and *Firmicutes* (101). The bacteria in the phylum *Bacteroidetes* are Gram-negative and not spore-forming. They are anaerobic but not sensitive to oxygen. Two major classes that belong to *Firmicutes* are Bacilli (gram-positive, obligate or facultatively aerobic) and *Clostridia* (Gram-positive, anaerobic). Although most of the bacteria in *Clostridia* Class do not produce spores, *Clostridium* species have endospores that allow them to survive unsuitable environments and recolonize in favorable conditions. In contrast, Actinobacteria is a phylum of Gram-positive bacteria. They are normally multiple branching rod shapes, non-motile, non-spore-forming, and anaerobic. *Bifidobacterium* is an important genus in Actinobacterium phylum. Proteobacteria inhabit in the gastrointestinal tract of all terrestrial vertebrates. Proteobacteria are Gram-negative, rod shape, non-spore-forming bacteria. Some

genera, including *Lactobacillus*, *Staphylococcus*, and *Escherichia*, are facultative anaerobic yet *Bacteroides* are obligate anaerobic bacteria (103).

The composition of gut microbiota is dynamic according to the host and selective environmental pressure, including chemical, nutritional, and immunological gradients along the alimentary tract. The bacterial growth is limited by a high acidic content, oxygen, and antimicrobial agents (104). The different microbiomes are influenced by microbial colonization and the environment. The pathophysiological states of a human individual are determined by the presence of these beneficial and disease-associated bacteria in the gut microbiomes (105). The microbiota avoids the host's immunity by employing a multifactorial and dynamic intestinal barrier. The barrier composes of integrated components, including physical, biochemical, and immunological factors (106). According to the large genome and metabolic component of gut microbiota, a wide range of beneficial properties is provided to the host. Microbes play important roles in maintaining the intestinal barrier integrity, providing nutrients such as vitamins and short-chain fatty acids (SCFAs), and protecting against pathogens. Propionate, butyrate, and acetate are the three main types of SCFA metabolized in the alimentary tract by the gut microbes. These SCFAs are mainly produced by the bacteria in the phylum *Bacteroidetes* and *Firmicutes* (107). They involve in the regulation of gene expression, chemotaxis, differentiation, proliferation, and apoptosis (108). Butyrate is not only the important energy source for colonocytes but also reported to have anti-inflammatory and anticancer activities (108-110). Interestingly, butyrate promotes the tight-junction assembly and mucin synthesis, which enhances the gut barrier integrity (110).

Modern investigation shows that 100-400 trillion microbes colonize and live in close symbiotic relationships with their hosts (111). The intestinal bacteria form a physical barrier by tightly adhere to mucus on the intestinal epithelium. These bacteria are provided to an infant during breastfeeding, which contains a high number of *Bifidobacteria* and *Lactobacillus* (112). Three bacterial genera that were found to be the majority of the gut microbiome in human adults are *Bacteroides*, *Parabacteroides*, and *Clostridium* (113).

The interaction between the immune cell of the host and the gut microbiota is mediated by receptors on the intestinal epithelial cells, including Toll-like receptors (TLRs) and nucleotide-binding and oligomerization domain-like receptors (NLRs). These receptors recognize the molecules such as peptidoglycans, lipid A, lipopolysaccharide, flagella, and microbial RNA/DNA (known as pathogen-associated molecular patterns or PAMPs). These receptors induce a signaling pathway that activates the production of interleukin-1 β (IL-1 β) and interleukin-18 (IL-18) (114). This inflammatory response leads to pyroptosis that is against the infection.

The physiological effects of the intestinal microbiota on a host are summarized in Figure 19. The intestinal microbiota exerts the effects both locally in the intestine and distant organs. The microbiota enhances immunity, mobility, and integrity of the intestine. At remote organs, the microbiota regulates immune defense against viral infection in the lungs, decreases synaptic connection which increases anxiety and perception to pain, modulates metabolisms of the liver, and associates with osteoclast in the bones.

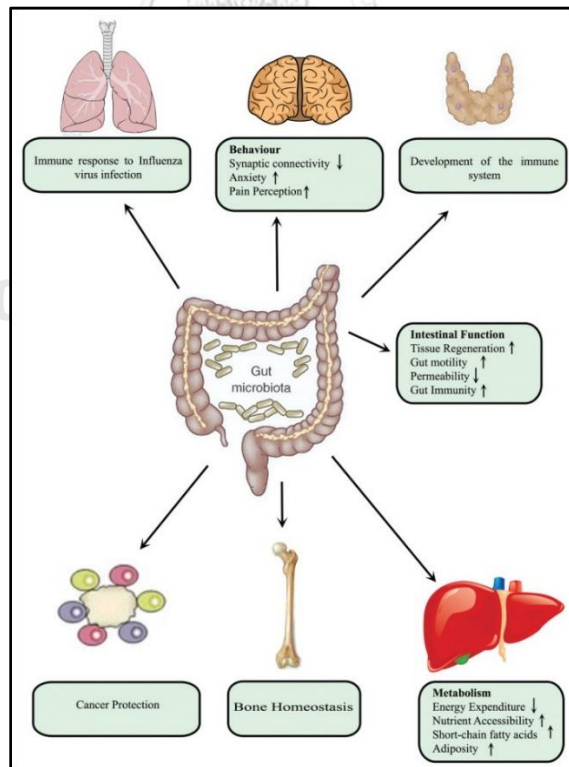


Figure 19. Microbial physiological impact on host (Al-Asmakh M. and Hedin L., 2015)

2.3.2. Gut dysbiosis

Host and microbes have developed interdependent relationships that provide mutual benefit for each other. When the microbial species in their host become imbalanced, the impairment of the intestinal barrier and inflammation can be induced, which is known as gut dysbiosis (115). Many diseases such as diabetes, obesity, inflammatory bowel disease (IBD), and cancer were reported involving gut dysbiosis (105).

Some health-promoting bacteria, such as *Faecalibacterium prausnitzii* was reported to predominate in healthy humans. At the same time, *Bacteroides* and *Ruminococcus gnavus* were reported to be associated with IBD. The study of obesity in an animal model reported the association between the low abundance of *Bacteroides* and obesity. Moreover, inflammatory cytokines such as TNF- α and IL-1 β were reported to be positively associated with *Firmicutes*. This indicates the potential association between gut dysbiosis and diseases (116).

The pathogenesis of gastrointestinal tract disease seems to be determined by the proportion between pathogenic microbes and beneficial microbes (117). The infection of *Clostridium difficile* that causes diarrhea and colitis was reported to associate with antibiotic use and depletion of *Ruminococcaceae*, *Lachnospiraceae*, and butyrogenic bacteria (118). Furthermore, the impairment of intestinal epithelium such as injury, loss of goblet cells, erosion, fibrosis, and ulceration that contributes to IBD also associates with the increasing *Pasteurellaceae*, *Veillonellaceae*, *Fusobacteriaceae*, and *Enterobacteriaceae* bacterial families. The increased gut permeability due to the decreased function of the intestinal barrier contributes to the increased susceptibility of bacterial endotoxins. However, it is still not clear whether the elevated intestinal permeability is a contributing factor or a consequence of the gastrointestinal disease (119). Heeney *et al.* (2018) has reported the decrease of beneficial bacteria, including *Lactobacilli* and *Bifidobacteria*, as well as increasing pathogenic and opportunistic bacteria (120). The increasing pathogenic bacteria promote the production and accumulation of toxic substances, including ammonia,

urea, creatinine, guanidine, indole, *p*-cresol, and trimethylamine-N-oxide (TMAO). Besides, the pathogenic bacteria induce the inflammation of epithelial tissue and contribute to declining tight junction proteins and allow the transport of toxic substances into the bloodstream via paracellular pathway (121).

2.3.3. Chronic kidney disease and microbiota changes

Regression of renal function results in the progression of uremia in CKD. The secreted urea into the gastrointestinal tract promotes the growth of urease-producing bacterial families and increases the conversion of urea into ammonia. Hence, the patients with ESRD are found to have bacterial families producing uricase, *p*-cresyl, and indole-forming bacteria predominate in their gastrointestinal tract (122, 123). Wang *et al.* (2015) reported a randomized, double-blind, placebo-controlled trial that probiotics treatment significantly decreased the inflammatory cytokines TNF- α , IL-5, and IL-6 and increased the anti-inflammatory cytokine IL-10 in the blood plasma of the peritoneal dialysis patients (14). Studies in the 5/6 nephrectomy rats and the patients with ESRD showed different intestinal microbial flora profiles compared to the healthy controls. Vasiri D. *et al.* (2013) reported the increased abundance of *Actinobacteria*, *Firmicutes*, and *Proteobacteria* in the patients with ESRD over the healthy individuals (124). Wang K. *et al.* (2012) also reported the decreased *Bifidobacterium catenulatum*, *Bifidobacterium longum*, *Bifidobacterium bifidum*, *Lactobacillus plantarum*, *Lactobacillus paracasei*, and *Klebsiella pneumoniae* in the peritoneal dialysis patients (125). In the patients with immunoglobulin A (IgA) nephropathy, the gut microbiota was significantly different from the healthy (126). Gut dysbiosis in KD patients worsens their renal progression due to the production of toxin, and increased toxin absorption from impaired intestinal epithelial integrity.

2.3.4. Probiotics

Probiotics are live microorganisms such as bacteria and fungi ingested to improve the balance of the intestinal microbiota. Probiotics provide beneficial effects to many physiological mechanisms in the body, including lowering intestinal pH,

limiting invasion and colonization of pathogenic bacteria, and modifying the immune response. Lactic acid-producing bacteria such as *Lactobacillus* and *Bifidobacterium* are recognized as common prebiotics and regulated as dietary supplements. Although the effectiveness of probiotics is not consistent in all species or strains of the microbes, strong evidence showed that some probiotics are effective for the treatment of acute diarrhea caused by rotavirus. Clinical studies reveal the effects of probiotics for the prevention of *Clostridium difficile* associated diarrhea, IBS, ulcerative colitis, and Crohn's disease, but the mechanisms are still not clear. Several billion bacterial cells are recommended to allow the colonization in the gut and provide a beneficial effect; however, there is no consensus about the minimum amount of the microbes (127).

The mechanisms that probiotic bacteria may promote the positive effects on the host health are demonstrated in Figure 20. Even though the beneficial effects of probiotic bacteria are not consistent in all strains, they downregulate the inflammatory mediators and increase epithelial barrier function (128).

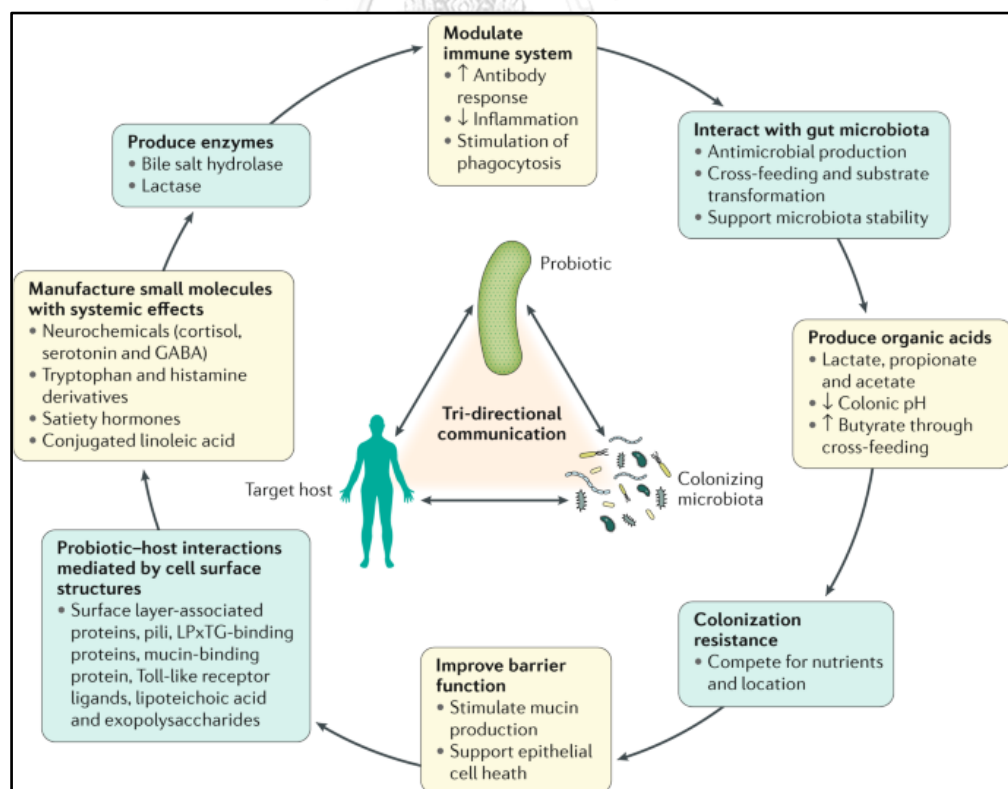


Figure 20. Microbial physiological impact on host (Al-Asmakh M. and Hedin L., 2015)

Many strains of *Bifidobacterium* (Figure 21A) and *Lactobacillus* (Figure 21B) were reported to have a beneficial effect on the body. *Bifidobacterium animalis* subspecies *lactis* has shown the effect in the gut-brain axis by modulating brain activity (129). Gao *et al.* (2015) reported an anti-inflammation property of *Lactobacillus reuteri* in the intestinal epithelium through histamine H₂ receptor-mediated suppression (130). In cystic fibrosis, the administration of *Lactobacillus rhamnosus* GG alleviated the intestinal inflammation in children patients (131). *Bifidobacterium longum*, acetate-producing bacteria, promotes intestinal epithelial integrity and protects the gut from enteropathogenic infection (132). *Lactobacillus acidophilus* NCFM (strain North Carolina Food Microbiology) exerts various benefits for the host, such as decreasing the occurrence of pediatric diarrhea, decreasing blood toxic amines level in dialysis-dependent CKD patients with small bowel bacterial overgrowth, and facilitating lactose digestion in lactose-intolerant individuals (133).

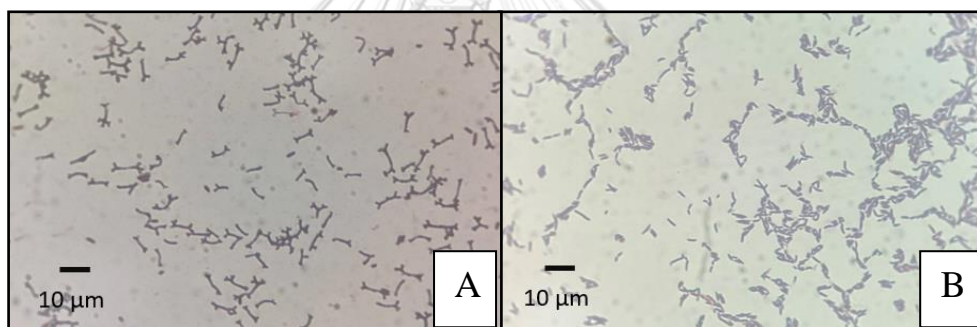


Figure 21. *Bifidobacterium* spp. (A) and *Lactobacillus* spp. (B)

The promotion of the intestinal epithelium integrity by probiotics was reported. In the *in vitro* study, *L. rhamnosus* GG, *L. rhamnosus* HN001, and *L. plantarum* 229V together with carbohydrate fraction from caprine milk promoted intestinal integrity of Caco-2:HT29-MTX co-culture by increasing TEER value (134).

2.3.5. Prebiotics

Prebiotic refers to “selectively fermented nondigestible food ingredients or substances that specifically support the growth and/or activity of health-promoting bacteria that colonize the gastrointestinal tract” (135). The colonic environment contributes to intestinal microbiota changes. Prebiotics are fermented in the colon and

altered intestinal microflora. Generally, intestinal bacteria have a saccharolytic capability that can be considered potentially beneficial. These metabolic profiles are typical for Lactobacilli and Bifidobacteria (136). The growth of fecal Bifidobacteria is promoted by the consumption of inulin, oligofructose, and fructooligosaccharide (FOS) (137). Moreover, acacia gum promotes a greater increase in Bifidobacteria and Lactobacilli than inulin, with fewer gastrointestinal side effects (138).

The health benefits of prebiotics are recognized in evidence-based reviews, typically including double-blind, randomized, controlled trials experiments. Many health issues are reported to be positively affected by the administration of probiotics, including cardiovascular disease, diabetes mellitus, laxation, appetite control, body weight, and cancers. The prebiotics can enhance the production of short-chained fatty acids and improve gut barrier function (136).

Chitosan oligosaccharide (COS), novel prebiotics, is an oligomer of β -(1 \rightarrow 4)-linked d-glucosamine derived from deacetylation and hydrolysis of chitin. It typically composes of 50-55 monomers with a molecular weight of less than 10,000 Da (Figure 22). The potential therapeutic applications of COS were reported as they have anti-inflammation properties, immunostimulating effects, anti-tumor activities, anti-obesity and lipid-lowering effects, anti-diabetic effect, anti-hypertensive effects, antimicrobial activities, and anti-oxidative effects (16).

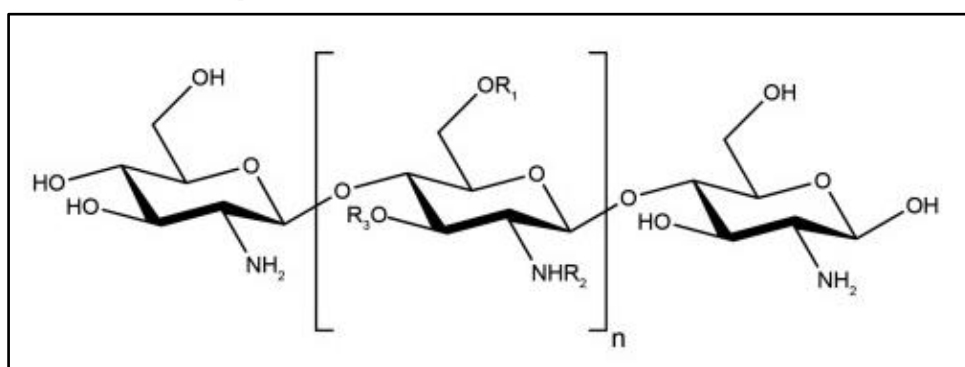


Figure 22. Chitosan oligosaccharide
(Muanprasat C. and Chatsudthipong V., 2017) (16)

Many studies revealed the role of COS in the suppression of inflammation *in vitro* and *in vivo*, the increased expression of tight junction protein in an intestinal epithelial cell, reducing paracellular transport of toxic substances through intestinal

epithelium, and reducing the loss of the epithelial barrier integrity through anti-inflammatory properties (17-19).

2.4 Measurement of diversity of intestinal bacteria

The marker gene in bacterial genome that is commonly used in the gut microbiome analysis is the ubiquitous 16S ribosomal RNA gene. It has a conserved regions which are highly conserved for all Prokaryote alternate with 9 variable regions (V1to V9), ideal primer binding sites for gene amplification. The variable regions are phylogenetically distinct for bacterial genera and species. Sequencing these regions enables the attempt to classify the bacteria and analyze the bacterial diversity. In bacterial diversity analysis, relative species abundance is usually determined. It measures that either a species is frequently or rarely found in a particular community-a species richness (139). Although the selection of the variable regions is controversial, the V1-V2 region and V3-V4 region are commonly used in gut microbiota studies. However, many studies suggest that V3-V4 region is more suitable not only in gut but also in vaginal microbiome analysis (140). The bioinformatic tool for microbiome analysis of 16S rRNA is QIIME (Quantitative Insights Into Microbial Ecology) (141). The species of interest can be divided into groups according to their genetic similarity, known as operation taxonomical unit (OTU) using the software tool.

2.5 Alpha and Beta Diversity

The diversity of the microbiome (in term of richness and evenness) then be analyzed in a single sample known as alpha diversity-basic characterization of a community (142). Several indices are commonly used in the estimation of the alpha diversity including richness, Chao1, Pielou's evenness, and Shannon index.

In an estimation of the bacterial diversity, Chao1 index was developed to calculate the expected OTUs based on the observed OTUs as shown in the following equation.

$$S_{\text{Chao1}} = S_{\text{obs}} + \frac{F_1(F_1-1)}{2(F_2+1)}$$

Where F_1 and F_2 are the count of the singletons-an OTU with only one sequence and doubletons-an OTU with two sequences, respectively. S_{obs} is the number of observed species (143).

Another factor that must be considered together with the richness is evenness. The richness considers only the number of species but does not consider the number of individuals in each species. The measurement of evenness is a measure of relative abundance of different species that occupy the community. When both richness and evenness are considerably high, the diversity is usually high as well (144). Shannon diversity index is an estimator of species richness and evenness, calculated by the following equation.

$$H = -\sum_{i=1}^s (p_i \ln p_i)$$

Where H is the Shannon index, s is the number of OTUs and p_i is the proportion of the community represented by OTU $_i$ (145).

Shannon index is directly proportional to the number of species present in the community and their relative abundances.

Pielou's evenness is a tool to measure the individuals of each species if any of them dominates the community (the index value closes to 0) or all the species occupy the community evenly (the index value closes to 1). Pielou evenness is calculated by the following equation.

$$J = \frac{H}{\ln N}$$

Where H is Shannon diversity index and N is the total number of the species in the community (146).

The relative abundance or the percentage of a particular taxon within a community or sample, typically calculated by dividing the number of individuals of a particular species by the total number of individuals in the sample, and then multiplying by 100 to express the result as a percentage. Relative abundance is an

important measurement as it provides the degree of distribution and evenness of different species within a community or sample.

The following equation shows the calculation of the relative abundance.

$$\text{Relative abundance} = \frac{\text{Number of individuals of species}}{\text{Total number of individual species in sample}} \times 100$$

The diversity measurements are also determined by the beta diversity which describes the differences in species composition or diversity of two or more populations or habitats. Higher values of beta diversity indices indicate a greater dissimilarity or turnover in species composition between populations or habitats, suggesting distinct ecological communities. Beta diversity helps understand the factors influencing spatial patterns of biodiversity, such as habitat heterogeneity, dispersal limitations, and environmental gradients. It provides insights into landscape-scale processes such as species migration, colonization, and extinction. Several indices are commonly used in the estimation of the alpha diversity including Bray-Curtis index, Jaccard index, and Simpson index.

The Bray-Curtis dissimilarity is a commonly used metric to quantify the dissimilarity in species composition between two samples or communities. It takes into account both the presence/absence and abundance of species. The formula for calculating the Bray-Curtis dissimilarity between two samples A and B is as follows.

$$\text{Bray-Curtis dissimilarity} = \frac{(\sum |a_i - b_i|)}{(\sum |a_i + b_i|)} \times 100$$

Where:

$|a_i - b_i|$ represents the absolute difference in abundance of species i between samples A and B.

\sum represents the summation across all species present in both samples.

a_i and b_i represent the abundances of species i in samples A and B, respectively.

Jaccard Index is an index that only considers the presence or absence of species and calculates the ratio of the number of species shared between two samples to the total number of unique species in both samples. It ranges from 0 (no shared species) to 1 (identical species composition). It is a simple and widely used metric to quantify the similarity or dissimilarity between two samples or communities based on the presence or absence of species. Jaccard is calculated by creating a matrix or table where rows represent the samples or communities being compared, and columns represent the species present in those samples, assign a value of 1 if a species is present in a sample, and 0 if it is absent. Then, count the number of species that are present in both samples (shared species) and the number of species that are present in only one of the samples (unique species), represented as n_{11} and as n_{10} and n_{01} , respectively. The Jaccard index is then calculated by the following equation.

$$\frac{n_{11}}{n_{10} + n_{01} + n_{11}}$$

Chapter III

Materials and Methods

3.1 *In vitro* study

3.1.1. Cell culture

Caco-2, human colon adenocarcinoma cells (147) were used in this research as it is a human intestinal epithelial cell that represent the barrier between luminal cavity and basement membrane. The cells were stored in glycerin at -80°C until they were required for the experiment. The cells were transferred into sterilized plate with medium containing high glucose DMEM supplemented with 10% V/V fetal bovine serum (FBS), 1% V/V penicillin, and 1% V/V streptomycin and incubated at 5% CO₂ and 37°C.

3.1.2. MTT-cell viability assay

Caco-2 cells were seeded in a 96-well plate with 15,000 cells per plate and incubated at 5% CO₂ and 37°C for 24 hours. After the confluent cell is about 80%, culture media were removed and washed with phosphate-buffered saline (PBS). Cells in the plate were added by DMEM (Dulbecco's modified eagle's medium) at pH 7.40 with the test substances (in this experiment-prebiotics) for 24 hours. Cell viability was evaluated by 3-(4,5-dimethylthiazol-2-yl)-2,5-diphenyltetrazolium bromide (MTT) assay. Only living cells containing NAD(P)H-dependent oxidoreductase enzymes were able to reduce the MTT to formazan, a purple-colored product with a maximum absorbance of 570 nm. Multidetecion microplate readers (Figure 23) were used to detect the absorbance of 570 nm on the culture plate. The cell viability of the different concentrations of each prebiotic treatment was compared to the cell viability of the control.



*Figure 23. Multidetection microplate reader
(Picture from product merchant company) (148)*

3.1.3. Transepithelial electrical resistance (TEER)

Caco-2 cells of 500,000 cells were seeded into transwell (ThinCert™, 0.4 μm pore size, 1.131 cm² culture surface) and incubated for 21 days in the medium containing high glucose DMEM supplemented with 10%V/V fetal bovine serum (FBS), 1%V/V penicillin, and 1% V/V streptomycin. After 21 days, the cells were serum-starved overnight (replaced by FBS-free media). The cells were measured TEER values by Epithelial Voltohmmeter (EVOM2, Figure 24)(148) to obtain TEER values at 0 hours. The cells in the transwell were treated by tested materials (in this experiment (prebiotics and probiotics). The cells from each treatment were incubated for 24 hours and proceeded TEER measurement by Epithelial Voltohmmeter (EVOM2) to obtain TEER values at 24 hours. Fold-changes were calculated from the proportion between TEER values at 24 hours and TEER values at 0 hours.

$$\text{Fold changes of TEER} = \frac{\text{TEER values at 24 hours}}{\text{TEER values at 0 hours}}$$



Figure 24. Epithelial Voltohmmeter
(Picture from product merchant company)(148)

3.1.4. Gene expression of tight junction proteins

The cells required for the evaluation of gene expression were collected in RNAlater™ (solution for RNA stabilization and storage, Thermo Fisher Scientific) to carry out RNA extraction. The extracted RNAs were carried out quantitative reverse transcription-polymerase chain reaction (RT-qPCR) for GAPDH (housekeeping gene), claudin-1, occludin, and zonula occludens-1 (tight junction proteins). The expression of each tight junction protein of each treatment was calculated relative to the GAPDH, the housekeeper. The relative expression was calculated by fold-changes from the control. The primers for PCR are shown in Figure 25 (149-151).

A	GAPDH-F	GTGAAGGTCGGAGTCAACGG	104
	GAPDH-R	TCGATGAAGGGGTCATTGATGG	
B	CLDN1-F	AAGTGCTTGGAAGACGATGA	275
	CLDN1-R	CTTGGTGTGGGTAAGAGGTT	
C	OCLN-F	CCAATGTCGAGGAGTGGG	237
	OCLN-R	CGCTGCTGTAACGAGGCT	
D	ZO1-F	CCAATGTCGAGGAGTGGG	183
	ZO1-R	CGCTGCTGTAACGAGGCT	

Figure 25. PCR primers sequence for RT-qPCR and product sizes; A. GAPDH, B. Claudin-1, C. Occludin, and D. Zonula occludens (149-151).

3.1.5. Bacterial isolation, screening, and identification

a) Fecal collection

Feces of healthy participants were collected from the research study “Association of gut microbiome in patients with chronic HCV infection receiving the combination regimen of Grazoprevir and Elbasvir therapy”, IRB number 378/61. The samples were collected in an anaerobic bag (BIOME-Preserve Microbiota Collection Kit). The feces underwent the following bacterial isolation within 6 hours.

b) Bacterial isolation

The isolation of Lactobacilli was carried out by the following steps. The feces of 0.5 g were put into 10 mL of sterile phosphate buffer saline solution (PBS) and well mixed. One mL of the solution was put into 9 mL of PBS to make serial ten-times dilutions. The procedure was repeated nine times to obtain the serial dilution of 10^{-9} . One hundred microliter of the dilution between 10^{-7} to 10^{-9} were spread in MRS agar plate (de Man, Rogosa, and Sharpe) and incubated at 37°C in an incubator for 48 hours inside 2.5 L rectangular jars contained AnaeroPack®-Anaero (Mitsubishi Gas Chemical Co., INC., Japan) to keep the anaerobic condition. According to oxygen-sensitive property of the *Bifidobacterium spp.*, the isolation processes had to carryout in the anaerobic chamber (Concept 400; Ruskinn Technology, UK). The atmospheric condition inside the chamber contained 80% N_2 , 10% H_2 , and 10% CO_2 . The aliquots were plated on modified Columbia agar (MCA) plates at 37°C for 48 to 72 hours (152).

A single colony from the culture was picked and streaked on another MRS medium. The plates were incubated at 37°C in an anaerobic incubator for 48 hours. The bacteria from every single colony were nominated and picked to carry out gram staining and catalase test (observing gas bubble after adding hydrogen peroxide). The gram-positive, rod-shaped, and catalase-negative bacteria which were compatible with *Lactobacillus* features were selected and then streaked on another MRS medium, then grew at 37°C in an anaerobic incubator for 48 hours for further examinations.

The isolation of Bifidobacteria was carried out by the following steps. The 0.5 g feces was put into 10 mL of sterile peptonated water (L-cysteine-HCl 3g/L, soy peptone 2 g/L) and well mixed. One mL of the solution was put into 9 mL of sterile peptonated water to make a ten times dilution. The procedure was repeated nine times to obtain the serial dilution of 10^{-4} . Each dilution was spread MCA medium (Modified Columbia blood agar) and incubated at 37°C in an anaerobic incubator for 72 hours for Bifidobacteria.

Every single colony grown on the plate was named, streaked on another MCA medium, and undergone Gram staining and catalase test. The gram-positive, Y-shaped, and catalase-negative bacteria, which was compatible with the phenotypic feature of Bifidobacteria, were selected to carry out PCR with the primers of *Bifidobacterium*-specific 16S rRNA gene (443 bp product) (153) and universal bacteria primers (1500 bp product), shown in Figure 27. The colonies that showed the PCR product of 443 bp with the specific primers were selected to carry out the Sanger sequencing for genotypic identification. The selected bacteria were grown in brain heart infusion (BHI) broth and incubated anaerobically at 37°C for 72 hours. The culture of the bacterial cells was well mixed with 40% glycerol of equal amount, incubated at 37°C for 1 hour. The bacteria were stored at -80°C for further experiment.

c) Screening of candidate probiotics

The isolated Bifidobacteria and Lactobacilli underwent the evaluation of TEER to select the candidate probiotics for further experiments in the animal. The competent Caco-2 cells were seeded into the transwell as mentioned beforehand and treated by 10^6 CFU/mL of the selected *Bifidobacterium* and *Lactobacillus* strains on the apical side of the transwell. The cells from each treatment were incubated for 24 hours and proceeded TEER measurement and calculated the fold change after 24 hours of the treatments. The bacterial isolates that provided high TEER value were kept in the stock library (at -80°C) for identification.

d) Bacterial identification

For bacterial genotypic identification, the selected bacterial colonies were undergone DNA extraction and PCR with a specific primers for the Lactobacilli 16S rRNA gene (341 bp product) and universal bacteria primers (1500 bp product), as shown in Figure 26 (154). The colonies that showed the PCR product of 341 bp with the specific primers were subsequently confirmed by the Sanger sequencing for strain identification. DNA extraction from the bacterial colonies was carried out using a DNA extraction kit. PCR was then performed to obtain a DNA product of the 16S rRNA gene, with a length of 1235 base pairs. The resulting DNA products were sent to Bionics Co., Ltd. (South Korea) for sequencing and the sequences were compared to the NCBI database.

The bacteria were stored in glycerol at -80°C for further experiment.

A	L341-F	AGCAGTAGGGAATCTTCCA
	L341-R	CACCGCTACACATGGAG
B	8F	AGAGTTTGATCCTGGCTCAG
	1492R	TACGGYTACCTTGTTACGACTT

Figure 26. Specific PCR primer sequence. A: Specific primers for Lactobacilli, B: Universal bacteria primers (154).

A	Bif194-F	GGGTGGTAATGCCGGATG
	Bif601-R	TAAGCGATGGACTTTCACACC
B	8F	AGAGTTTGATCCTGGCTCAG
	1492R	TACGGYTACCTTGTTACGACTT

Figure 27. Specific PCR primers sequence. A: Specific primers for Bifidobacterium, B: Universal bacteria primers (153).

3.1.6. Prebiotics preliminary test

The proper concentrations of chitosan oligosaccharide (COS), inulin, and resistant maltodextrin were evaluated by MTT assay (155). The cells were treated by each of the prebiotic at the concentration of 0 (untreated control), 10, 50, 100, 500, and 1000 $\mu\text{g/mL}$, and 0.3% hydrogen peroxide (H_2O_2) and incubated in 5% atmospheric CO_2 at 37°C for 24 hours. The cells then were carried out the MTT viability assay as mentioned.

The properties of the prebiotics in an enhancing intestinal epithelial barrier were investigated by the evaluation of TEER value and gene expression of tight junction proteins.

The evaluation of TEER value was set up in two settings, normal condition, and inflammatory condition. In a normal condition, the cells were treated both in the apical and basolateral sides of the cell with; 1) 0.005% acetic acid as vehicle control, 2) 100 $\mu\text{g/mL}$ COS (the concentration tested to be non-cytotoxic), 3) 100 $\mu\text{g/mL}$ Inulin, 4) 100 $\mu\text{g/mL}$ FOS, 5) 100 $\mu\text{g/mL}$ resistant maltodextrin, or 6) 0.06 $\mu\text{g/mL}$ TGF- β (transforming growth factor-beta, a cytokine that protects intestinal integrity) (156) as a positive control. In an inflammatory condition, the cells were treated both in the apical side and basolateral side of the cell with 0.01 $\mu\text{g/mL}$ TNF- α (tumor necrosis factor-alpha, proinflammatory cytokine) and; 1) 0.005% acetic acid as vehicle control, 2) 100 $\mu\text{g/mL}$ COS, 3) 100 $\mu\text{g/mL}$ Inulin, 4) 100 $\mu\text{g/mL}$ resistant maltodextrin, or 5) 0.06 $\mu\text{g/mL}$ TGF- β . The cells from both conditions were incubated after the treatments for 24 hours and proceeded TEER measurement by Epithelial Voltohmmeter (EVOM2) to obtain TEER values at 24 hours. Fold-changes were calculated from the proportion between TEER values at 24 hours and TEER values at 0 hours.

The cells that had been measured the TEER values were immediately collected from the transwell plate into RNeasyTM to carry out RNA extraction for the evaluation of gene expression of the tight junction proteins. The extracted RNAs were carried out RT-qPCR for GAPDH (housekeeping gene), claudin-1, occludin, and zonula occludens-1 (tight junction proteins). The expression of each tight junction

protein of each treatment was calculated relative to the housekeeper. The relative expression was calculated by fold-changes from the control. The primers for PCR are shown in Figure 27.

3.1.7. Treatment preparation

a) Prebiotic treatments

The dose calculation in animal was based on the Nair and Jacon's guideline (157). The prebiotic dose in animal equals to 0.162 times recommended human dose as shown in the

	Recommended human dose (mg/kg/day)	Rats dose (mg/kg/day)
COS	100	16
Inulin	330	54
Maltodextrin	330	54

Table 3.

Table 3. Dose of prebiotics in animal experiment

	Recommended human dose (mg/kg/day)	Rats dose (mg/kg/day)
COS	100	16
Inulin	330	54
Maltodextrin	330	54

The prebiotic treatments were prepared by following a set of procedures to obtain their respective stocks. Inulin and resistant maltodextrin were dissolved in 1% acetic acid at a concentration of 300 mg/mL. Chitosan oligosaccharide, due to its poor solubility, was dissolved in 1% acetic acid at a concentration of 50 mg/mL and shaken vigorously for 6 hours. The prepared stocks of prebiotics were then diluted with 1% phosphoric acid, taking into account the body weight of the rats. Each rat was orally administered with approximately 0.5 mL of the corresponding prebiotic treatment daily.

b) Commercial probiotics

Lactobacillus casei was prepared from 80 mL of commercial yogurt which contains 8×10^9 CFU/ml. A bottle (80 mL) was centrifuged at 5000 G for 15 minutes, the supernatant was discarded, and the pellet was resuspended into 1.6 mL of phosphate buffer saline (PBS). A concentration of approximately 5×10^9 CFU/mL was obtained. The final volume of 0.2 mL was fed to the animals every day for 10^8 CFU per day.

c) Synbiotic treatments

Selected *Lactobacillus* and *Bifidobacterium* were grown in an MRS and MCA medium, respectively, and incubated at 37°C in an anaerobic incubator for 48 hours. The concentration of the bacterial cells was calculated by undergoing serial dilution. Each dilution was measured by the optical spectrophotometry absorbance of 600 nm wavelength and undergone plate spreading. The plates were incubated anaerobically for 24 hours and counted for colony formation. The numbers of colony-forming units were calculated relative to the absorbances to create a graph. The concentration of the bacterial cultures was obtained from the slope of the graph. A particular volume of the bacterial culture was calculated to centrifuge and resuspended in 2 mL of PBS to obtain the concentration of 5×10^9 CFU/mL. Each experimental rat was fed with 10^9 CFU per day.

There were two synbiotic formulae used in the experiment. The first formula composed of the prebiotics, COS and inulin, together with both *Lactobacillus spp.* and *Bifidobacterium spp.* isolated from the aforementioned experiments. The second formula composed of all three prebiotics, COS, inulin, and resistant maltodextrin, together with both *Lactobacillus spp.* and *Bifidobacterium spp.*

3.2 *In vivo* study

The probiotics that have good characteristics in enhancing TEER value and identified the species were chosen to use in the animal experiment. In the animal model, Jcl/SDT 4-week old male rats purchased from Nomura Siam International Co.Ltd were used.

3.2.1. Animal preparation and CKD induction

Rats were raised in the Animal Center at the Faculty of Medicine, Chulalongkorn University, in 35×75×18 cm (width×length×height) cage, at 22°C, under 12/12 light and dark cycle, 40-60% relative humidity, with *ad libitum* for food (C.P. 082) (148) and drink. Rats were acclimatized for two weeks before the initiation of the experiment. The rats were randomly allocated into eight groups, namely: 1) control group that did not receive cisplatin injection (Control), 2) CKD induced rat treated by phosphate buffer saline vehicle (CKD), 3) CKD induced rat treated by chitosan oligosaccharide (COS), 4) CKD induced rat treated by inulin (Inulin), 5) CKD induced rat treated by maltodextrin (Maltodextrin), 6) CKD induced rat treated by *Lactobacillus casei* (*L. casei*), 7) CKD induced rat treated by mixture of COS, inulin, *Lactobacillus salivarius*, and *Bifidobacterium longum* (Synbiotics 1), and 8) CKD induced rat treated by mixture of COS, inulin, resistant maltodextrin, *Lactobacillus salivarius*, and *Bifidobacterium longum* (Synbiotics 2), with 6 animals in each group (158). The rats in the control group were injected with 1 mL normal saline intraperitoneally, and the others were induced for CKD by 10 mg/kg rat's body weight of cisplatin intraperitoneal injection (159). All rats were raised for five weeks after the injection to allow the acute renal injury subsided. The blood and feces of rats were collected before all treatments. The phosphoric acid was diluted to obtain 1%

(w/w) phosphate and applied in the drinking water of the animals along with the treatments in the experiment.

All the groups in the animal experiment is shown in the Table 4.



Table 4. Groups in animal experiment

Group	CKD induced	Prebiotics			Probiotics
		COS	Inulin	maltodextrin	
Control	-	-	-	-	-
CKD	+	-	-	-	-
COS	+	16 mg/kg	-	-	-
Inulin	+	-	54 mg/kg	-	-
Maltodextrin	+	-	-	54 mg/kg	-
L. casei	+	-	-	-	<i>Lactobacillus casei</i>
Synbiotics1	+	16 mg/kg	54 mg/kg	-	<i>Lactobacillus</i> and <i>Bifidobacterium</i>
Synbiotics2	+	16 mg/kg	54 mg/kg	54 mg/kg	<i>Lactobacillus</i> and <i>Bifidobacterium</i>

3.2.2. Blood, feces, and organ collection

Blood samples of approximately 0.5 mL were collected from the tail vein (160) in heparinized 1.5 mL microcentrifuge tubes. The blood plasma was obtained by centrifugation at 2500 G for 10 minutes and stored at -80°C. Fresh fecal samples were collected from the rats and stored in DNA/RNA Shield® reagent (ZYMO Research) at -80°C.

Blood samples were collected from all rats prior to cisplatin administration, initiation of treatments, and on the day of sacrifice. At the end of the twelve-week study period, the rats were euthanized via long exposure to CO₂. Blood samples of the rats on the day of sacrifice were collected via cardiac puncture. The kidneys were split longitudinally. Half of the kidney specimens were collected in 4% paraformaldehyde and stored at 4°C, and the other half collected in RNAlater™ and store at -80°C. The jejunum section of the intestine was cut into 1 cm pieces and stored at -80°C, while fecal samples were collected in DNA/RNA Shield® reagent (ZYMO Research) and

stored at -80°C . The remaining sections of the intestine and right femur bones were collected and stored in paraformaldehyde at 4°C .

3.2.3. Gene expression of tight junction protein

RNA was extracted from the jejunum parts of the intestinal tissue and subjected to quantitative reverse transcription-polymerase chain reaction (RT-qPCR) using primers for GAPDH (housekeeping gene), occludin, and zonula occludens-1 (tight junction proteins). The relative expression of each tight junction protein in each treatment was determined by calculating fold-changes relative to the control and normalizing to the housekeeping gene. The PCR primers sequences are provided in Figure 25.

3.2.4. Serum calcium-phosphate profiling

The concentration of calcium and phosphate levels in the samples were analyzed using automated Alinity ci system at the Department of Laboratory Medicine, Faculty of Medicine, Chulalongkorn University (161).

The concentration of serum parathyroid hormone (PTH) from each treatment was analyzed using enzyme-linked immunosorbent assay (ELISA) of a parathyroid hormone ELISA kit in 96-well plates (Wuhan Fine Biotech Co., Ltd.). The optical densities were measured at a wavelength of 450 nm using multidetection microplate readers.

3.2.5. Histopathological evaluation

The tissue samples underwent permanent slide-making processes at the Department of Pathology, Faculty of Medicine, Chulalongkorn University. Hematoxylin and eosin (H&E) staining was performed on sections of kidney and jejunum tissues to stain the nucleus and cytoplasm.

The collected femoral bones were fixed, decalcified in 0.5% nitric acid for 7 days, sectioned, stained with H&E, and subjected to histopathological examination. The tissues were evaluated by a pathologist from the Department of Pathology, Faculty of Medicine, Chulalongkorn University.

The kidney injury were scored according to glomerular lesion from 0-4 described by Rossert *et.al.*, 2000 (162) and the fibrosis area described Cohen *et. al.*, 2020 (163). The epithelial changes of jejunum were evaluated by March score from 0-4 described by Rostom *et. al.*, 2006 (164). The bone mineral density of femur bone is determined by structure and quantity of trabecular bone described by Chen *et. al.*, 2014 (165).

3.2.6. Intestinal microbiota analysis

DNA extraction from fecal samples was carried out using the ZymoBIOMICS™ DNA Miniprep Kit (Zymo Research Corp.) following the manufacturer's instructions. The concentration and purity of the extracted DNA were assessed using a DeNovix™ UV-Vis spectrophotometer and stored at -20°C until further analysis.

The intestinal microbiome profiling was carried out using the 16S/ITS Microbiome Profiling Service by Modgut Genomic Service (Mod Gut Company Limited at King Mongkut's University of Technology Thonburi. The target sequences in V3-V4 region of 16S rRNA gene were amplified. The library of DNA was quantified. The positive control for library preparation and negative controls were included to evaluate the level of bioburden carried by the process. The final library was sequenced on Illumina® MiSeq™ with a v3 reagent kit (600 cycles). The sequencing was performed with 10% PhiX spike-in.

The raw read from Illumina® MiSeq™ was demultiplexed and removed non-biological nucleotide (primers and adapters). DADA2 pipeline was performed to create an amplicon sequence variant (ASV) table. Uclust from QIIME v.1.9.1 was achieved to assign taxonomy with reference database. The number of microbial taxonomic groups in the samples determines their richness, while the distribution of abundances of the groups determines their evenness.

For data visualization, summary of ecological communities of gut microbiota with respect to its richness and evenness refers to the Alpha diversity (Shannon index and Pielou's evenness) was analyzed. The beta diversity was represent as principal

coordinate analysis (PCoA). The top relative abundance taxa were generated by the average abundance of each taxa in each group divided by the total abundance of the taxa. The composition bar plot of top relative abundance taxa was generated with in-house scripts using R program. The relative abundance of the bacteria was analyzed and correlated with the physiological parameters.

3.2.7. Statistical analysis

SPSS version 22.0 was used for statistical analysis in the present study. Continuous data was tested by Student t-test for two independent groups comparison and ANOVA with post-hoc Bonferrini test for more than 2-groups comparison and Mann-Whitney U test for non-parametric valuables. In an animal experiment, Student t-test for 2 independent groups comparison, Kruskal-Wallis test for means difference in non-parametric data. Chi-square test was used in histological analysis. Pearson correlation was used to evaluate the correlation. Significant differences were considered when $p < 0.05$. Figures, diagrams, and graphs were generated using Prism 9 Windows 64-bit Version 9.5.1.733.

3.2.8. Ethical consideration

The study was conducted under the agreement with the Helsinki Declaration and Good Clinical Practice guidelines (166) for participants whom will provide feces and procedures of the Institutional Animal Care and Use Committee (IACUC) for the experimental animals (167). All the procedures were approved by the Institutional Review Board of the Faculty of Medicine, Chulalongkorn University (IRB number 914/64). The protocols of the animal experiment were approved by the Chulalongkorn University Animal Care and Use Committee (CU-ACUC protocol number 004/2563).

Chapter 4

Results

4.1 Isolation and screening of bacteria

The fecal samples were subjected to serial dilution and the resulting dilutions were plated onto selection agar plates specific for Bifidobacteria (MCA) and Lactobacilli (MRS). After incubation, individual colonies were selected and assigned a numerical code, as illustrated in Figure 28.

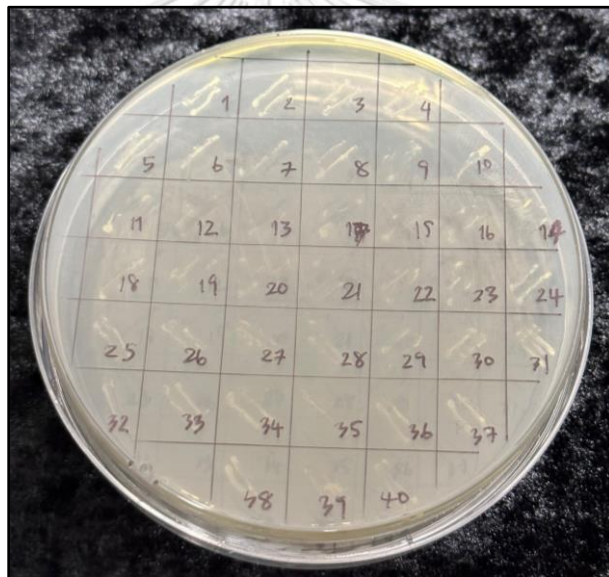


Figure 28. Media screened bacterial colonies

Each bacterial colony was subjected to Gram staining and catalase testing. The colonies that were observed to have a rod-shaped morphology and were catalase-negative were selected to be grown on another agar plate, as illustrated in Figure 29.

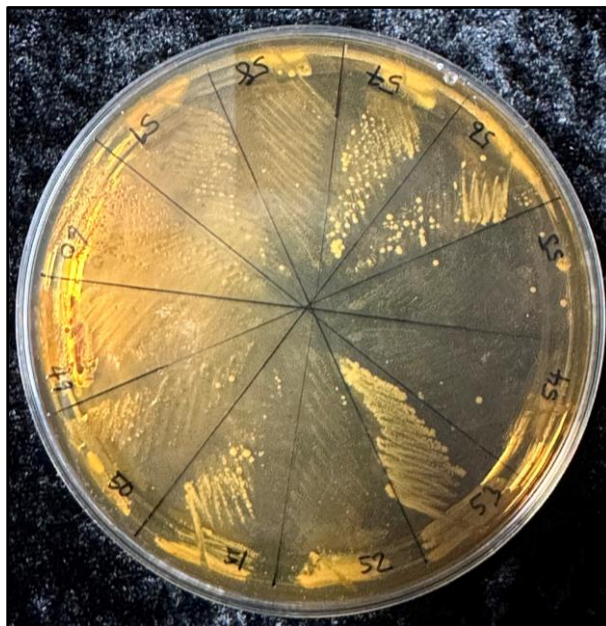


Figure 29. Shape and catalase screened bacterial colonies

The bacterial colonies were evaluated for their effect on the TEER value of Caco-2 cells. The percentage of TEER change in the cells 24 hours after treatment with the candidate bacteria is presented in Table 5. Bacterial colonies that potentially increased the TEER value of the cells were selected for identification of the species using Sanger sequencing. The identification results for 18 bacteria are shown in Table 6.

Bifidobacterium longum and *Lactobacillus salivarius* isolate number BFS3-09 and LBR2-28, respectively, were selected for further experiments, as they contained the desirable properties including anti-inflammation and TEER-promotion. In addition, both species was approved to be used as the food probiotic based on the regulation of the Thai Ministry of Public Health (168), which listed these two species along with *Lactobacillus crispatus* as being present in the high %TEER list.

Table 5. %TEER compared to control in Caco-2 cells treated by candidate bacterial colonies

Colony	% TEER	Colony	% TEER	Colony	% TEER
BFS3-3	108.00	LBR2-3	168.12	BFS3-1	4.41
BFS3-6	121.77	LB1-2	180.14	BFS3-2	149.09
BFS3-8	79.30	LBS6-69	167.62	BFS3-4	69.69
BFS3-11	16.52	LBR2-17	170.84	BFS3-5	122.85
BFS3-14	85.78	LBR2-1	80.59	BFS3-7	126.31
BFS3-15	99.29	BFS5-2	38.31	BFS3-09	139.36
BFS3-28	91.45	BFM3-8	191.00	BFS3-10	98.49
BFS3-30	97.45	BFS3-7	102.95	BFS3-12	126.61
BFS3-31	47.87	BFM1-5	160.65	BFS3-13	110.54
BFS3-32	7.31	BFS2-6	186.89	BFS3-18	127.76
BFS3-33	5.12	BFS2-11	11.24	BFS3-19	3.44
BFS3-34	4.47	BFS1-3	177.44	BFS3-20	104.21
BFS3-35	5.53	BFM0-7	27.99	BFS3-24	117.52
BFS3-36	4.46	BFM2-6	186.47	BFS3-25	151.85
BFS3-48	108.00	BFBB	214.36	S3B01	96.28
BFS3-37	0.52	BFM2-1	175.90	S3B02	104.23
BFS3-43	0	BFM2-2	196.83	S3B03	94.13
BFS3-44	0.20	BFM8-3	194.42	S3B04	110.53
BFS3-45	3.31	BFM3-3	40.15	S3B06	105.71
BFS3-46	57.30	BFM8-4	194.10	S3B07	110.00
BFS3-09	139.36	LBS1-71	129.26	S3B08	6.24
B27	80.25	LBR2-14	141.96	S3B09	47.62
B40	62.06	S1.67	69.67	S3B11	98.35
B51	102.76	S1.68	67.76	S3B13	101.50
B52	97.88	S1.71	120.57	S3B15	113.06
B53	96.35	S1.74	94.30	S3B18	100.23
B54	96.96	S2.1	83.53	S3B19	108.23
B55	108.05	S3.4	19.21	S3B20	99.16
B56	100.05	S1.45	74.99	S3B21	98.79
B57	110.15	S1.47	112.67	S2.07	108.71
B58	115.33	S1.52	110.41	S2.58	99.93
B59	96.87	S1.55	67.81	S1.8	18.30
B60	39.08	S1.34	30.53	S1.9	31.46
B62	91.61	S1.38	9.92	S1.10	10.82
B21	106.58	S1.25	46.15	S1.12	127.72

Table 6. Bacterial identification results from 16S rRNA gene sequence
The percentage relatives to the PBS control

Isolate	Blast results	%TEER	%IL-8 expression
BFM2-2	<i>Bifidobacterium longum</i>	129.26	44.32
BFM2-6	<i>Bifidobacterium longum</i>	122.46	95.44
BFM8-3	<i>Bifidobacterium longum</i>	127.68	89.23
BFS2-6	<i>Bifidobacterium longum</i>	122.73	42.53
LBS1-71	<i>Weissella confusa</i>	120.57	70.17
LBS3-B02	<i>Weissella confusa</i>	104.23	25.38
LBS3-B04	<i>Weissella confusa</i>	110.53	20.41
LBS3-B07	<i>Weissella confusa</i>	110.00	20.88
LBS3-B15	<i>Weissella confusa</i>	113.06	12.26
LBS3-B19	<i>Weissella confusa</i>	108.23	32.79
LBS1-35	<i>Weissella confusa</i>	123.99	75.56
LBS2-07	<i>Weissella confusa</i>	108.71	21.69
LBS2-14	<i>Lactobacillus crispatus</i>	141.96	76.09
LBS2-28	<i>Lactobacillus salivarius</i>	121.05	68.38
LBS3-B22	<i>Weissella confusa</i>	101.51	89.94
BFS3-09	<i>Bifidobacterium longum</i>	139.36	27.13
BFS3-46	<i>Bifidobacterium longum</i>	115.15	56.08
BFS3-58	<i>Bifidobacterium longum</i>	115.33	7.63

4.2 Prebiotic

4.2.1. MTT cell viability assay

According to the results of the cell viability assay, treatment with chitosan oligosaccharide (COS) and inulin at a concentration of 1000 $\mu\text{g/mL}$ reduced the viability of Caco-2 cells compared to phosphate buffer saline (PBS). However, only resistant maltodextrin treatment at a concentration of 500 $\mu\text{g/mL}$ showed a significant decrease in cell viability, as shown in Figure 30. Therefore, a concentration of 100 $\mu\text{g/mL}$ was selected for subsequent experiments with prebiotics.

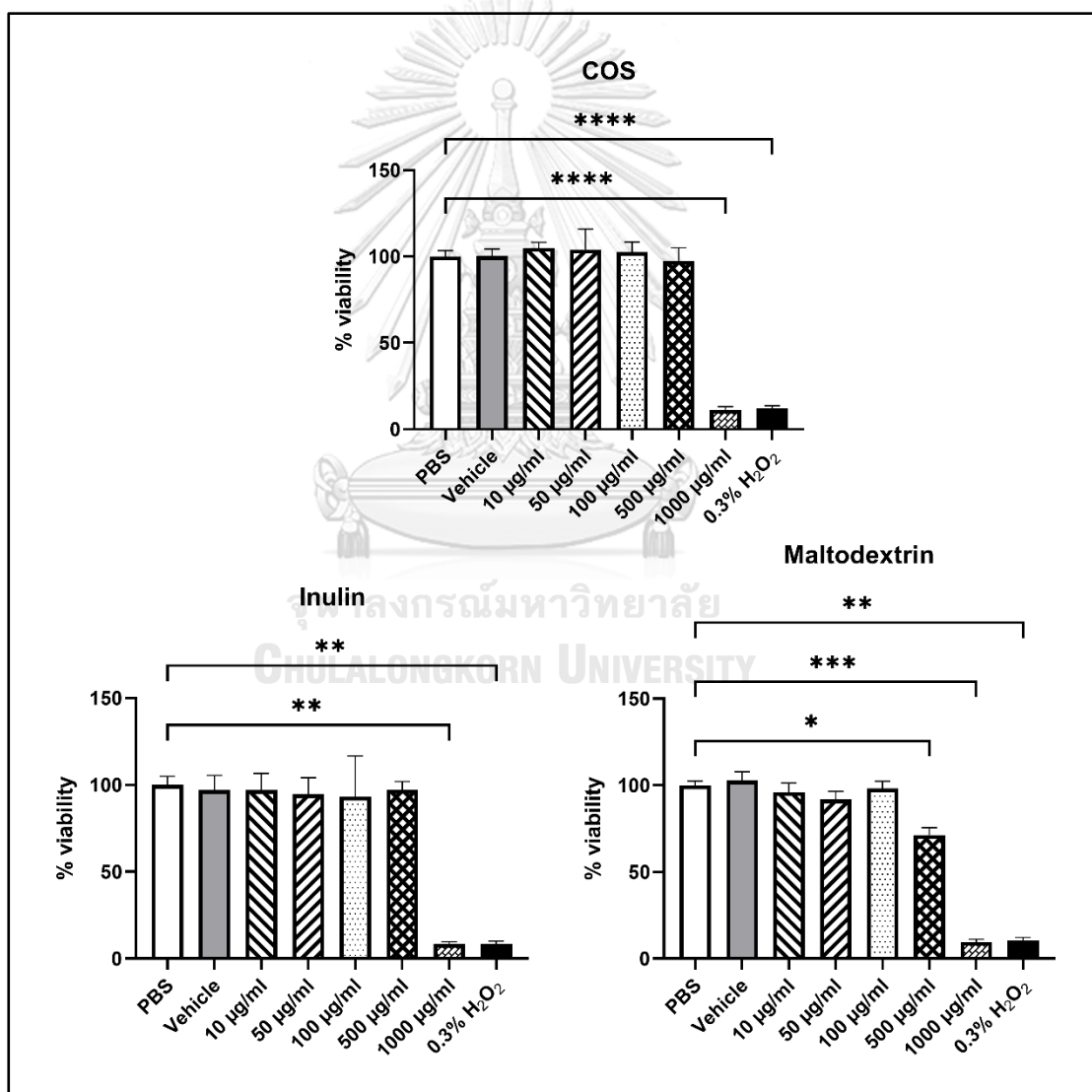


Figure 30. MTT cell viability of Caco-2 cells treated by various concentrations of prebiotics
 * represents p -value < 0.05 , ** represents p -value < 0.01 , *** represents p -value < 0.001 ,
 and **** represent p -value < 0.0001

4.2.2. TEER

In a normal setting, treatment with 60 ng/mL TGF- β significantly increased the transepithelial electrical resistance (TEER) value of Caco-2 cells. Treatment with 100 μ g/mL inulin and resistant maltodextrin also resulted in a promising increase in TEER compared to the control, although statistical significance was not achieved. Under inflammatory conditions induced by 50 ng/mL TNF- α , co-treatment with 100 μ g/mL inulin, resistant maltodextrin, and 60 ng/mL TGF- β restored TEER values to levels similar to those observed in the normal setting. These findings suggest that prebiotics have the potential to attenuate the effects of inflammatory cytokines.

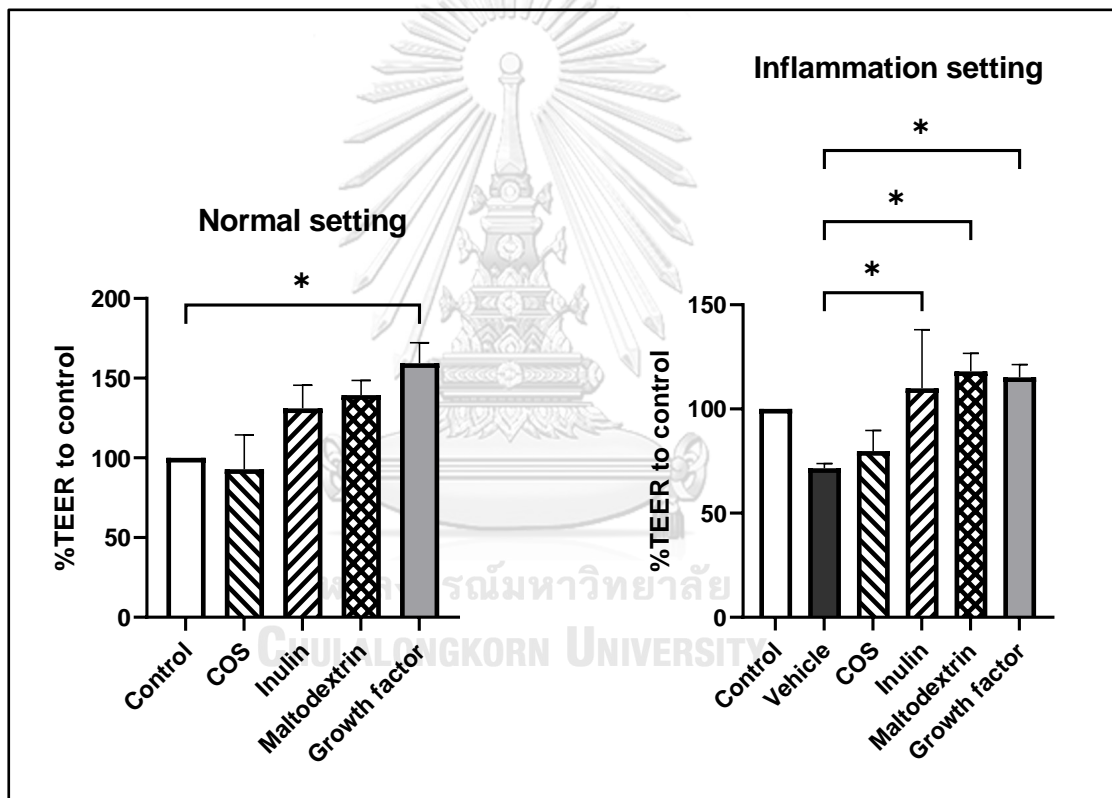


Figure 31. %TEER compared to control of Caco-2 cells treated by prebiotics
* represents p -value <0.05

4.2.3. Gene expression of tight junction proteins

The expression of tight junction protein mRNA was evaluated using RT-PCR. Cells treated with prebiotics were collected and extracted with TRIzol reagent. The relative expression of each target gene was calculated compared to the control. The findings suggest that the prebiotics utilized in the study may have increased the expression of tight junction protein at the mRNA level, as depicted in Figure 32.

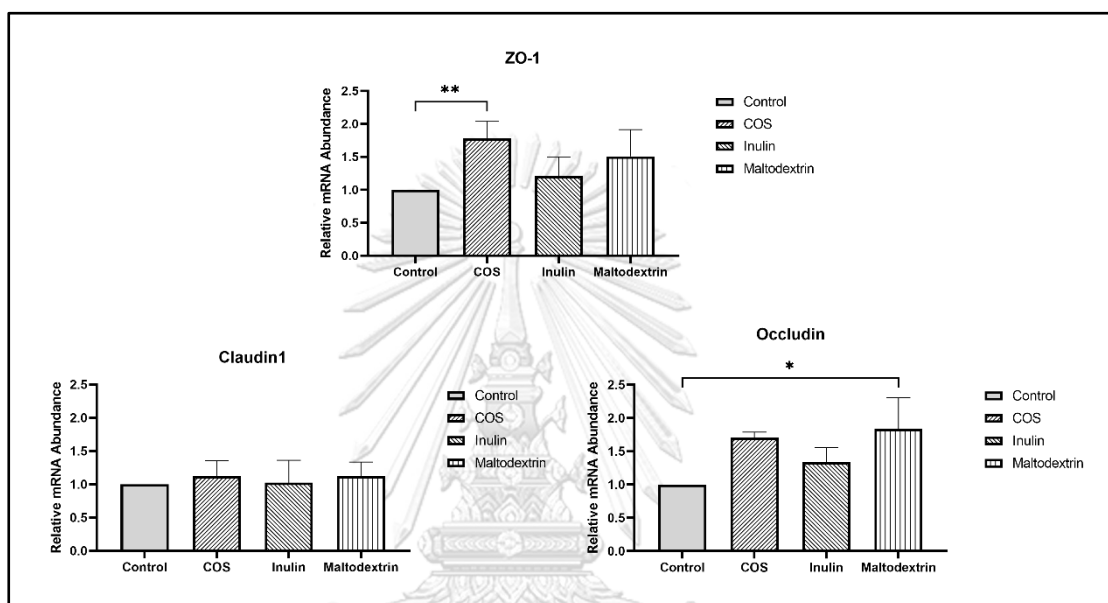


Figure 32. Expression of tight junction mRNA in Caco-2 cells treated by prebiotics.

* represents p -value < 0.05 , ** represents p -value < 0.01

4.3 Animal experiments

To induce chronic kidney disease, 4-week-old rats were intraperitoneally injected with 5 mg/kg of cisplatin twice a week (totaling 10 mg/kg) within a week, followed by a five-week recovery period to allow for acute kidney injury to recover. Rats without cisplatin injection were assigned to the control group. All rats were given drinking water containing 1% orthophosphoric acid and daily treatments were initiated.

4.3.1. Body weight

Throughout the course of the experiment, the body weight of the rats was recorded. The results indicate that all rats experienced an increase in weight, ranging

from 10-20%, from the start to the end of the experiment as depicted in (Figure 33). At the beginning of the experiment, the weight of the healthy rats in the control group was significantly greater than that of the CKD induced rats ($p=0.0151$). However, no significant difference in weight was observed between the CKD induced rats and other experimental groups.

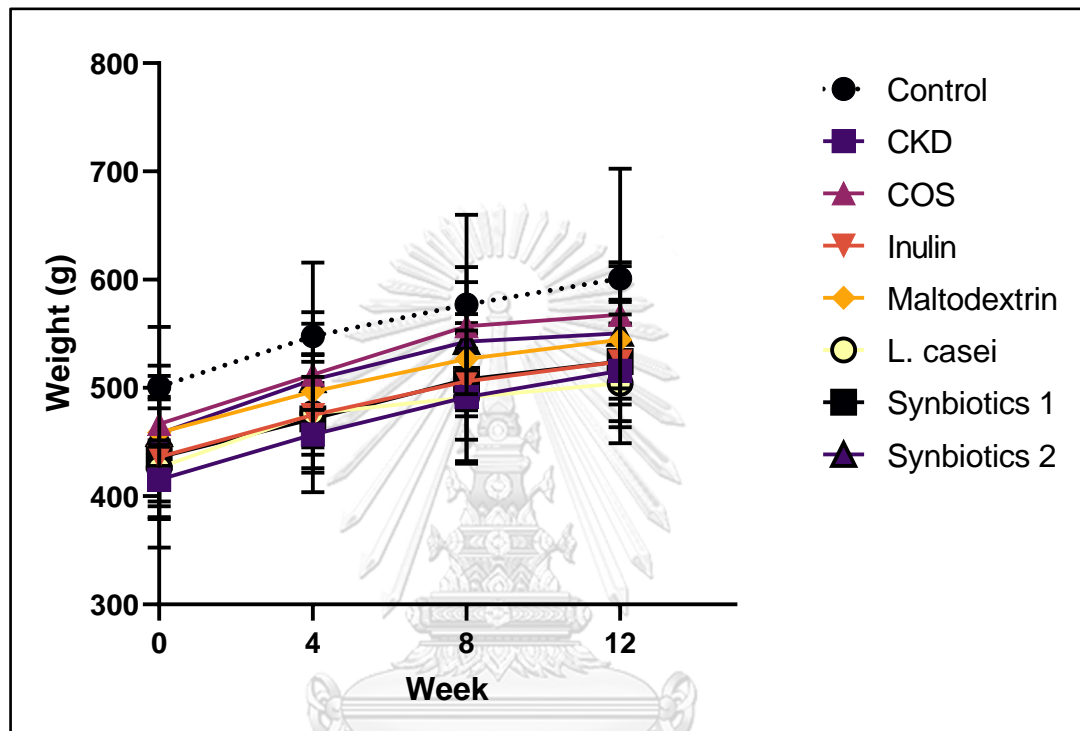


Figure 33. Weight of the rats

4.3.2. Serum creatinine

Serum creatinine levels of the rats injected with cisplatin peritoneally were significantly higher ($p<0.05$) than those in the controlled group at week 0 (the day of starting treatments) as shown in the Figure 34, indicating the nephrotoxicity induced by cisplatin, while the elevated serum creatinine at the 4th week establishing the chronic kidney disease model in cisplatin-injected rats. Throughout the experiment, the serum creatinine levels of rats with CKD that received treatment with all tested interventions (COS, inulin, maltodextrin, L. casei, synbiotics 1, and synbiotics 2) did not significantly differ from those of CKD rats treated with PBS, indicating that the interventions did not improve kidney function in CKD rats. However, the

interventions did not demonstrate any adverse effects on the kidney function of CKD rats.

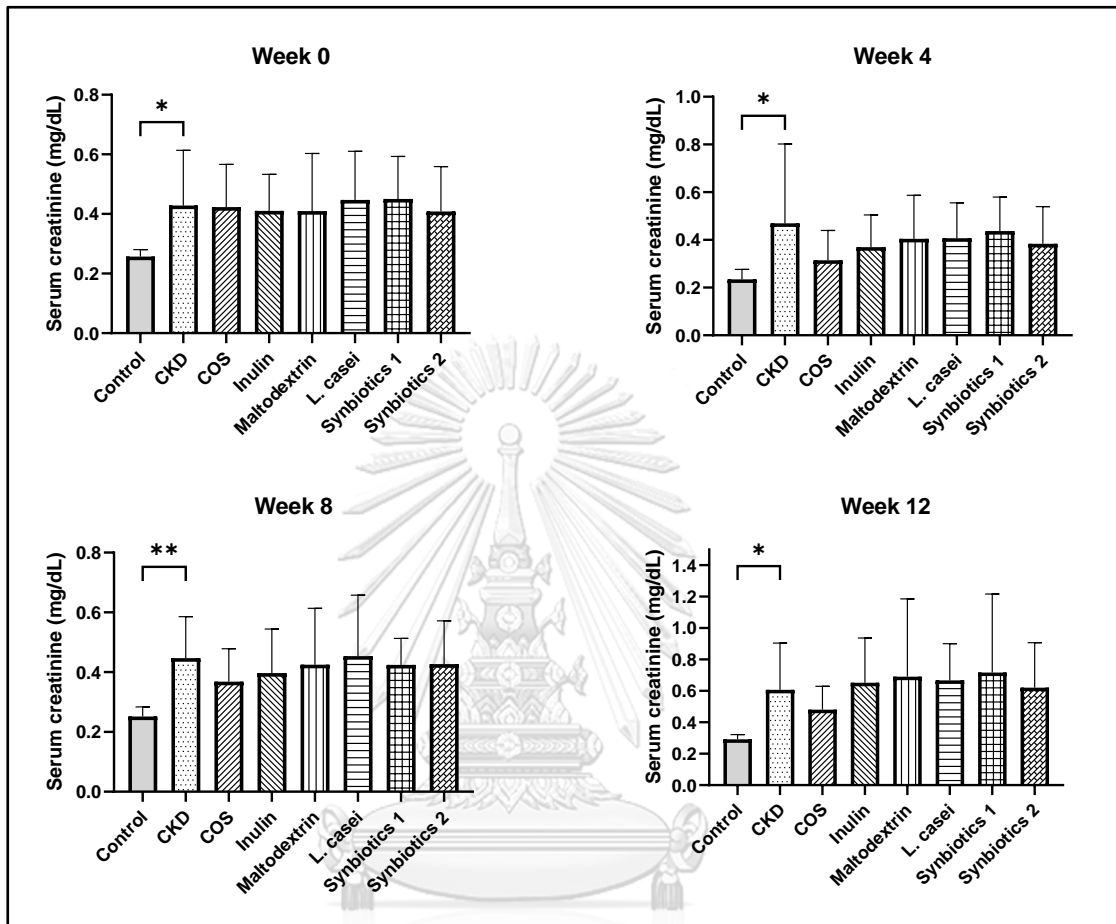


Figure 34. Serum creatinine
* represents p -value < 0.05

4.3.3. Serum phosphate

A 1% solution of phosphoric acid (H_3PO_4) was administered in the rats' drinking water on the first day of treatment. The serum phosphate levels of the rats were measured at week 4, 8, and 12, as depicted in Figure 35. At week 4, the rats treated with *L. casei*, synbiotics 1, and synbiotics 2 showed significantly lower serum phosphate level than those with CKD. At week 8, only synbiotics 1 and synbiotics 2 demonstrated lower serum phosphate level than CKD. At the end of the experiment, only synbiotics 1 showed lower serum phosphate level compared to CKD.

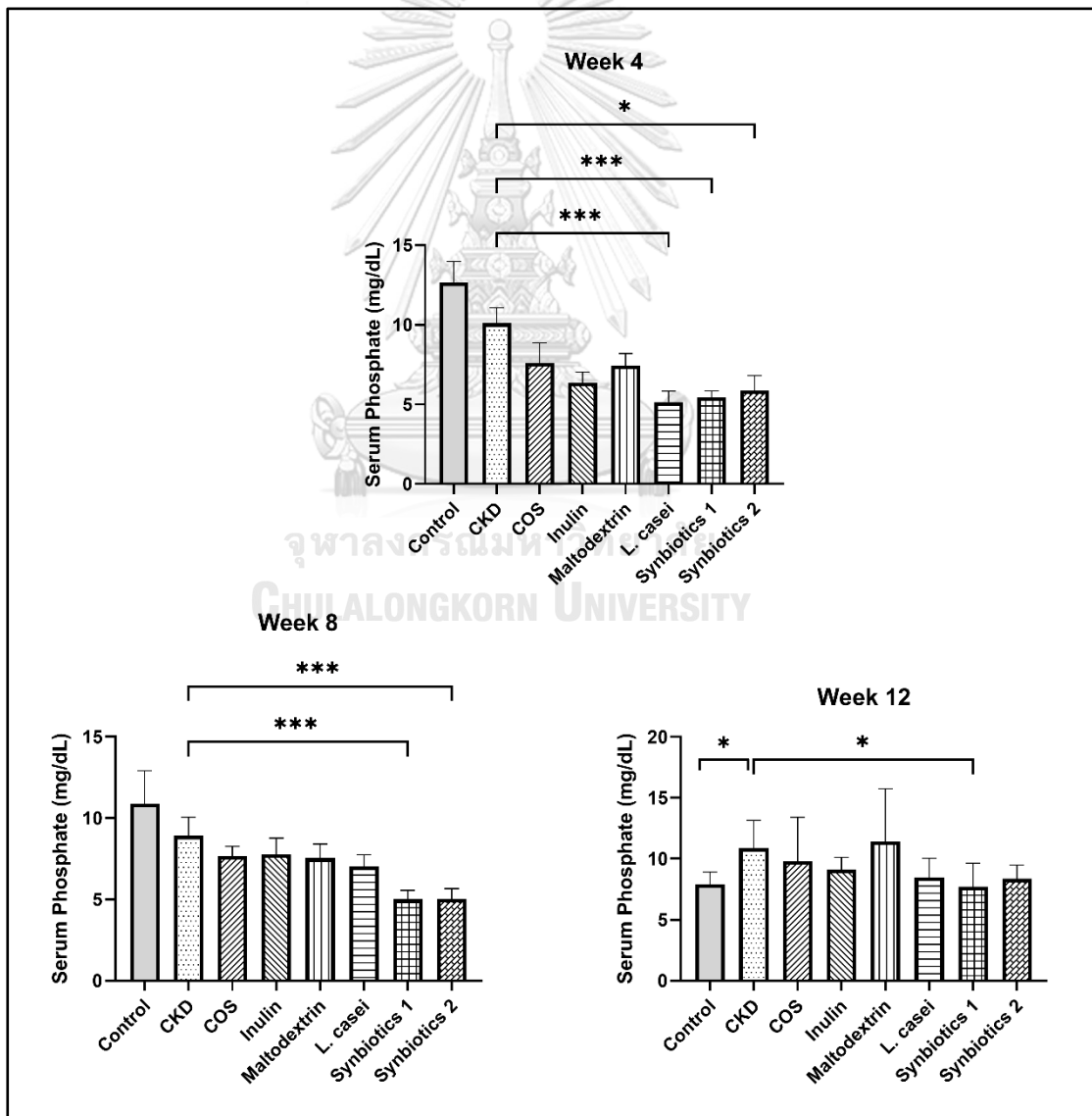


Figure 35. Serum phosphate

* represents p -value < 0.05 , ** represents p -value < 0.01 , *** represents p -value < 0.001 ,

The serum phosphate level in rats with chronic kidney disease in all treatment groups showed a tendency to increase, indicating the progression of the hyperphosphatemic effect of chronic kidney disease. In contrast, the serum phosphate levels in the control group tended to decrease, as shown in Figure 36.

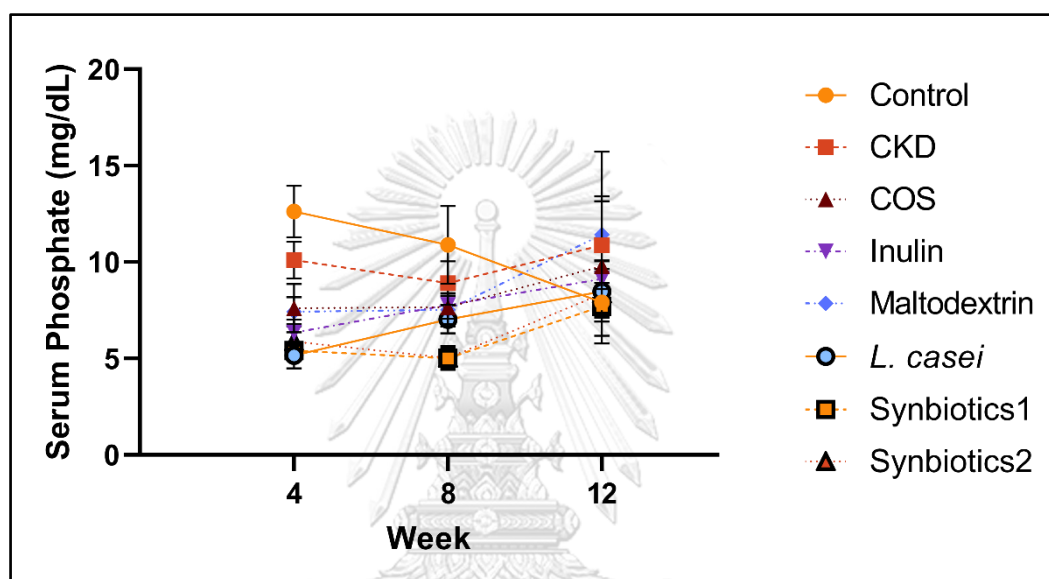


Figure 36. Serum phosphate changes

4.3.1. Parathyroid hormone

Parathyroid hormone (PTH) levels were measured in the serum at week 12. It was found that the CKD rats in all groups developed hyperparathyroidism, their serum PTH level were approximately 400 ng/mL. Results indicated that the serum PTH levels in the Synbiotics 1 group were significantly lower than those observed in the CKD group ($p=0.046$). Although the *L. casei* group exhibited similar PTH levels to the Synbiotics 1 group, the difference was not statistically significant relative to the CKD group ($p=0.0984$), as demonstrated in

Figure 37. Furthermore, the week-12 serum phosphate to serum PTH ratio was calculated. Findings revealed that the phosphate to PTH ratio in the CKD group

was significantly greater than that observed in the control group ($p=0.0175$), whereas no significant differences were noted among the other treatment groups.

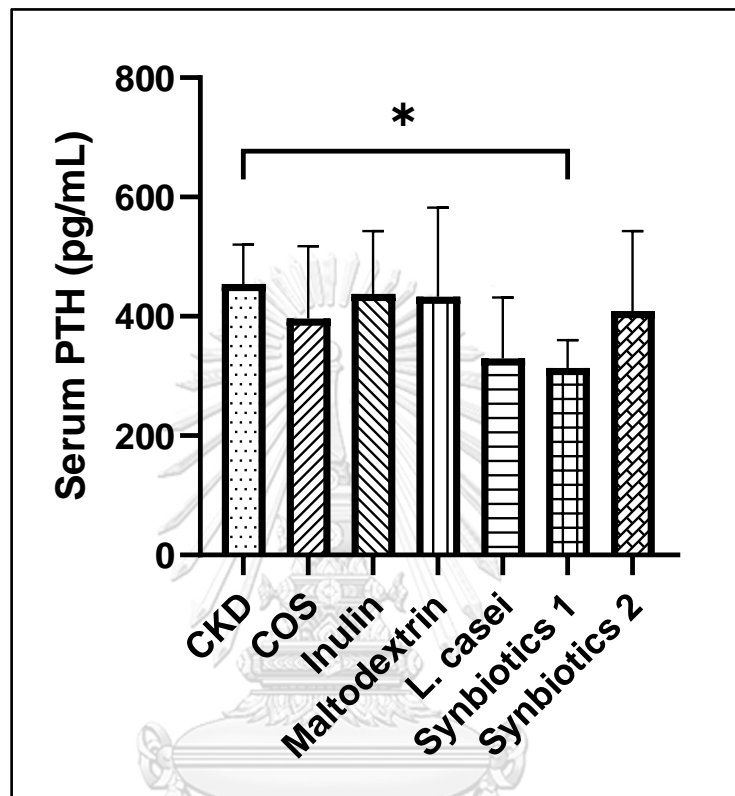


Figure 37. Serum parathyroid hormone
* represents p -value <0.05

4.3.2. Urine phosphate and calcium excretion rate

The urine of the rats was collected one day prior to sacrifice, and the levels of phosphate, calcium, and creatinine were determined. The ratio between urine phosphate (mg/dL) and urine creatinine (mg/dL) was calculated to determine the urine phosphate excretion rate, as well as the ratio between urine calcium (mg/dL) and urine

creatinine (mg/dL) to determine the urine calcium excretion rate

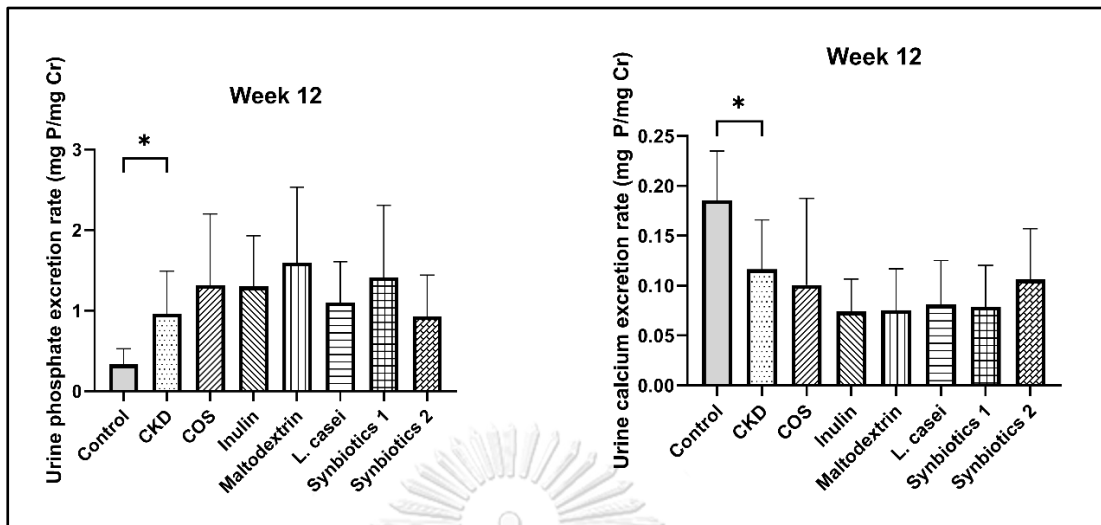


Figure 38). While the excreted phosphate in the urine of the CKD group was greater than that observed in the control group, no significant differences were found among the other treatment groups. Significant amounts of calcium were excreted in the urine of the control group compared to the CKD group. However, no significant differences were found in the excreted calcium levels in the urine among the other treatment groups.

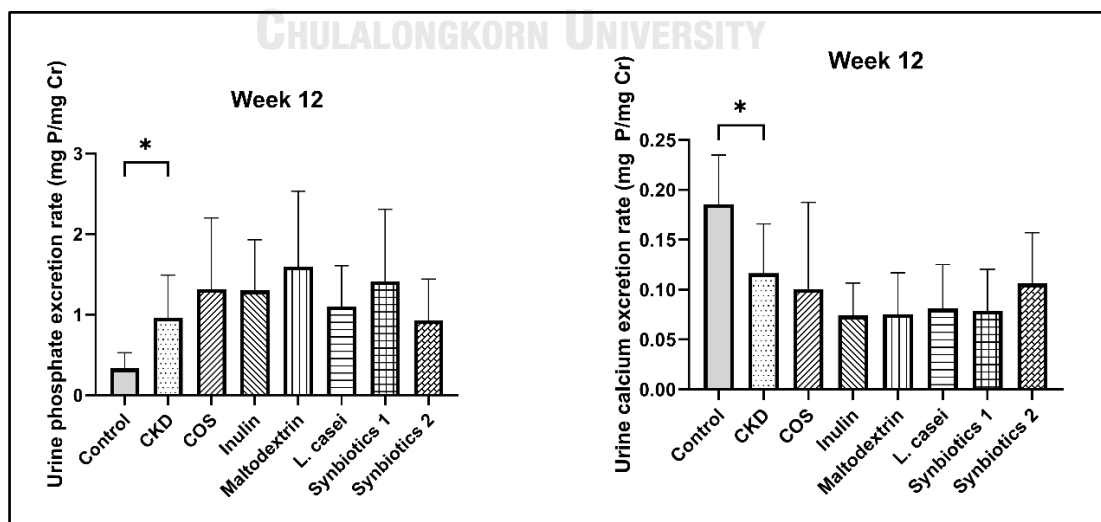


Figure 38. Urine phosphate and calcium excretion rate
* represents p-value <0.05

4.3.3. Gene expression of tight junction proteins

RNA was extracted from the jejunum of rats and subsequently quantified using RT-PCR. The relative expression was then determined with respect to the CKD group. The primers utilized targeted two tight junction genes, namely zonula occludens type 1 (ZO-1) and occludin (OCLN), with glyceraldehyde-3-phosphate dehydrogenase (GAPDH) serving as the housekeeping gene. While no significant difference in the expression of these genes was observed, a trend towards a higher expression of tight junction proteins was noted in the control group relative to the CKD group. Notably, the expression of both target genes was observed to increase in the Synbiotics 2 group.

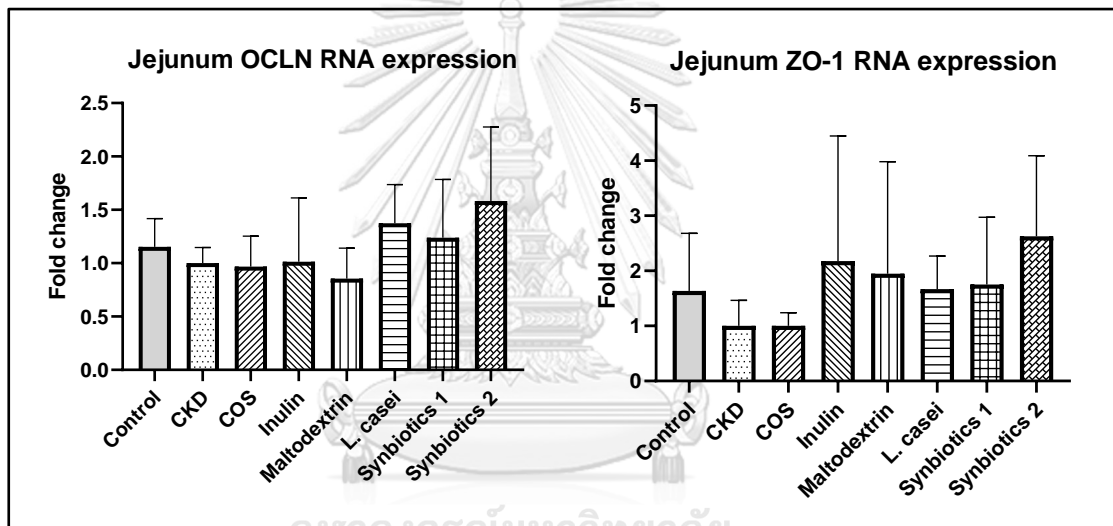


Figure 39. RNA expression of tight junction protein in jejunum

4.3.4. Histopathological examination

i) Kidney

In the kidney of chronic kidney disease induced rats, tubular necrosis (degeneration) was observed (absence of nucleus), glomerular necrosis, multiple tubular dilation, according to the effect of cisplatin in the induction of renal epithelial cell death (169) as shown in Figure 40 The glomerular lesion score in CKD groups was not significantly different from any treatment.

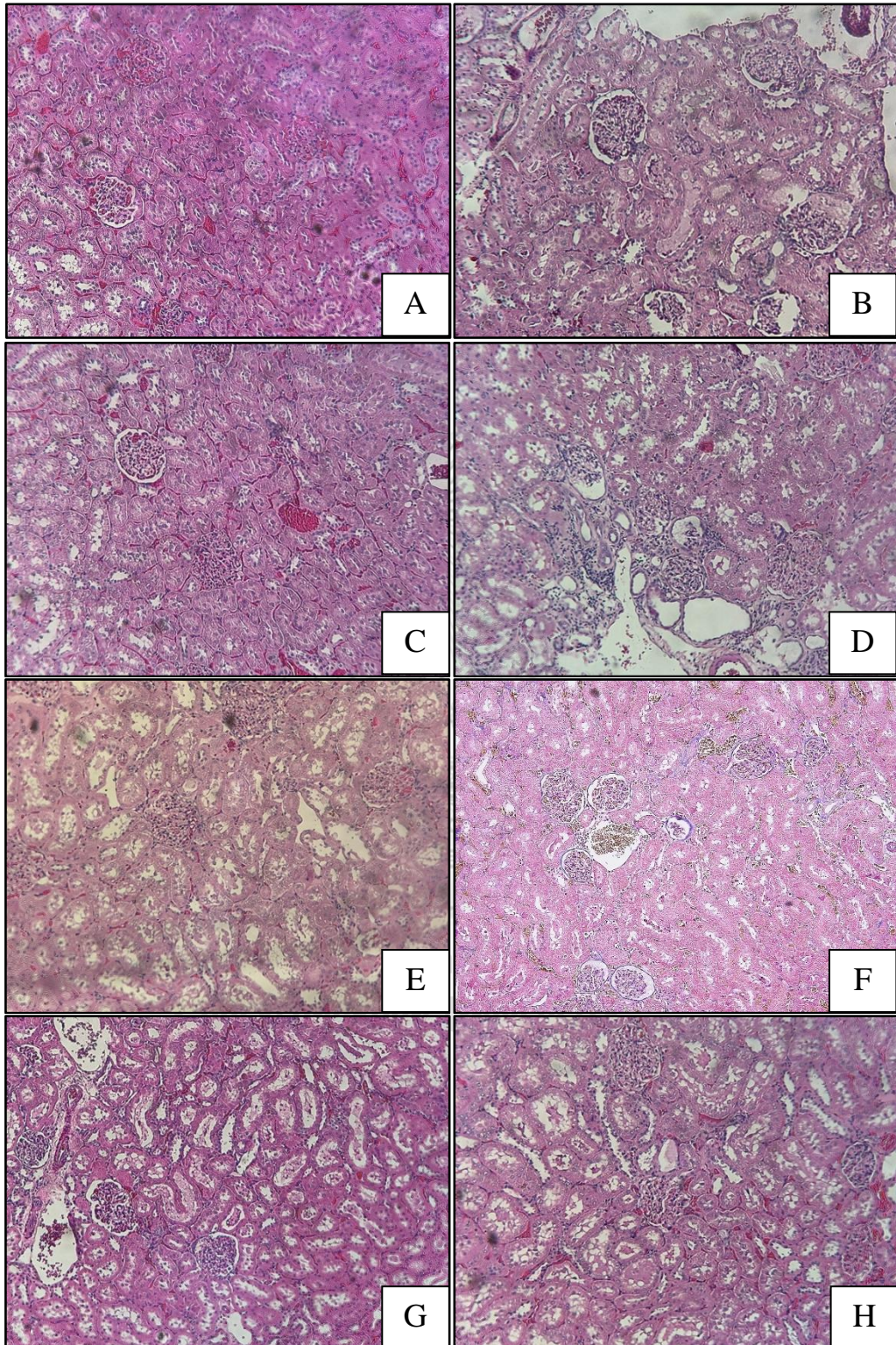
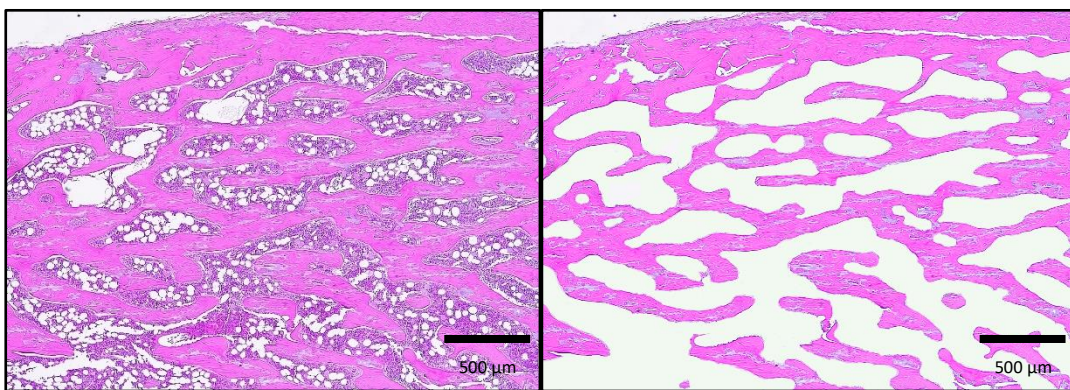


Figure 40. H&E-stained kidney section demonstrating glomeruli and tubules.

A) Control. B) CKD, C) COS, D) Inulin, E) Maltodextrin, F) *L. casei*, G) Synbiotic 1, and H) Synbiotic2 group: The image shows the renal cortex with glomeruli and tubule. The glomeruli appear as round structures with clear, visible nuclei, while the tubules appear as a network of small, interconnected structures.

ii) Femur bone

Histopathological examination of femur bones was conducted to evaluate the effects of CKD on bone density as shown in Figure 41 to Figure 48. The results showed that bone density observed in the trabecular bone in CKD rats was not significantly different from that of normal rats, indicating that mild CKD did not induce osteoporosis in the CKD rat model. The evaluation of the effects of treatments on bone density in this study was not carried out.



*Figure 41. Trabecular bone stained with H&E of Control group:
The left panel shows the original image, with bone marrow visible as purple-stained areas.
The right panel shows the same image with the bone marrow deleted, revealing the structure
of the trabecular bone.*

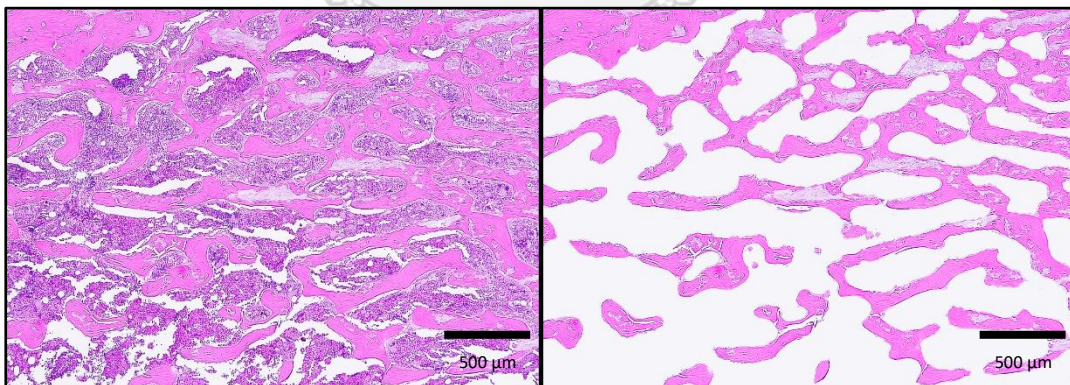


*Figure 42. Trabecular bone stained with H&E of CKD group:
The left panel shows the original image, with bone marrow visible as purple-stained areas.
The right panel shows the same image with the bone marrow deleted, revealing the structure
of the trabecular bone.*

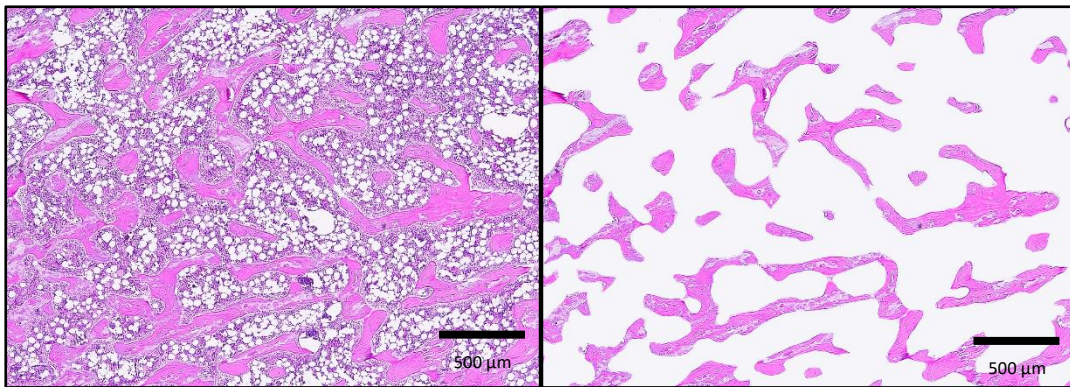


*Figure 43. Trabecular bone stained with H&E of COS group:
The left panel shows the original image, with bone marrow visible as purple-stained areas.
The right panel shows the same image with the bone marrow deleted, revealing the structure
of the trabecular bone.*

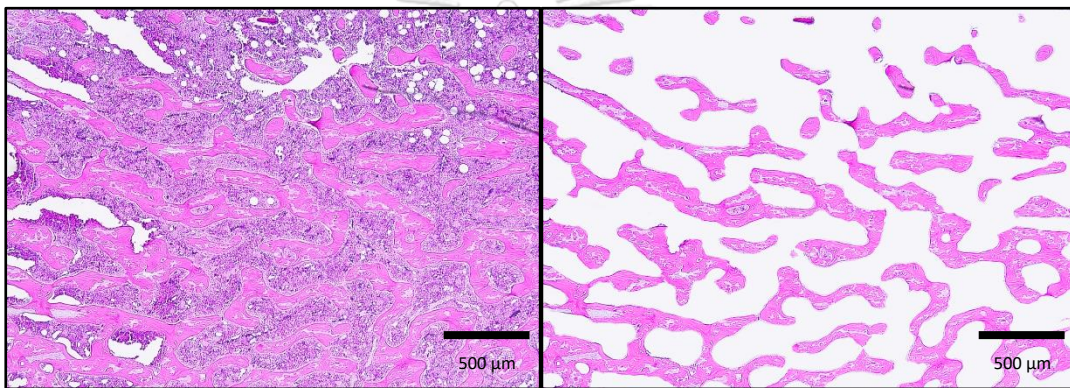


*Figure 44. Trabecular bone stained with H&E of Inulin group:
The left panel shows the original image, with bone marrow visible as purple-stained areas.
The right panel shows the same image with the bone marrow deleted, revealing the structure
of the trabecular bone.*

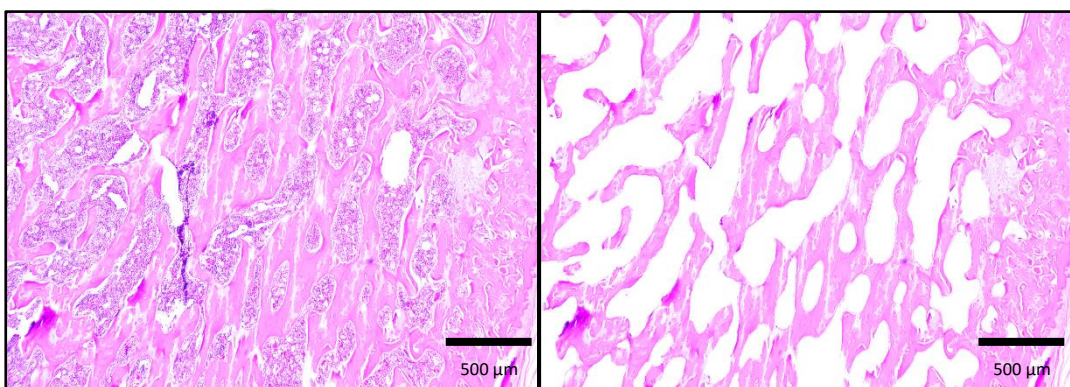


*Figure 45. Trabecular bone stained with H&E of Maltodextrin group:
The left panel shows the original image, with bone marrow visible as purple-stained areas.
The right panel shows the same image with the bone marrow deleted, revealing the structure
of the trabecular bone.*

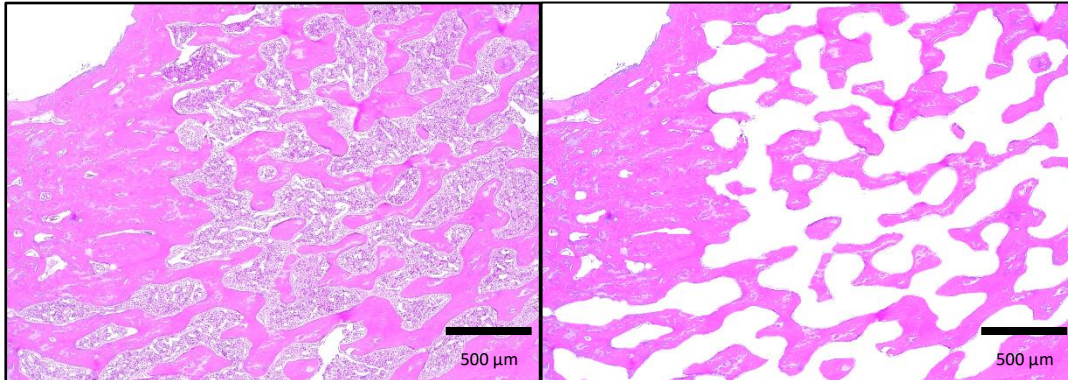


*Figure 46. Trabecular bone stained with H&E of L. casei group:
The left panel shows the original image, with bone marrow visible as purple-stained areas.
The right panel shows the same image with the bone marrow deleted, revealing the structure
of the trabecular bone.*

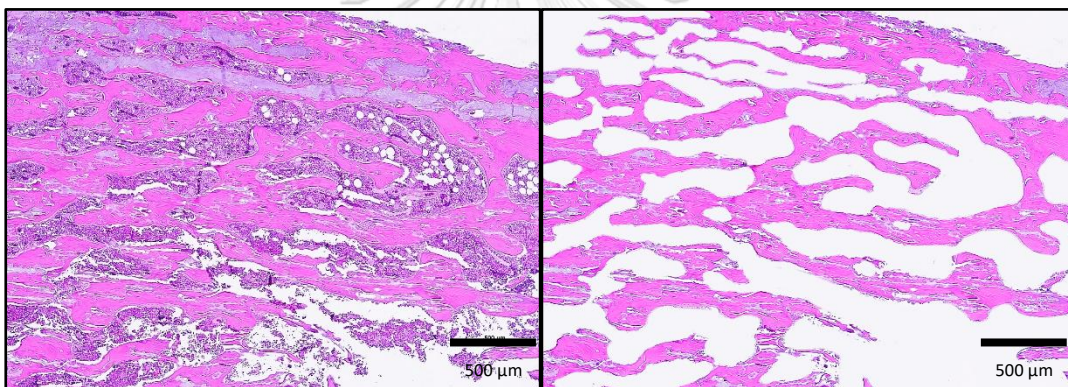


*Figure 47. Trabecular bone stained with H&E of Synbiotic 1 group:
The left panel shows the original image, with bone marrow visible as purple-stained areas.
The right panel shows the same image with the bone marrow deleted, revealing the structure
of the trabecular bone.*

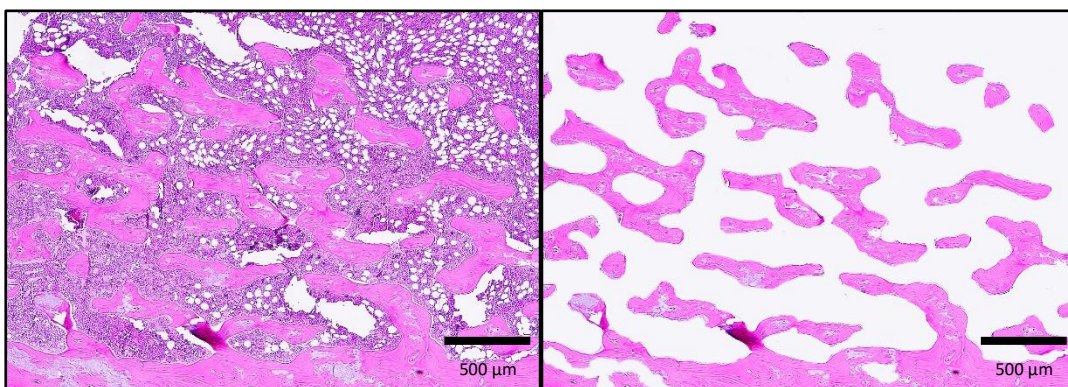


*Figure 48. Trabecular bone stained with H&E of Synbiotic 2 group:
The left panel shows the original image, with bone marrow visible as purple-stained areas.
The right panel shows the same image with the bone marrow deleted, revealing the structure
of the trabecular bone.*

iii) Jejunum

Immunohistochemical staining of the jejunum with anti-ZO-1 antibody showed the decreased in the positive area in CKD group compared to the Control group as shown in Figure 49 and Figure 50. The positive area of staining increased in the rats treated by Synbiotic 1 showing in Figure 55. The medians and IQR of the score are shown Figure 57.

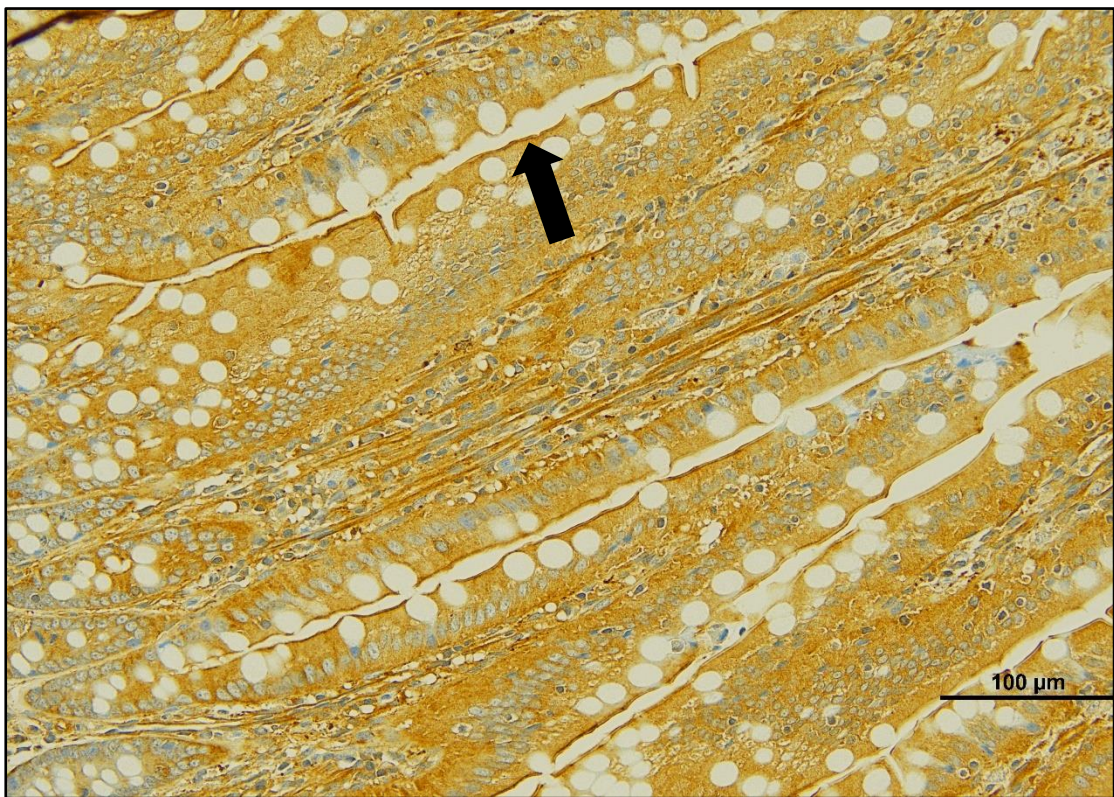


Figure 49. Immunohistochemical staining of the jejunum with anti-ZO-1 antibody of Control group:

The image shows the localization of the tight junction protein ZO-1 in the intestinal epithelial cells of the jejunum. ZO-1 appears as a continuous line of brown staining at the apical surface of the epithelial cells, outlining the cell borders (black arrow).

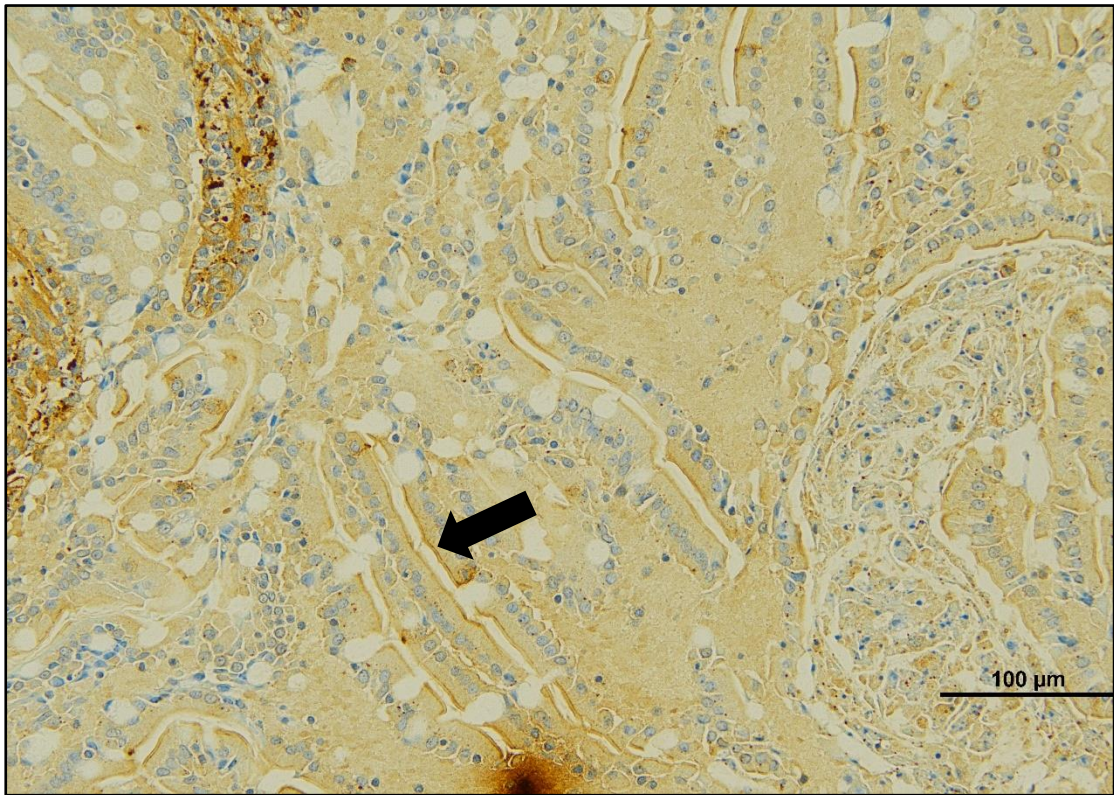


Figure 50. Immunohistochemical staining of the jejunum with anti-ZO-1 antibody of CKD group:

The image shows the localization of the tight junction protein ZO-1 in the intestinal epithelial cells of the jejunum. ZO-1 appears as a continuous line of brown staining at the apical surface of the epithelial cells, outlining the cell borders (black arrow).

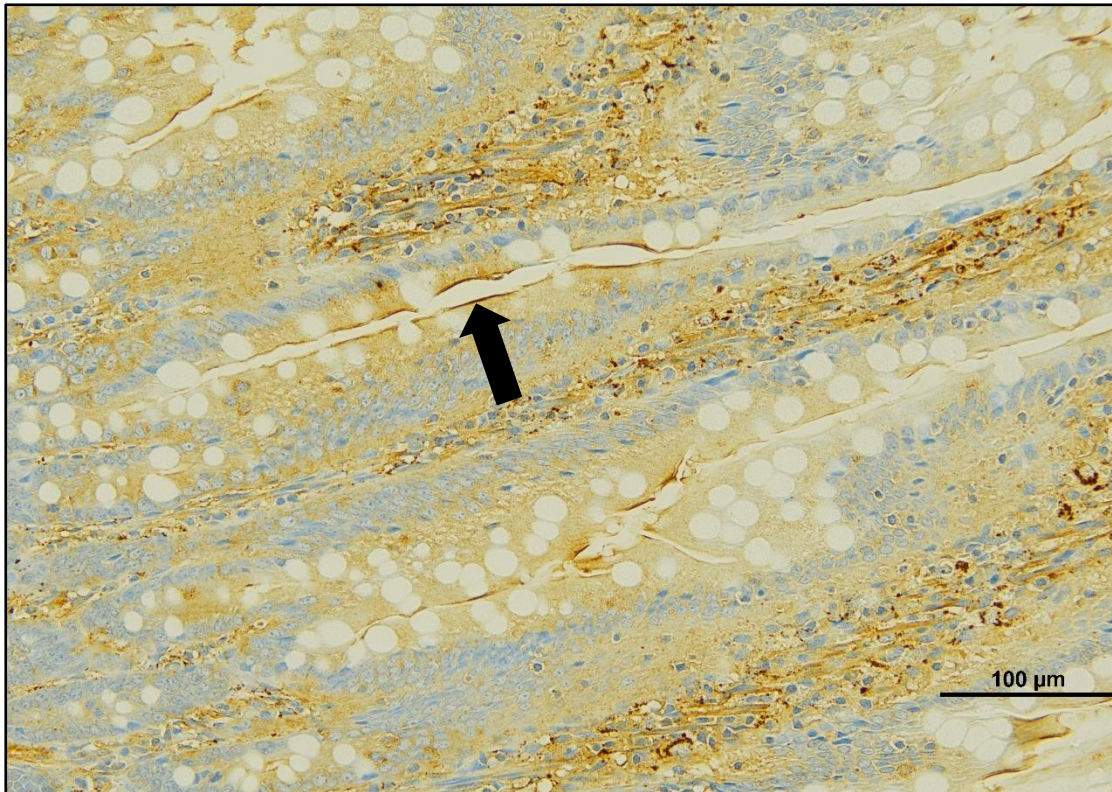


Figure 51. Immunohistochemical staining of the jejunum with anti-ZO-1 antibody of COS group:

The image shows the localization of the tight junction protein ZO-1 in the intestinal epithelial cells of the jejunum. ZO-1 appears as a continuous line of brown staining at the apical surface of the epithelial cells, outlining the cell borders (black arrow).

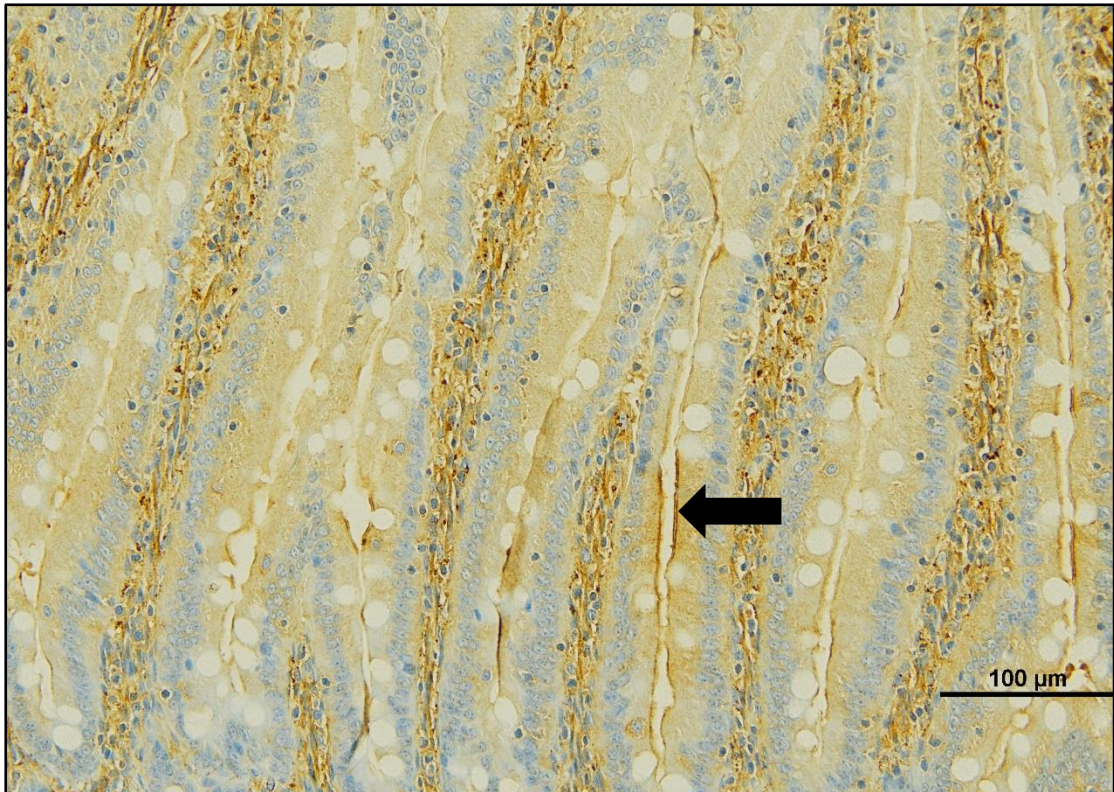


Figure 52. Immunohistochemical staining of the jejunum with anti-ZO-1 antibody of Inulin group:

The image shows the localization of the tight junction protein ZO-1 in the intestinal epithelial cells of the jejunum. ZO-1 appears as a continuous line of brown staining at the apical surface of the epithelial cells, outlining the cell borders (black arrow).

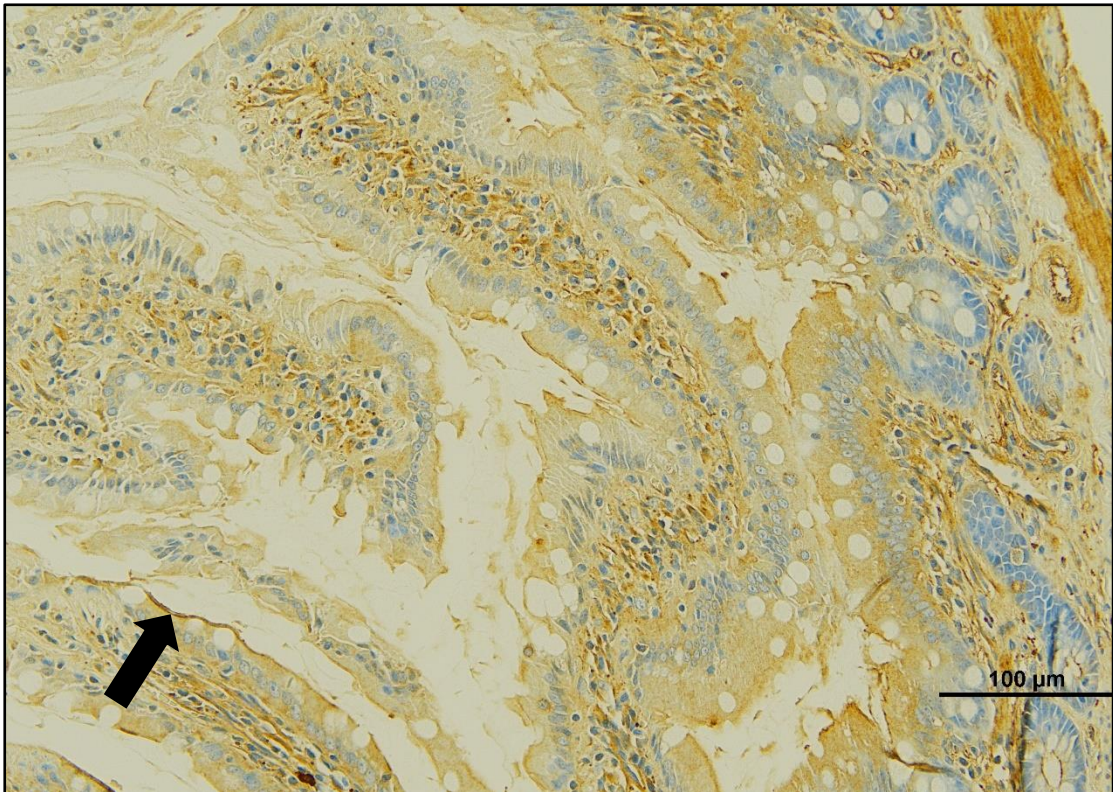


Figure 53. Immunohistochemical staining of the jejunum with anti-ZO-1 antibody of Maltodextrin group:

The image shows the localization of the tight junction protein ZO-1 in the intestinal epithelial cells of the jejunum. ZO-1 appears as a continuous line of brown staining at the apical surface of the epithelial cells, outlining the cell borders (black arrow).

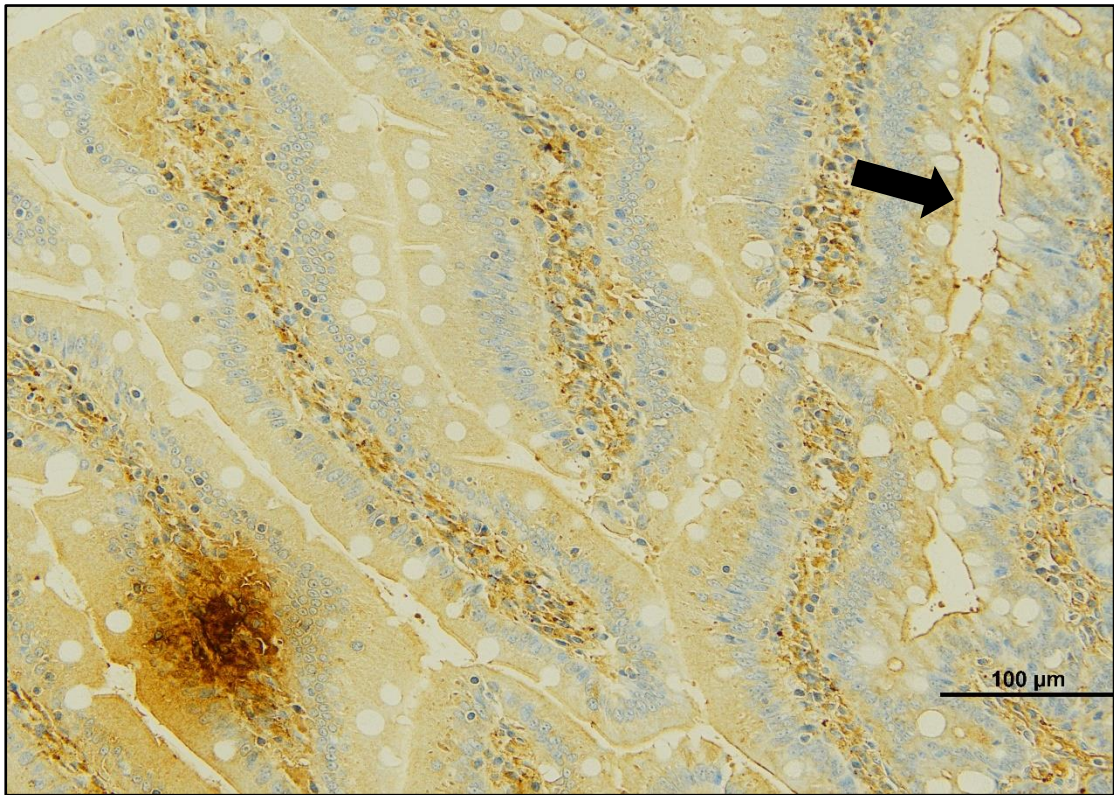


Figure 54. Immunohistochemical staining of the jejunum with anti-ZO-1 antibody of L. casei group:

The image shows the localization of the tight junction protein ZO-1 in the intestinal epithelial cells of the jejunum. ZO-1 appears as a continuous line of brown staining at the apical surface of the epithelial cells, outlining the cell borders (black arrow).

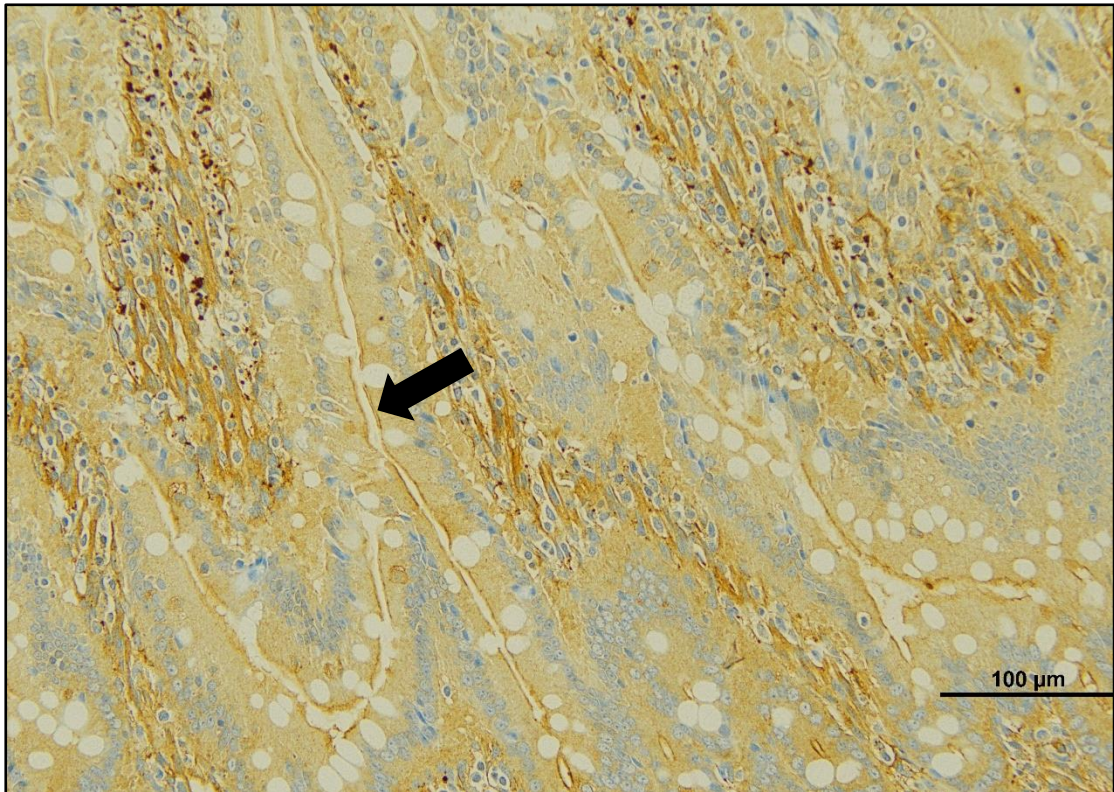


Figure 55. Immunohistochemical staining of the jejunum with anti-ZO-1 antibody of Synbiotic 1 group:

The image shows the localization of the tight junction protein ZO-1 in the intestinal epithelial cells of the jejunum. ZO-1 appears as a continuous line of brown staining at the apical surface of the epithelial cells, outlining the cell borders (black arrow).

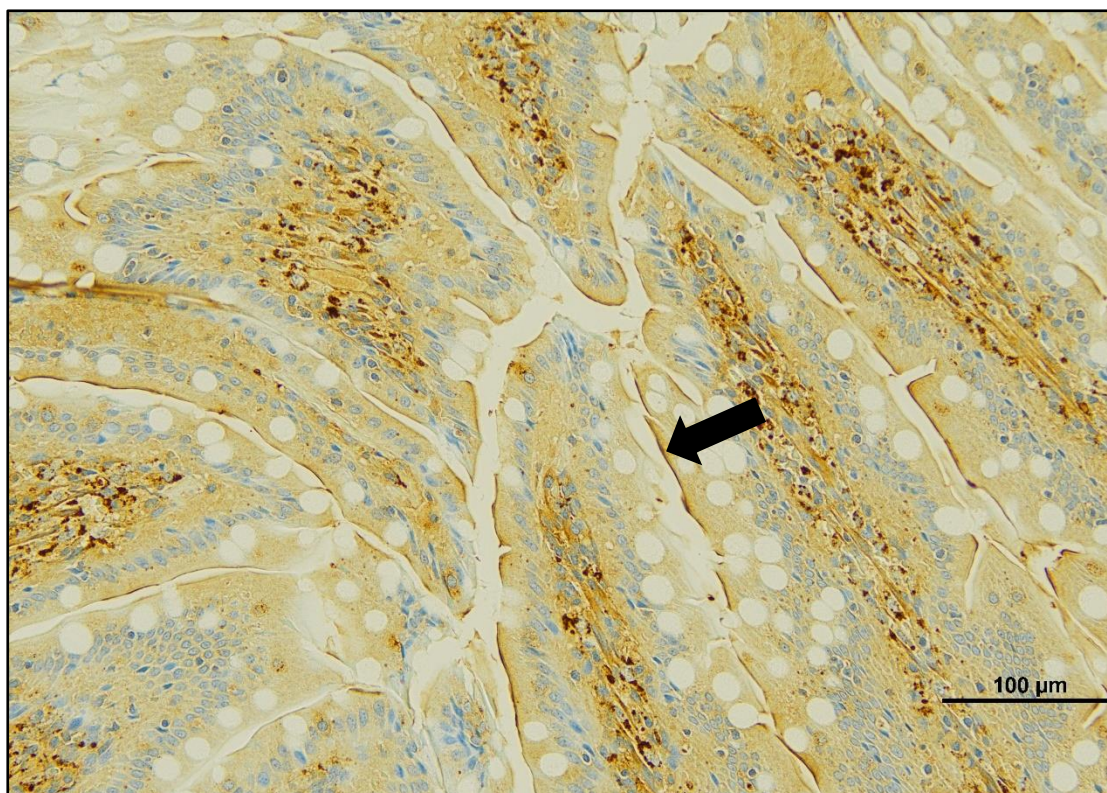


Figure 56. Immunohistochemical staining of the jejunum with anti-ZO-1 antibody of Synbiotic 2 group:

The image shows the localization of the tight junction protein ZO-1 in the intestinal epithelial cells of the jejunum. ZO-1 appears as a continuous line of brown staining at the apical surface of the epithelial cells, outlining the cell borders (black arrow).

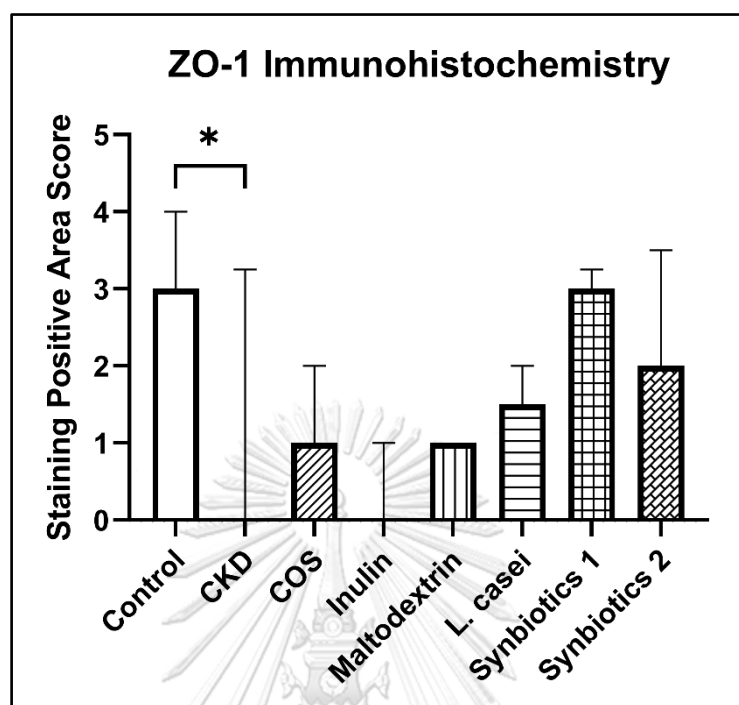


Figure 57. Median and IQR of the staining positive area score of the anti-ZO-1 antibody on rats jejunum.

* represents p -value <0.05

ZO-1 staining	Percent positive	Score
Negative	$<5\%$	0
Mild	5-25%	1
Focal	25-50%	2
Multifocal	50-75%	3
Pitch	$>75\%$	4

4.3.5. Correlation test

Parathyroid hormone (PTH) plays an important role in serum calcium and phosphate homeostasis by induction of bone resorption and urinary reabsorption. The correlation between serum PTH versus urinary phosphate and calcium via urine were evaluated. The Pearson correlation coefficient between serum PTH and serum phosphate at week 12 was 0.193, while the correlation coefficient between serum PTH and serum calcium was 0.341. In addition, a correlation coefficient of 0.436 was observed between serum calcium and serum phosphate. These findings suggested a weak correlation between serum PTH and both calcium and phosphate, while a moderate correlation was noted between serum calcium and serum phosphate.

PTH regulates urine phosphate via urinary excretion. Weak correlation between PTH and urine phosphate excretion rate (Pearson correlation coefficient of 0.151) and between serum PTH and calcium excretion rate (Pearson correlation coefficient of 0.170) were demonstrated in the present study.

Correlation between the RNA expression of ZO-1 and OCLN is strong (Pearson correlation coefficient of 0.87, $p=0.0001$). The correlation between serum PTH and the expression of ZO-1 is 0.256. The correlation is weak but statistical significant ($p = 0.035$).



4.3.6. Fecal Microbiota Analysis

a. Sequencing quality

In 16S rRNA gene sequencing, a sequencing depth of 10,000-20,000 reads per sample is commonly employed as a minimum threshold to ensure dependable taxonomic classification of the microbial community (141).

Figure 58 shows the alpha rarefaction of the phylogenetic diversity, observed features, and Shannon index of all the samples assigned to the sequencing. The sequencing depth is sufficient to capture the full diversity of microbial communities as the curves reach a plateau.

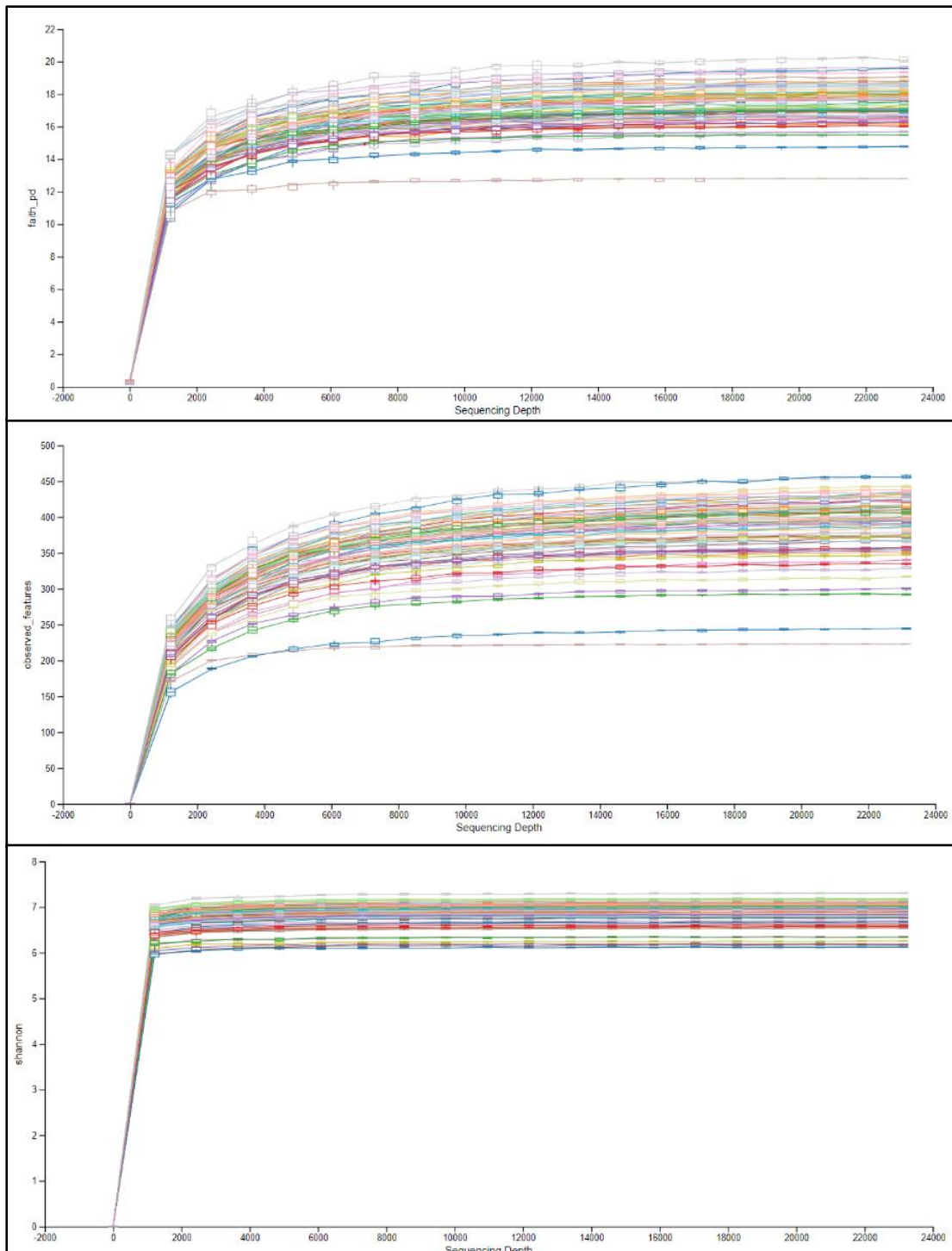


Figure 58. Alpha rarefaction

Table 7. shows the frequency per sample of all 70 fecal specimens, and the minimum frequency of 23278 reads was utilized to estimate the relative abundance of microbial communities.

Table 7 Summary of the sample frequency

	Frequency
Minimum frequency	23278.0
First quartile	50505.0
Median frequency	55031.5
Third quartile	59902.75
Maximum frequency	79791.0
Mean frequency	55931.7

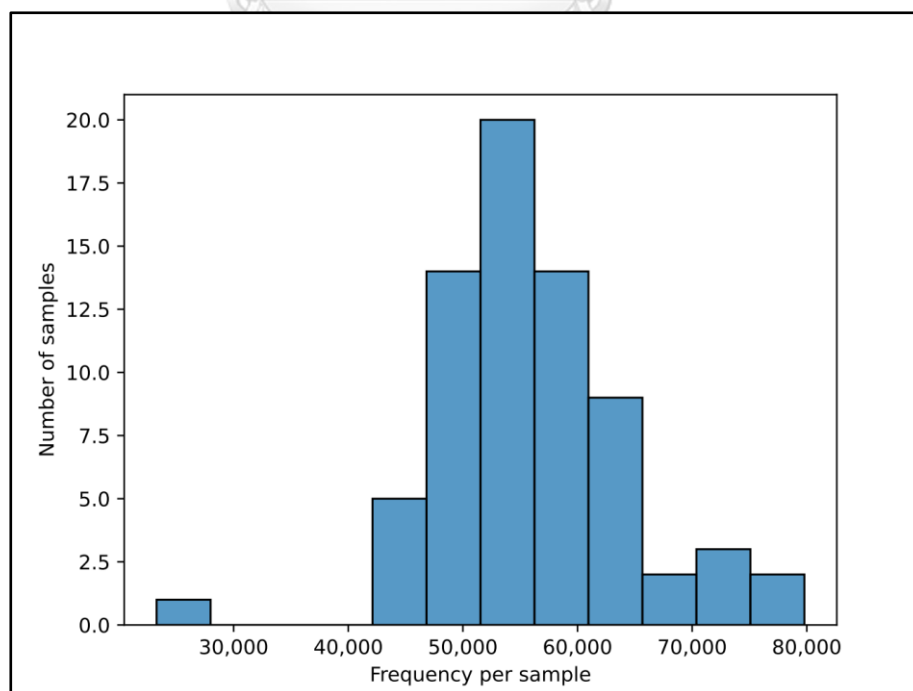


Figure 59. Histogram of the frequency per sample

b. Alpha diversity

Shannon indices of the bacterial populations were determined and compared for the significant changes via using a Wilcoxon signed-rank test. The results showed that, when all 35 samples from 8 groups were combined, the Shannon diversity of the post-treatment group was significantly higher than the pre-treatment stages (p -values = 0.0005), as shown in Figure 60 (p -values = 0.0005). However, when the samples were grouped based on treatment, no significant difference was found, as shown in Figure 61 with p -value that tested by Wilcoxon signed-rank test. Moreover, no significant difference was found in both week 0 and week 12, using Kruskal-Wallis test with the p -value of 0.05 as shown in Figure 62.

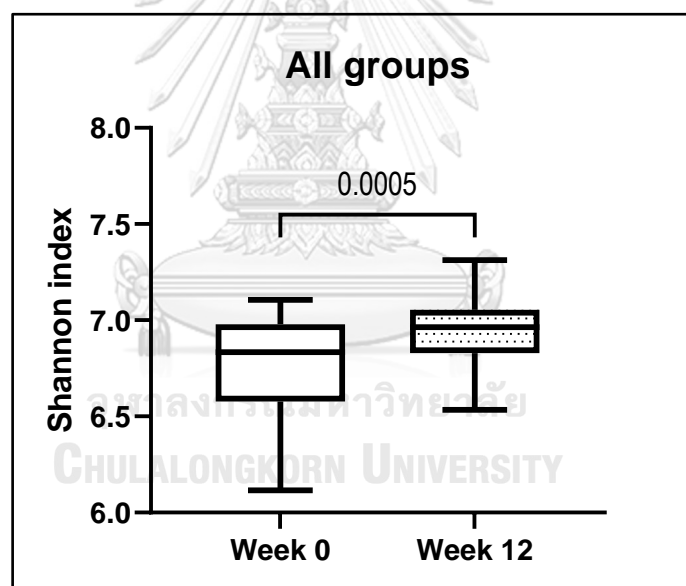


Figure 60. Shannon index of all groups comparing pre-treatment and post-treatment is represented in median and interquartile range. Shannon index of bacterial populations at week 12 was significantly higher than week 0 with p -value = 0.0005 tested by Wilcoxon signed-rank.

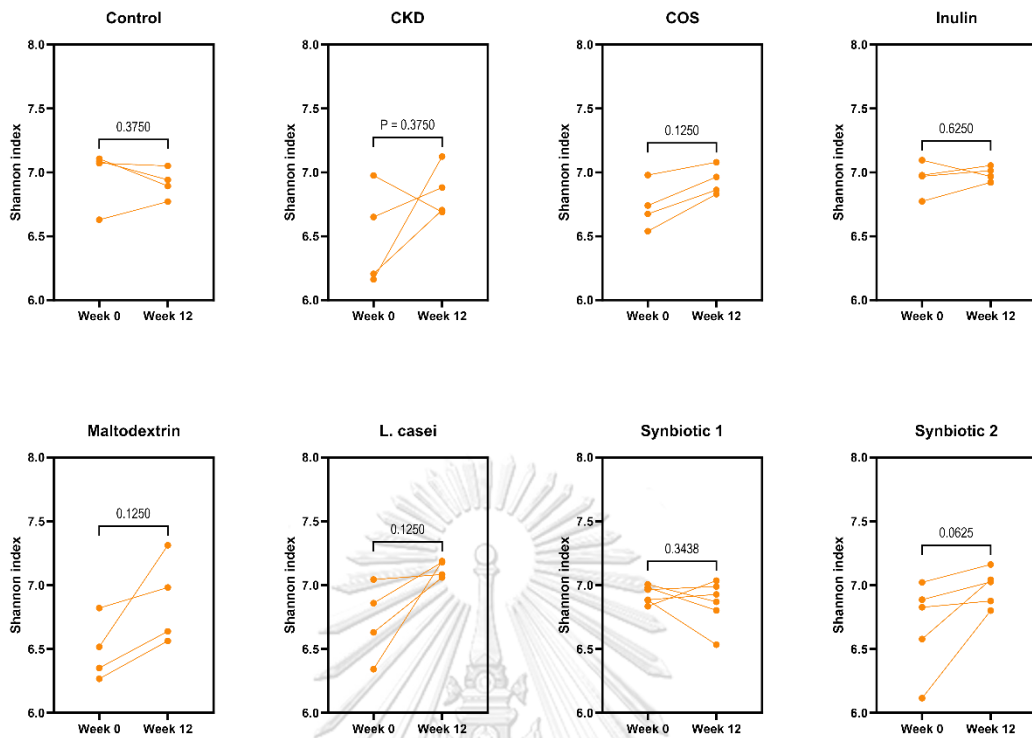


Figure 61. Shannon index of each groups comparing pre-treatment and post-treatment is represented in median and interquartile range. Significant difference was not found in any treatment (p-values from Wilcoxon signed-rank test were shown in each graph)

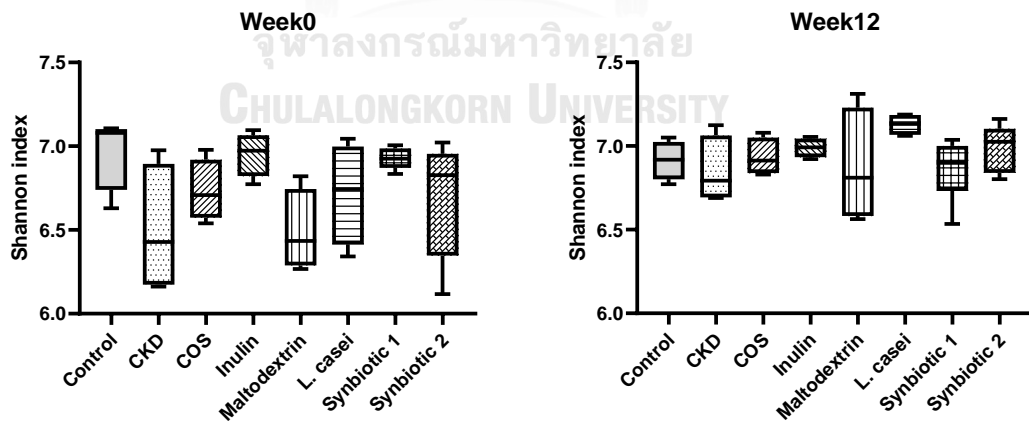


Figure 62. Shannon index of pre-treatment and post treatment comparing all groups are represented in median and interquartile range. Shannon diversity of all groups were not significantly different. (Kruskal-Wallis test: p-value = 0.0717 at week 0 and p-value = 0.202 at week 12)

Pielou's evenness of pre-treatment (week 0) and post-treatment (week 12) in treatment were compared using Wilcoxon signed-rank test. The results indicated that Pielou's evenness of the post-treatment group was significantly higher than pre-treatment stages when all 35 samples from 8 groups were combined as shown in Figure 63. However, Figure 64 demonstrates that when the Wilcoxon signed-rank test was conducted separately for each group of treatment, no significant difference was found in any group.

Furthermore, Pielou's evenness of the fecal bacteria at week 0 and week 12 were determined and compared using Kruskal-Wallis test. A significant difference was found at week 0 with p-value of 0.006. However, there was no significant difference in the Pielou's evenness at week 12, with a p-value of 0.1985, as shown in Figure 65. The results were further analyzed for the significant difference among each group using Mann Whitney test. Results indicated that the Pielou's evenness of the CKD group was significantly lower than the Control group, but not in the other groups.

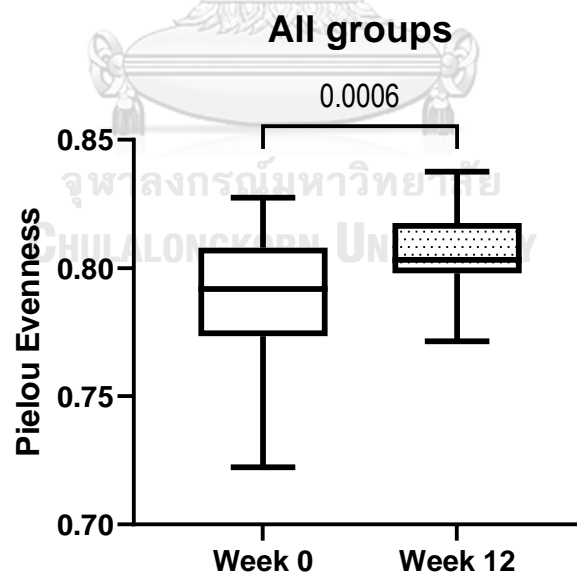


Figure 63. Pielou's evenness of all groups comparing pre-treatment and post-treatment is represented in median and interquartile range.

Pielou's evenness of bacterial populations at week 12 was significantly higher than week 0 with p-value = 0.0006 tested by Wilcoxon signed-rank.

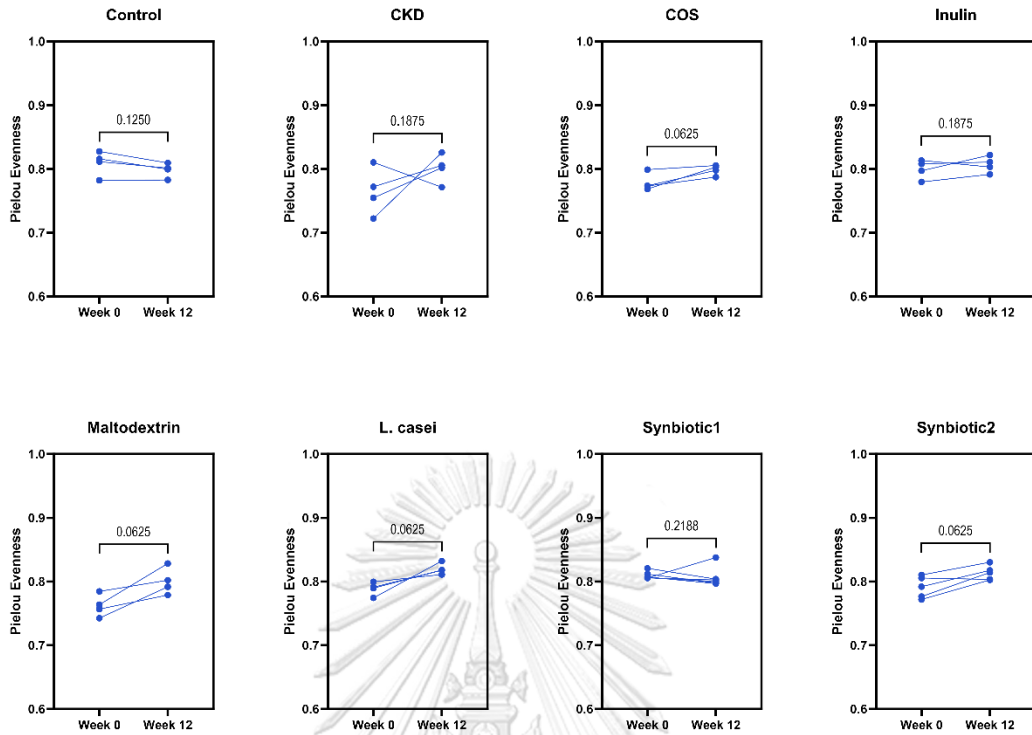


Figure 64. Pielou's evenness of each groups comparing pre-treatment and post-treatment is represented in median and interquartile range. Significant difference was not found in any treatment (p -values from Wilcoxon signed-rank test were shown in each graph)

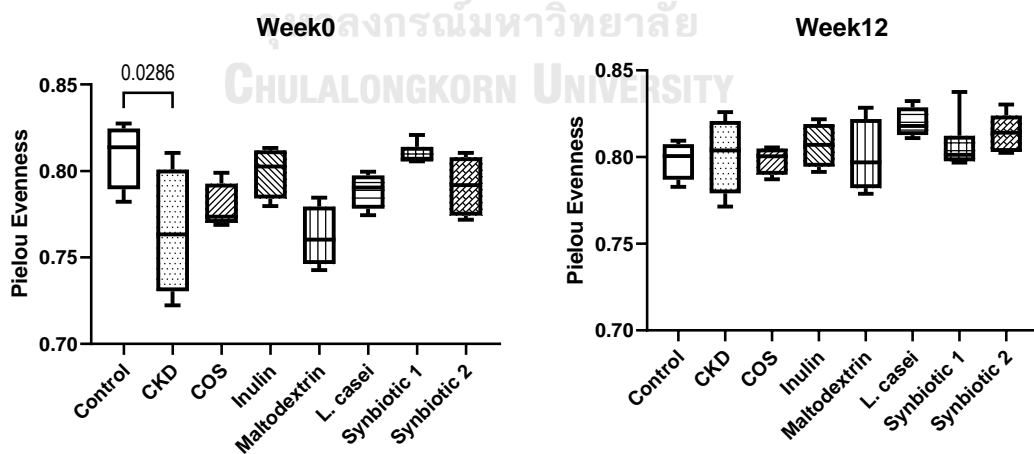
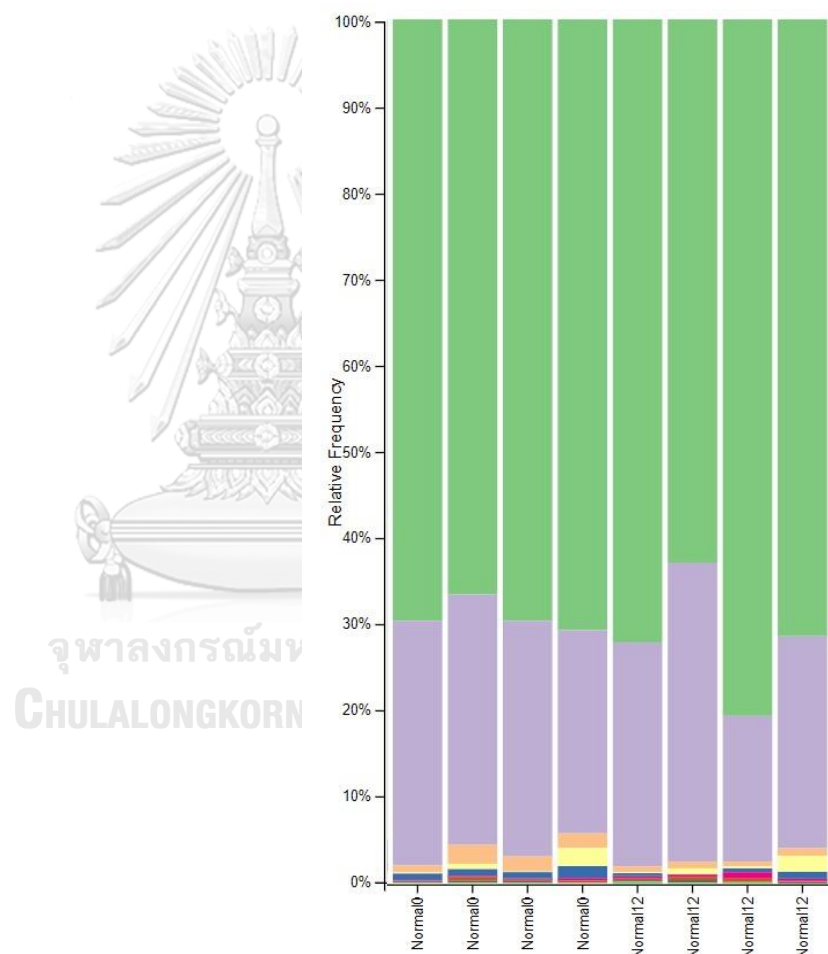


Figure 65. Pielou's evenness of pre-treatment and post treatment comparing all groups. Pielou's evenness of all groups at week 0 were significantly different (Kruskal-Wallis test: p -value = 0.009). The difference was not significant at week 12 (Kruskal-Wallis test: p -value = 0.1985)

c. Relative abundance

The relative abundance (percentage of a particular species or taxon within a community) is calculated by dividing the number of reads of a particular species by the total number of reads in the sample and then multiplying by 100 to express the result as a percentage.

The relative abundances of the fecal microbiota were analyzed. The bacterial Phyla of each group in week 0 (pre-treatment) and week 12 (post-treatment) are



shown as median \pm interquartile length in

Table 8 through Table 15. The Wilcoxon signed-rank test was utilized to determine the statistical significance between pre-treatment and post-treatment, and p-values are indicated in the tables with an asterisk to signify statistical significance at $p < 0.05$. The stacked bars representing the proportion of each phylum in each individual sample were shown together with the tables.



จุฬาลงกรณ์มหาวิทยาลัย
CHULALONGKORN UNIVERSITY

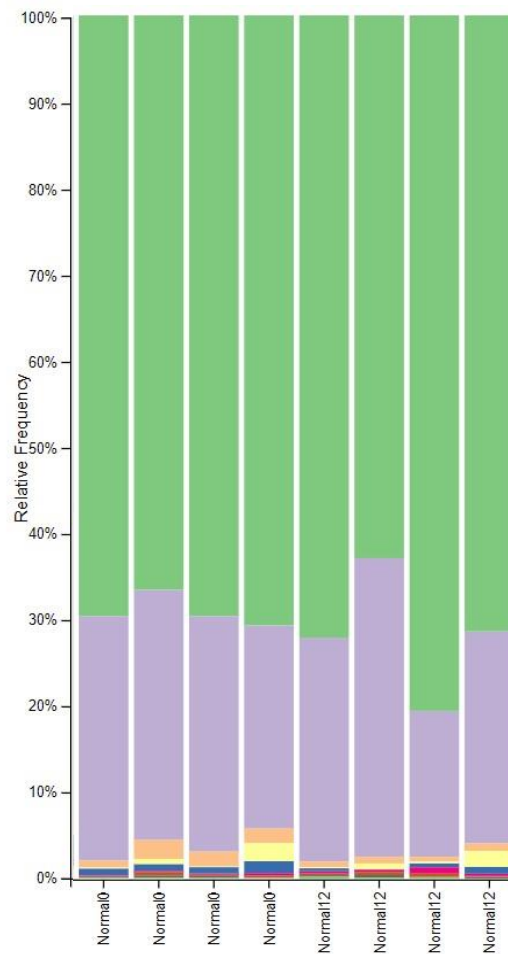


Table 8 Relative abundance of the bacterial Phyla in Control group (median \pm IQR)

Control	Week 0	Week 12	p-value
Phylum			
Actinobacteriota	0.094 \pm 0.130	0.140 \pm 0.122	0.465
Bacteroidota	13.882 \pm 2.176	12.602 \pm 6.816	0.715
Campylobacterota	0.096 \pm 0.076	0.098 \pm 0.081	0.465
Cyanobacteria	0.853 \pm 0.519	0.361 \pm 0.130	0.068
Deferribacterota	0.013 \pm 0.023	0.000 \pm 0.000	0.109
Desulfobacterota	0.385 \pm 0.239	0.204 \pm 0.294	0.068
Elusimicrobiota	0.000 \pm 0.000	0.000 \pm 0.000	1.000
Firmicutes	34.771 \pm 1.549	35.837 \pm 6.733	0.465
Patescibacteria	0.077 \pm 0.072	0.132 \pm 0.182	0.144
Proteobacteria	0.059 \pm 0.023	0.105 \pm 0.083	0.144
Spirochaetota	0.017 \pm 0.018	0.002 \pm 0.008	0.066
Verrucomicrobiota	0.173 \pm 0.819	0.223 \pm 0.712	0.715

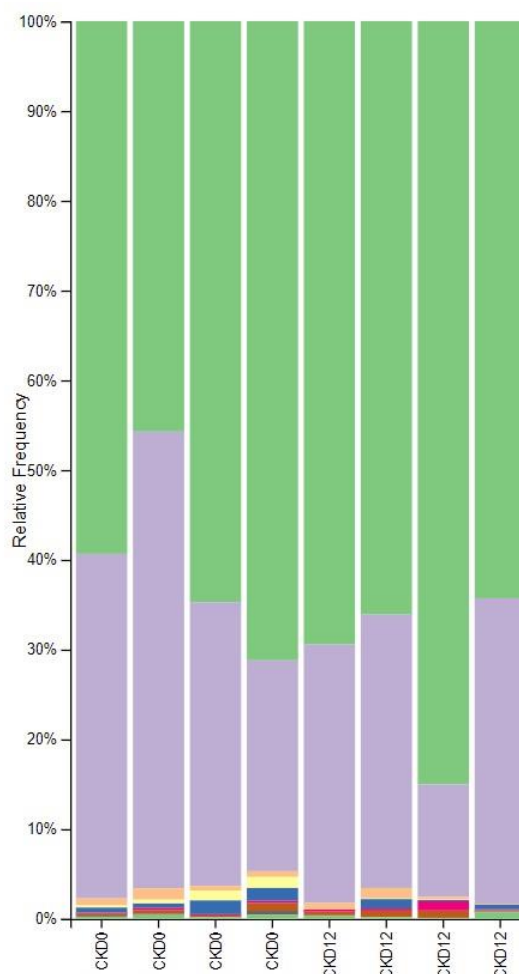


Table 9 Relative abundance of the bacterial Phyla in CKD group (median \pm IQR)

CKD	Week 0	Week 12	p-value
Phylum			
Actinobacteriota	0.165 \pm 0.271	0.292 \pm 0.182	0.715
Bacteroidota	17.497 \pm 11.114	8.266 \pm 11.447	0.273
Campylobacterota	0.069 \pm 0.172	0.051 \pm 0.077	0.109
Cyanobacteria	0.359 \pm 0.299	0.450 \pm 0.211	0.068
Deferribacterota	0.000 \pm 0.008	0.000 \pm 0.000	0.317
Desulfobacterota	0.507 \pm 0.507	0.442 \pm 0.121	0.273
Elusimicrobiota	0.000 \pm 0.000	0.000 \pm 0.260	1.000
Firmicutes	31.013 \pm 10.224	8.185 \pm 37.364	0.144
Patescibacteria	0.096 \pm 0.074	0.361 \pm 0.374	0.715
Proteobacteria	0.165 \pm 0.117	0.248 \pm 0.151	0.715
Spirochaetota	0.000 \pm 0.000	0.000 \pm 0.000	1.000
Verrucomicrobiota	0.371 \pm 0.455	0.043 \pm 0.083	0.068

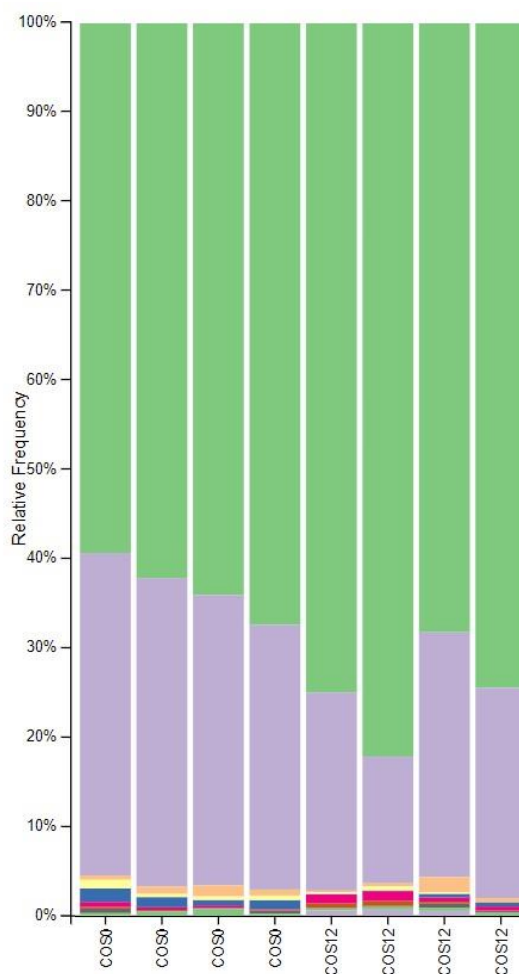


Table 10 Relative abundance of the bacterial Phyla in COS group (median \pm IQR)

COS	Week 0	Week 12	p-value
Phylum			
Actinobacteriota	0.061 \pm 0.058	0.182 \pm 0.225	0.144
Bacteroidota	16.777 \pm 2.682	11.447 \pm 5.116	0.068
Campylobacterota	0.112 \pm 0.219	0.077 \pm 0.170	0.715
Cyanobacteria	0.378 \pm 0.304	0.211 \pm 0.587	0.465
Deferribacterota	0.000 \pm 0.013	0.000 \pm 0.010	0.655
Desulfobacterota	0.541 \pm 0.352	0.121 \pm 0.173	0.068
Elusimicrobiota	0.000 \pm 0.000	0.260 \pm 0.253	0.109
Firmicutes	31.559 \pm 3.260	37.364 \pm 5.284	0.068
Patescibacteria	0.144 \pm 0.180	0.374 \pm 0.304	0.068
Proteobacteria	0.174 \pm 0.228	0.151 \pm 0.031	0.465
Spirochaetota	0.000 \pm 0.000	0.000 \pm 0.000	1.000
Verrucomicrobiota	0.225 \pm 0.247	0.083 \pm 0.173	0.144

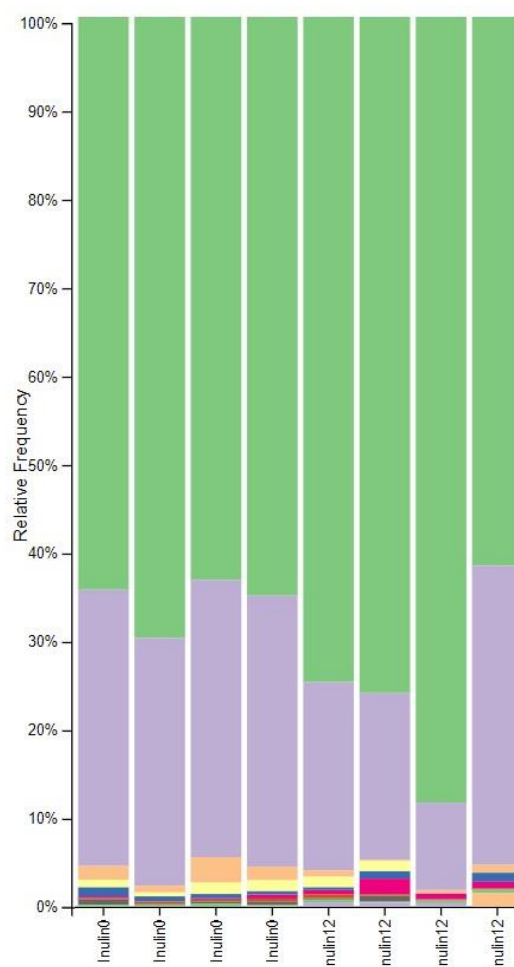


Table 11 Relative abundance of the bacterial Phyla in Inulin group (median \pm IQR)

Inulin	Week 0		Week 12		p-value
Phylum					
Actinobacteriota	0.121	\pm 0.058	0.080	\pm 0.133	0.715
Bacteroidota	15.379	\pm 1.303	9.978	\pm 9.228	0.144
Campylobacterota	0.173	\pm 0.191	0.053	\pm 0.242	0.715
Cyanobacteria	0.772	\pm 0.804	0.262	\pm 0.320	0.068
Deferribacterota	0.002	\pm 0.017	0.000	\pm 0.006	0.180
Desulfobacterota	0.259	\pm 0.247	0.293	\pm 0.446	0.715
Elusimicrobiota	0.000	\pm 0.000	0.207	\pm 0.196	0.109
Firmicutes	32.360	\pm 2.523	37.689	\pm 10.143	0.144
Patescibacteria	0.082	\pm 0.158	0.345	\pm 0.477	0.068
Proteobacteria	0.091	\pm 0.077	0.149	\pm 0.106	0.465
Spirochaetota	0.000	\pm 0.003	0.000	\pm 0.561	0.655
Verrucomicrobiota	0.500	\pm 0.359	0.282	\pm 0.571	0.465

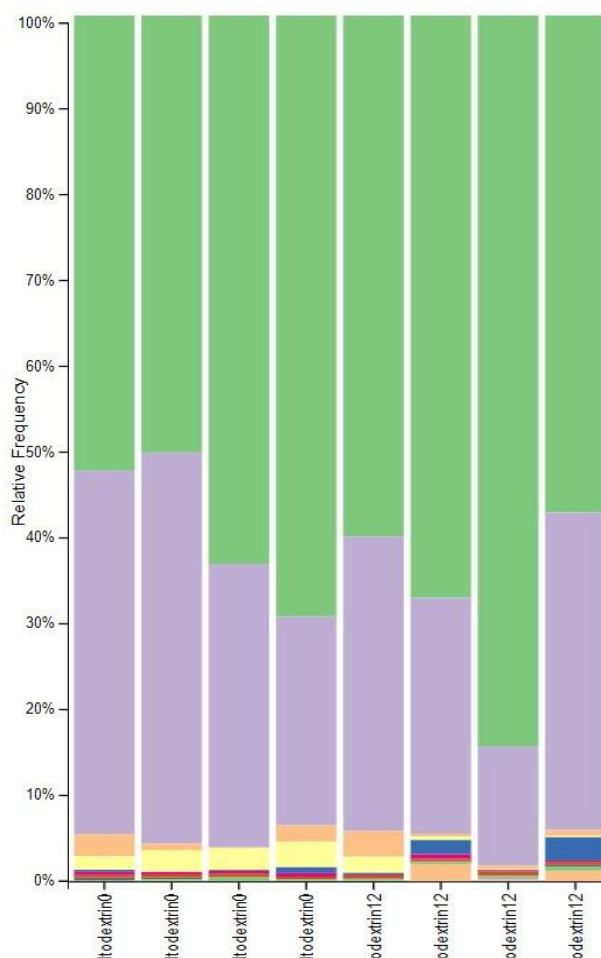


Table 12 Relative abundance of the bacterial Phyla in Maltodextrin group (median \pm IQR)

Maltodextrin	Week 0	Week 12	p-value
Phylum			
Actinobacteriota	0.153 \pm 0.070	0.163 \pm 0.075	0.465
Bacteroidota	18.695 \pm 9.044	15.327 \pm 9.440	0.273
Campylobacterota	0.076 \pm 0.125	0.049 \pm 0.088	1.000
Cyanobacteria	0.658 \pm 1.049	0.266 \pm 1.043	0.465
Deferribacterota	0.000 \pm 0.005	0.001 \pm 0.010	0.180
Desulfobacterota	0.093 \pm 0.268	0.467 \pm 1.175	0.465
Elusimicrobiota	0.000 \pm 0.000	0.000 \pm 0.079	0.317
Firmicutes	28.980 \pm 8.442	31.869 \pm 11.015	0.273
Patescibacteria	0.174 \pm 0.058	0.079 \pm 0.145	0.273
Proteobacteria	0.088 \pm 0.123	0.102 \pm 0.097	0.465
Spirochaetota	0.000 \pm 0.000	0.338 \pm 0.859	0.109
Verrucomicrobiota	1.236 \pm 0.508	0.134 \pm 0.686	0.144

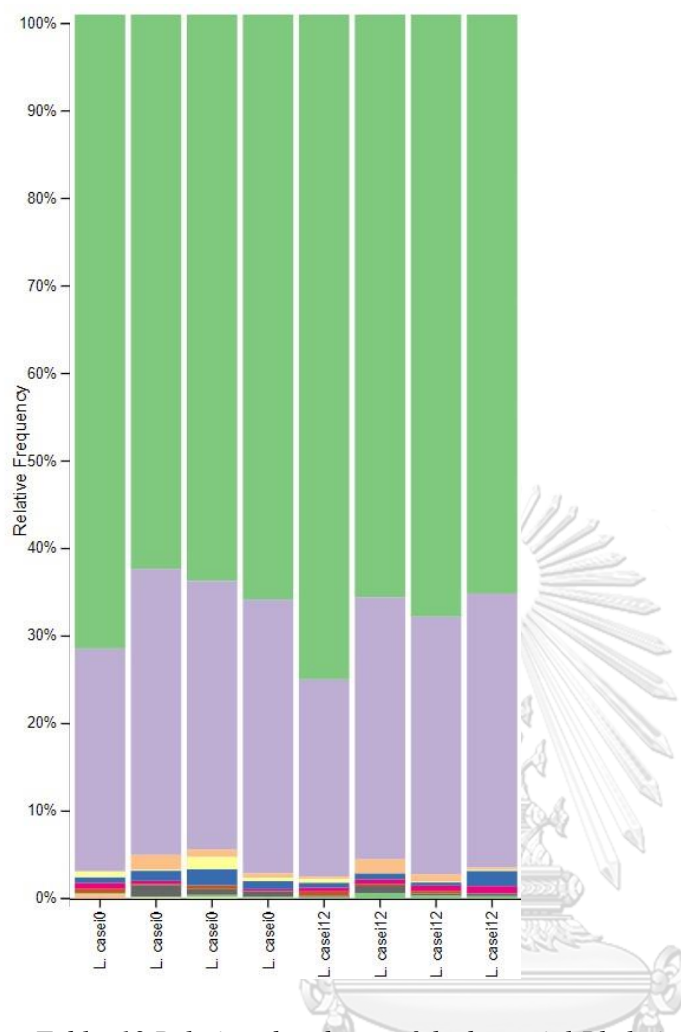


Table 13 Relative abundance of the bacterial Phyla in *L. casei* group (median \pm IQR)

L. casei	Week 0	Week 12	p-value
Phylum			
Actinobacteriota	0.131 \pm 0.203	0.124 \pm 0.184	0.465
Bacteroidota	15.348 \pm 2.767	14.703 \pm 3.316	0.144
Campylobacterota	0.318 \pm 0.505	0.147 \pm 0.243	0.144
Cyanobacteria	0.332 \pm 0.645	0.271 \pm 0.571	0.465
Deferribacterota	0.035 \pm 0.061	0.000 \pm 0.000	0.109
Desulfobacterota	0.525 \pm 0.466	0.311 \pm 0.525	0.465
Elusimicrobiota	0.000 \pm 0.000	0.000 \pm 0.000	1.000
Firmicutes	32.559 \pm 3.647	33.511 \pm 3.923	0.144
Patescibacteria	0.136 \pm 0.255	0.276 \pm 0.139	0.273
Proteobacteria	0.065 \pm 0.064	0.144 \pm 0.189	0.068
Spirochaetota	0.000 \pm 0.172	0.000 \pm 0.000	0.317
Verrucomicrobiota	0.242 \pm 0.508	0.045 \pm 0.157	0.068

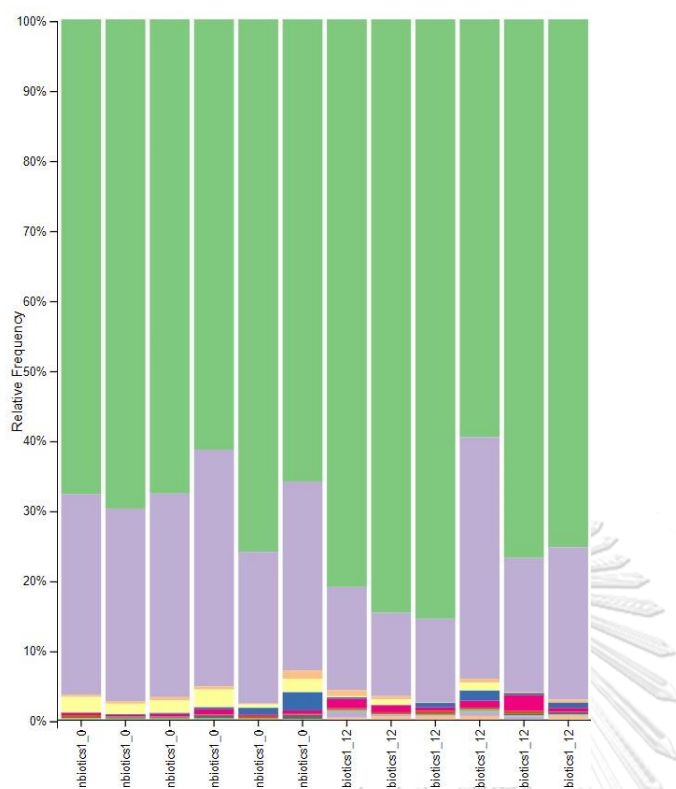


Table 14 Relative abundance of the bacterial Phyla in Synbiotic1 group (median \pm IQR)

Synbiotic 1	Week 0	Week 12	p-value
Phylum			
Actinobacteriota	0.054 \pm 0.095	0.169 \pm 0.177	0.249
Bacteroidota	14.018 \pm 4.805	10.223 \pm 8.785	0.046*
Campylobacterota	0.164 \pm 0.238	0.075 \pm 0.119	0.173
Cyanobacteria	0.227 \pm 0.387	0.152 \pm 0.240	0.917
Deferribacterota	0.000 \pm 0.008	0.006 \pm 0.028	0.109
Desulfobacterota	0.318 \pm 0.996	0.347 \pm 0.461	0.917
Elusimicrobiota	0.000 \pm 0.000	0.139 \pm 0.229	0.028*
Firmicutes	33.435 \pm 5.679	38.078 \pm 9.919	0.075
Patescibacteria	0.216 \pm 0.217	0.390 \pm 0.717	0.028*
Proteobacteria	0.056 \pm 0.048	0.071 \pm 0.102	0.599
Spirochaetota	0.005 \pm 0.011	0.230 \pm 0.198	0.046*
Verrucomicrobiota	0.917 \pm 0.778	0.005 \pm 0.406	0.028*

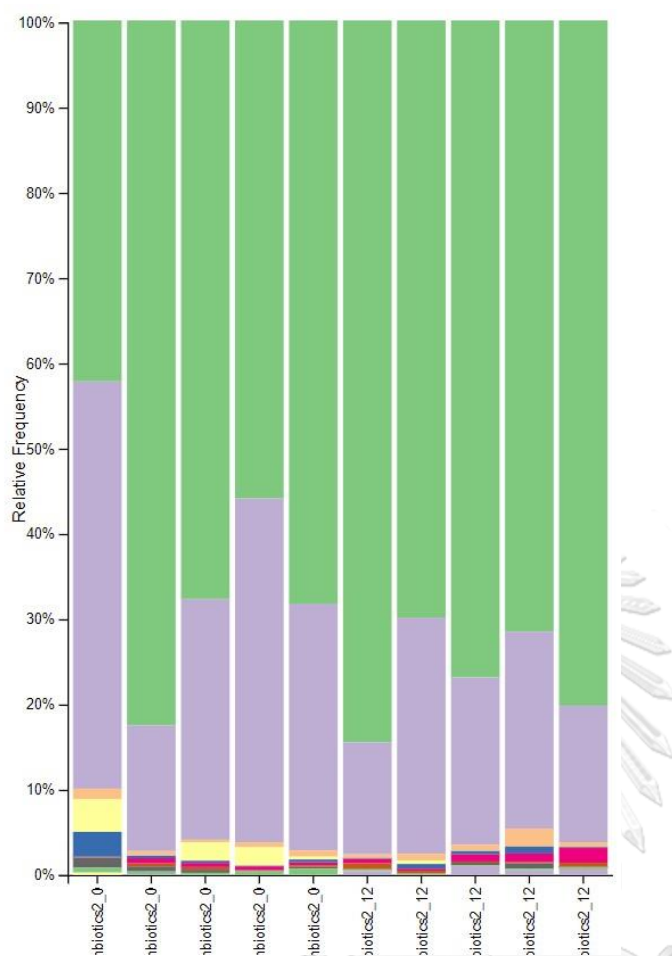


Table 15 Relative abundance of the bacterial Phyla in Synbiotic2 group (median \pm IQR)

Synbiotic 2	Week 0	Week 12	p-value
Phylum			
Actinobacteriota	0.130 \pm 0.092	0.115 \pm 0.147	0.500
Bacteroidota	14.250 \pm 9.653	10.656 \pm 4.795	0.225
Campylobacterota	0.144 \pm 0.246	0.100 \pm 0.231	0.345
Cyanobacteria	0.263 \pm 0.186	0.377 \pm 0.584	0.500
Deferribacterota	0.005 \pm 0.011	0.003 \pm 0.008	0.109
Desulfobacterota	0.147 \pm 0.089	0.233 \pm 0.286	0.893
Elusimicrobiota	0.000 \pm 0.034	0.292 \pm 0.393	0.080
Firmicutes	34.002 \pm 10.025	37.102 \pm 4.523	0.225
Patescibacteria	0.236 \pm 0.106	0.457 \pm 0.577	0.138
Proteobacteria	0.187 \pm 0.195	0.078 \pm 0.054	0.043*
Spirochaetota	0.000 \pm 0.000	0.000 \pm 0.010	0.655
Verrucomicrobiota	0.611 \pm 1.017	0.002 \pm 0.157	0.138

Based on the findings of the relative abundance analysis of bacterial Phyla, statistically significant changes were observed only in the groups treated with Synbiotic 1 and Synbiotic 2. Specifically, within the Synbiotic 1 group, there was a significant decrease in the relative abundance of Bacteroidota, while the relative abundance of Elusimicrobiota, Patescibacteria, and Spirochaetota showed a significant increase. Nonetheless, a significant decrease in the relative abundance of Proteobacteria was detected in the group administered with Synbiotics 2.

A non-parametric statistical analysis was conducted to evaluate the differences between the 8 groups at week 0 in the study for all Phyla. The Kruskal-Wallis test was used to compare the medians of the groups. The results showed a significant difference between at least one of the groups ($p < 0.05$) in the Phylum Proteobacteria and Spirochetota. A Mann-Whitney U test between the Control and CKD group showed the significant difference of the Phylum Proteobacteria with the p-value of 0.021 and the Phylum Spirochetota with p-value of 0.013.

The relative abundances of Firmicutes and Bacteroidota were used to determine the Firmicutes/Bacteroidota ratio. The results indicated that the Firmicutes to Bacteroidota ratio in week 12 significantly increased from week 0 when all samples were calculated together, as shown in Figure 66. However, when it was calculated separately, significant increase was

found only in the Synbiotic 1 group, as shown in

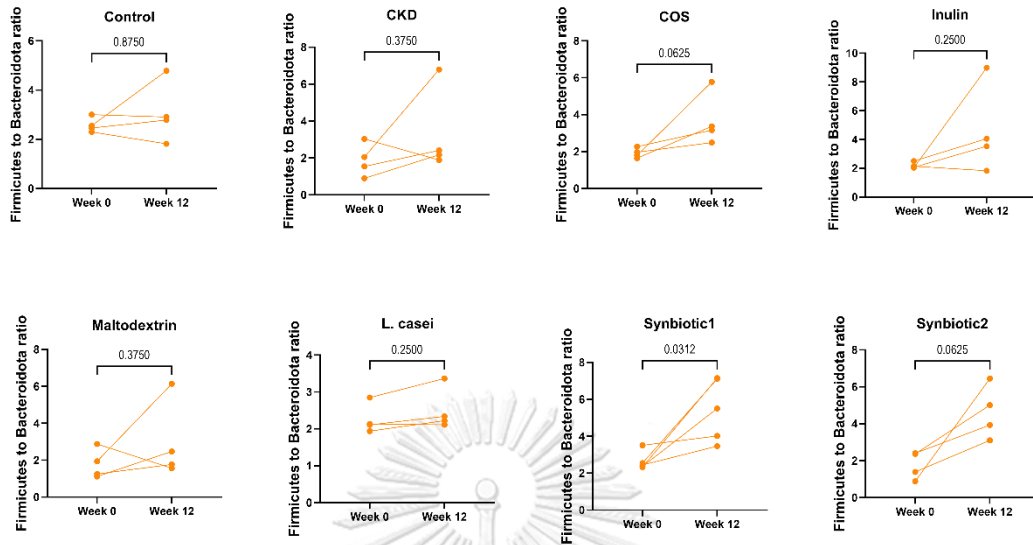


Figure 67.

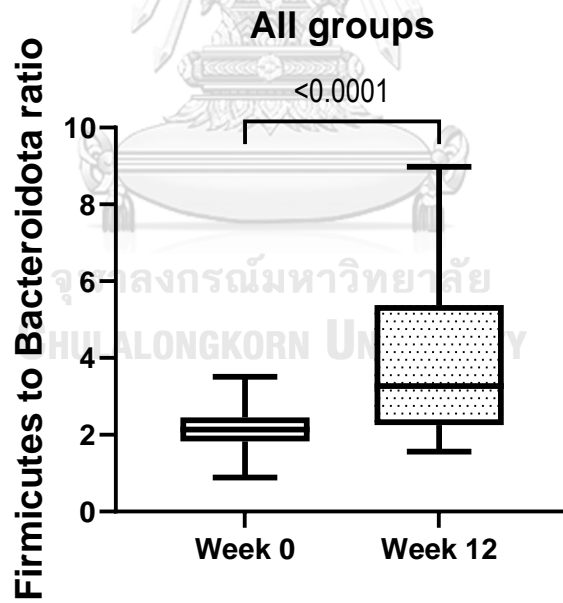


Figure 66. Firmicutes to Bacteroidota ratio of all groups comparing pre-treatment and post-treatment is represented in median and interquartile range.

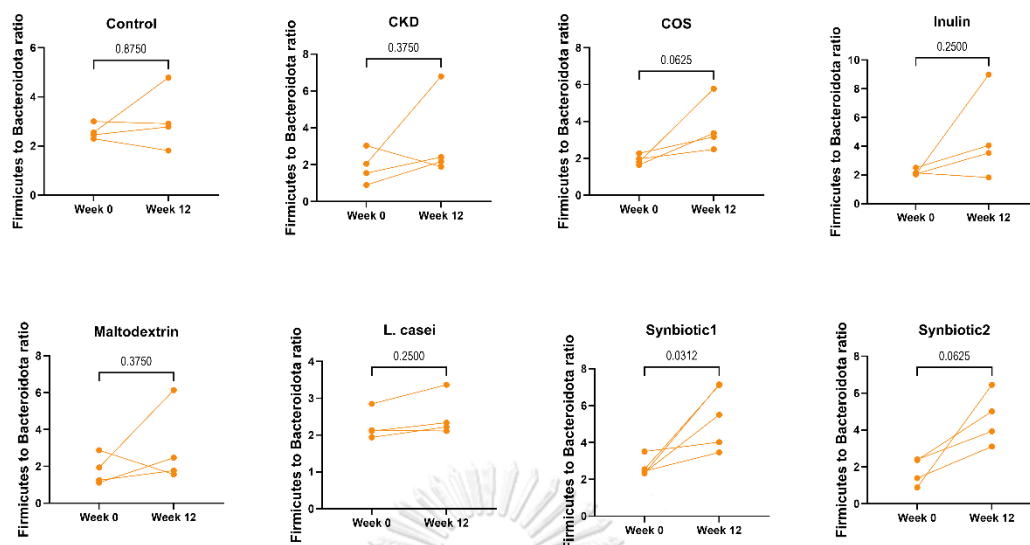


Figure 67. Firmicutes to Bacteroidota ratio of each groups comparing pre-treatment and post-treatment is represented in median and interquartile range.

The relative abundances in the Genus level were determined. The top 20 most abundant of bacterial Genera of each group in week 0 and week 12 are shown as median \pm interquartile length in Table 16 through Table 23. The significant changes of the abundance were determined using Wilcoxon signed-rank test. The significant change in the relative abundance were not found in Control, CKD, COS, Inulin, Maltodextrin, and L. casei group. However, 30 genera in Synbiotic 1 and 4 Genera in Synbiotic 2 group significantly changed. Table 24 and Table 25 show median of the difference in the relative abundance between week 12 and week 0 of Synbiotic 1 and Synbiotic 2 group, respectively. Population enrichment in 19 Genera and population depletion in 11 Genera were found in Synbiotic 1 group, as shown in Table 24. Moreover, population enrichment was also found in 4 Genera in Synbiotic 2 group, as shown in Table 25.

Table 16. Top 20 of relative abundance (%) from week 12 of the bacterial Genera in Control group (median ± IQR) showing on week 0 and week 12.

Control Genus	Week 0	Week 12
Muribaculaceae	17.110 ± 3.187	19.667 ± 8.719
<i>Ruminococcus</i>	5.204 ± 3.860	6.002 ± 0.701
UCG_005	1.558 ± 1.114	4.338 ± 3.343
Lachnospiraceae_NK4A136	6.987 ± 7.206	3.637 ± 6.778
Prevotellaceae_UCG_001	6.038 ± 4.367	3.067 ± 4.924
<i>Colidextribacter</i>	2.682 ± 1.083	2.903 ± 3.268
<i>Clostridia</i> _UCG_014	2.112 ± 1.190	2.803 ± 1.510
<i>Oscillibacter</i>	1.729 ± 0.539	1.965 ± 0.394
<i>Lactobacillus</i>	1.807 ± 0.528	1.783 ± 1.446
<i>Monoglobus</i>	0.631 ± 0.616	1.284 ± 0.852
<i>Bacteroides</i>	1.342 ± 0.535	1.212 ± 0.572
<i>Eubacterium siraeum</i>	1.442 ± 1.330	1.171 ± 1.103
<i>Eubacterium xylanophilum</i>	0.817 ± 0.505	1.055 ± 0.920
<i>Acetitomaculum</i>	0.000 ± 1.559	0.914 ± 2.097
<i>Roseburia</i>	1.885 ± 1.780	0.897 ± 1.808
RF39	1.081 ± 0.271	0.888 ± 0.343
<i>Gastranaerophilales</i>	1.705 ± 1.037	0.722 ± 0.259
<i>Phascolarctobacterium</i>	0.596 ± 0.939	0.685 ± 1.899
<i>Eubacterium coprostanoligenes</i>	0.908 ± 1.841	0.601 ± 0.909
Prevotellaceae_NK3B31	1.902 ± 3.409	0.536 ± 0.814

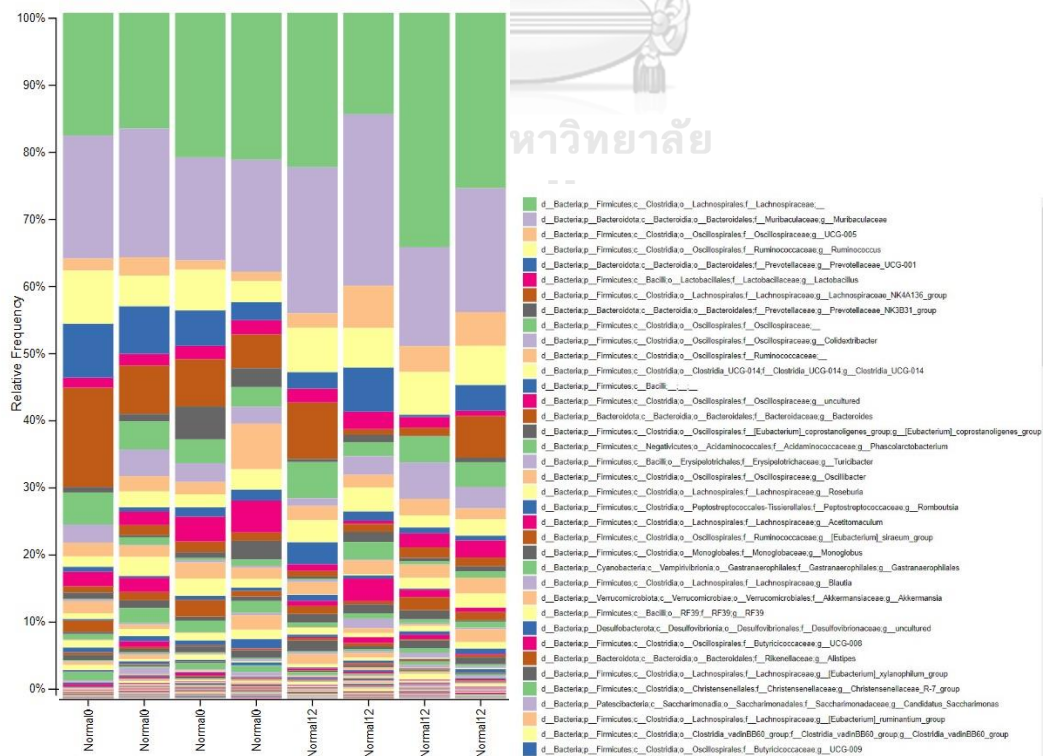


Table 17. Top 20 of relative abundance (%) from week 12 of the bacterial Genera in CKD group (median \pm IQR) showing on week 0 and week 12.

CKD	Week 0	Week 12
Genus		
Muribaculaceae	18.241 \pm 8.406	24.593 \pm 12.668
<i>Ruminococcus</i>	2.183 \pm 2.563	10.514 \pm 7.193
UCG_005	5.688 \pm 6.273	8.485 \pm 5.883
Lachnospiraceae_NK4A136	3.493 \pm 1.989	2.829 \pm 1.011
Prevotellaceae_UCG_001	1.297 \pm 1.115	2.641 \pm 0.906
<i>Colidextribacter</i>	0.205 \pm 0.522	2.481 \pm 1.788
<i>Clostridia</i> _UCG_014	0.558 \pm 0.555	2.248 \pm 1.418
<i>Oscillibacter</i>	1.431 \pm 0.998	1.936 \pm 1.805
<i>Lactobacillus</i>	1.308 \pm 1.636	1.822 \pm 0.795
<i>Monoglobus</i>	1.327 \pm 2.023	1.818 \pm 1.312
<i>Bacteroides</i>	0.000 \pm 0.052	1.716 \pm 1.529
<i>Eubacterium siraeum</i>	7.223 \pm 6.879	1.316 \pm 1.292
<i>Eubacterium xylanophilum</i>	0.596 \pm 0.826	1.152 \pm 1.244
<i>Acetivomaculum</i>	0.093 \pm 0.307	1.078 \pm 1.300
<i>Roseburia</i>	0.132 \pm 0.136	0.711 \pm 0.589
RF39	0.220 \pm 0.199	0.642 \pm 2.536
<i>Gastranaerophilales</i>	2.669 \pm 1.385	0.638 \pm 0.636
<i>Phascolarctobacterium</i>	0.086 \pm 0.401	0.581 \pm 0.841
<i>Eubacterium coprostanoligenes</i>	0.130 \pm 0.099	0.573 \pm 0.278
Prevotellaceae_NK3B31	0.718 \pm 0.599	0.495 \pm 0.900

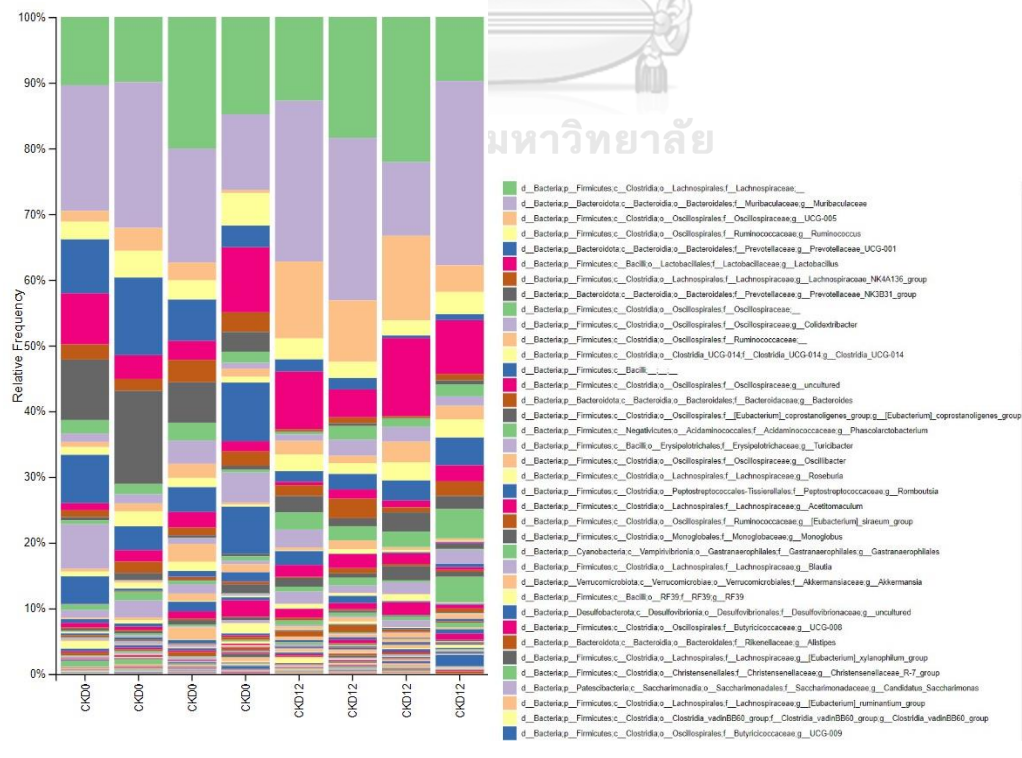


Table 18. Top 20 of relative abundance (%) from week 12 of the bacterial Genera in COS group (median \pm IQR) showing on week 0 and week 12.

COS	Week 0	Week 12
Genus		
Muribaculaceae	13.573 \pm 9.007	15.611 \pm 9.515
UCG_005	2.021 \pm 2.421	6.745 \pm 3.494
<i>Ruminococcus</i>	5.554 \pm 3.248	6.590 \pm 0.730
<i>Lactobacillus</i>	2.155 \pm 1.789	6.408 \pm 6.578
<i>Clostridia_UCG_014</i>	1.772 \pm 0.672	3.501 \pm 1.884
Lachnospiraceae_NK4A136	4.502 \pm 3.490	2.276 \pm 1.715
<i>Colidextribacter</i>	1.984 \pm 1.378	2.215 \pm 1.786
<i>Phascolarctobacterium</i>	0.525 \pm 0.156	2.019 \pm 1.161
<i>Monoglobus</i>	0.065 \pm 0.308	1.826 \pm 2.145
Prevotellaceae_UCG_001	5.943 \pm 1.681	1.567 \pm 4.034
<i>Roseburia</i>	1.599 \pm 1.459	1.377 \pm 1.239
<i>Acetitomaculum</i>	0.115 \pm 0.363	1.249 \pm 2.485
RF39	0.642 \pm 0.517	1.150 \pm 0.645
<i>Eubacterium coprostanoligenes</i>	1.206 \pm 1.759	1.014 \pm 1.529
<i>Bacteroides</i>	1.513 \pm 0.920	1.005 \pm 2.334
<i>Eubacterium siraeum</i>	0.398 \pm 0.247	0.925 \pm 0.791
<i>Eubacterium xylanophilum</i>	0.447 \pm 0.442	0.852 \pm 0.804
<i>Alistipes</i>	0.333 \pm 2.818	0.834 \pm 1.982
<i>Candidatus saccharimonas</i>	0.287 \pm 0.360	0.748 \pm 0.607
UCG_008	0.249 \pm 0.160	0.702 \pm 0.887

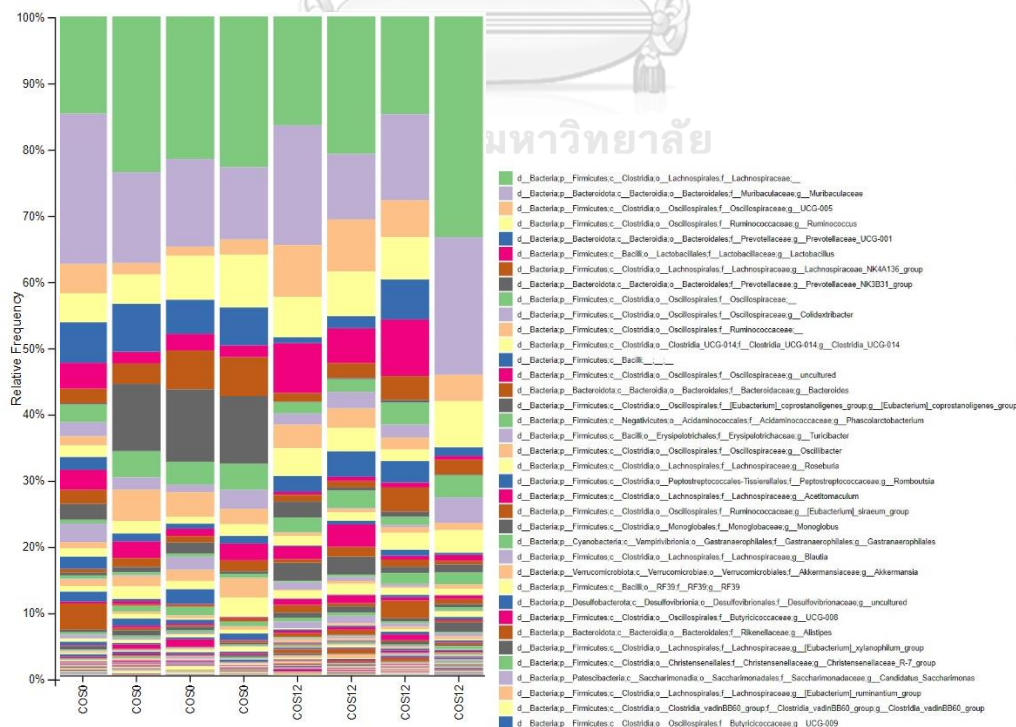


Table 19. Top 20 of relative abundance (%) from week 12 of the bacterial Genera in Inulin group (median ± IQR) showing on week 0 and week 12.

Inulin	Week 0	Week 12
Genus		
Muribaculaceae	19.535 ± 7.347	15.068 ± 13.394
UCG_005	2.457 ± 2.188	7.545 ± 8.018
<i>Colidextribacter</i>	2.034 ± 1.007	3.929 ± 4.439
<i>Ruminococcus</i>	6.319 ± 1.103	3.732 ± 2.671
<i>Clostridia_UCG_014</i>	2.518 ± 0.735	2.734 ± 0.775
<i>Eubacterium coprostanoligenes</i>	1.316 ± 0.490	2.447 ± 1.038
<i>Oscillibacter</i>	1.236 ± 0.408	2.137 ± 2.370
<i>Phascolarctobacterium</i>	0.795 ± 1.098	1.893 ± 2.009
<i>Lactobacillus</i>	4.197 ± 0.279	1.671 ± 3.798
Lachnospiraceae_NK4A136	1.831 ± 1.911	1.573 ± 3.195
Prevotellaceae_UCG_001	5.801 ± 2.315	1.534 ± 3.445
<i>Acetitomaculum</i>	0.804 ± 1.301	1.327 ± 2.341
<i>Monoglobus</i>	0.545 ± 1.032	1.273 ± 1.576
<i>Bacteroides</i>	0.847 ± 0.401	1.068 ± 0.553
<i>Alistipes</i>	0.374 ± 0.464	1.063 ± 1.016
<i>Eubacterium ruminantium</i>	0.000 ± 0.000	1.022 ± 0.956
<i>Eubacterium siraeum</i>	1.359 ± 0.463	0.973 ± 0.853
<i>Roseburia</i>	1.329 ± 1.102	0.869 ± 0.506
<i>Candidatus saccharimonas</i>	0.164 ± 0.316	0.689 ± 0.954
RF39	0.540 ± 0.982	0.622 ± 0.654

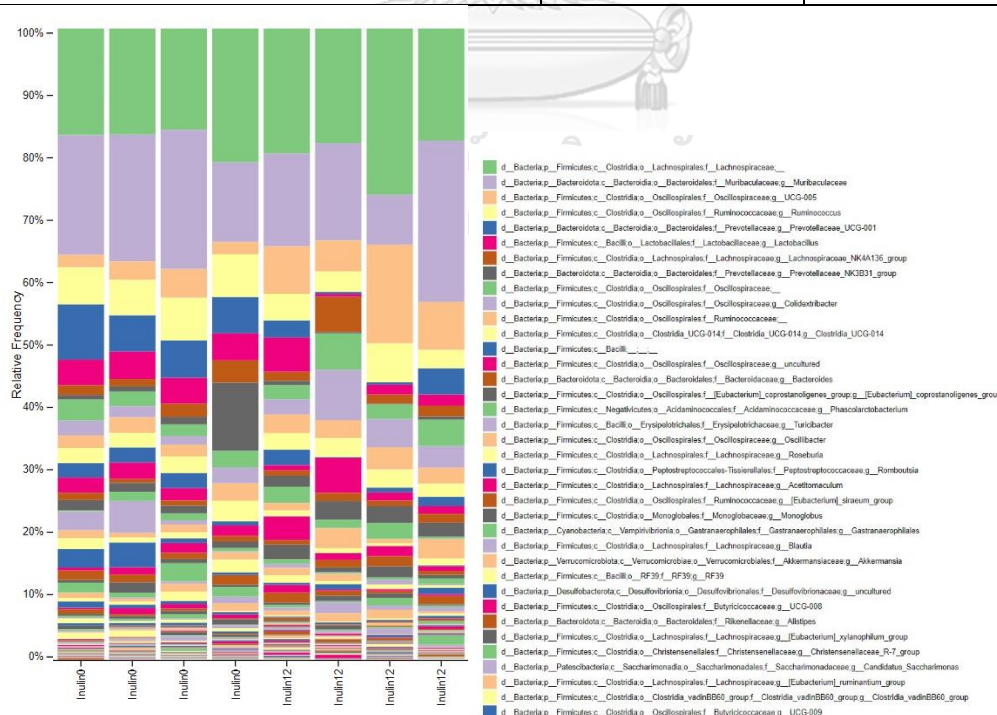


Table 20. Top 20 of relative abundance (%) from week 12 of the bacterial Genera in Maltodextrin group (median ± IQR) showing on week 0 and week 12.

Maltodextrin	Week 0	Week 12
Genus		
Muribaculaceae	17.664 ± 4.673	23.199 ± 13.534
UCG_005	2.373 ± 0.827	6.350 ± 10.674
<i>Lactobacillus</i>	6.806 ± 2.072	4.420 ± 3.768
<i>Ruminococcus</i>	3.750 ± 3.611	2.972 ± 1.755
Prevotellaceae_UCG_001	7.041 ± 4.237	2.565 ± 1.464
<i>Colidextribacter</i>	0.830 ± 1.376	2.202 ± 2.949
<i>Clostridia</i> _UCG_014	1.913 ± 1.511	2.114 ± 1.181
<i>Monoglobus</i>	0.488 ± 1.231	1.511 ± 1.903
<i>Eubacterium coprostanoligenes</i>	1.163 ± 1.577	1.429 ± 2.191
<i>Phascolarctobacterium</i>	0.841 ± 0.895	1.385 ± 2.231
Lachnospiraceae_NK4A136	2.213 ± 1.886	1.182 ± 2.002
<i>Oscillibacter</i>	0.508 ± 1.097	1.130 ± 2.150
<i>Acetitomaculum</i>	0.162 ± 1.104	1.022 ± 1.887
<i>Roseburia</i>	0.281 ± 1.972	0.888 ± 1.048
<i>Bacteroides</i>	1.027 ± 1.511	0.869 ± 1.308
UCG_008	0.465 ± 0.442	0.644 ± 1.424
<i>Gastranaerophilales</i>	1.316 ± 2.097	0.532 ± 2.087
<i>Romboutsia</i>	2.129 ± 5.993	0.525 ± 4.614
<i>Allobaculum</i>	0.063 ± 0.126	0.523 ± 1.413
<i>Blautia</i>	0.527 ± 0.361	0.508 ± 4.217

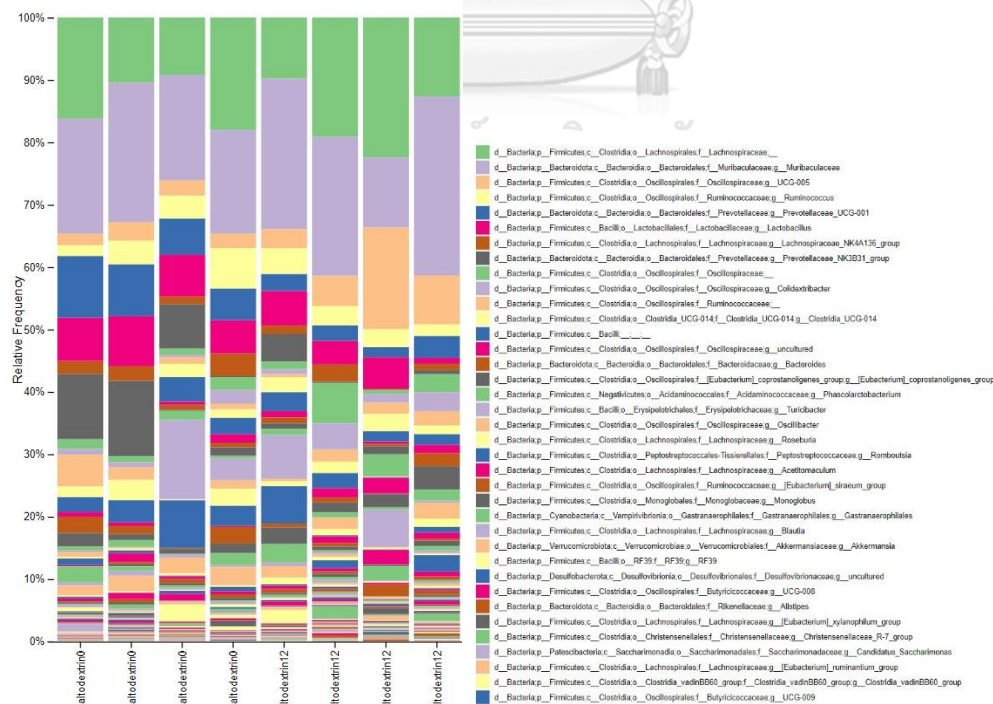


Table 21. Top 20 of relative abundance (%) from week 12 of the bacterial Genera in *L. casei* group (median \pm IQR) showing on week 0 and week 12.

L. casei	Week 0	Week 12
Genus		
Muribaculaceae	15.461 \pm 6.477	22.405 \pm 4.432
UCG_005	1.442 \pm 7.408	5.018 \pm 3.614
<i>Ruminococcus</i>	3.791 \pm 4.833	4.150 \pm 1.721
<i>Colidextribacter</i>	3.168 \pm 0.442	3.955 \pm 3.282
Lachnospiraceae_NK4A136	5.531 \pm 5.998	3.225 \pm 2.800
<i>Eubacterium coprostanoligenes</i>	0.685 \pm 0.707	2.853 \pm 1.583
<i>Clostridia</i> _UCG_014	1.513 \pm 1.928	2.256 \pm 0.695
<i>Alistipes</i>	0.281 \pm 0.312	2.181 \pm 1.898
<i>Eubacterium siraeum</i>	0.551 \pm 1.183	1.599 \pm 1.250
<i>Oscillibacter</i>	1.379 \pm 0.911	1.459 \pm 1.357
Prevotellaceae_Ga6A1	0.692 \pm 1.350	1.405 \pm 1.693
<i>Acetitomaculum</i>	0.039 \pm 0.412	1.403 \pm 1.988
<i>Monoglobus</i>	0.203 \pm 0.992	1.364 \pm 1.132
<i>Roseburia</i>	0.465 \pm 0.412	1.251 \pm 0.635
<i>Phascolarctobacterium</i>	0.990 \pm 2.937	1.104 \pm 1.955
<i>Eubacterium ruminantium</i>	0.668 \pm 1.136	1.022 \pm 1.570
RF39	0.609 \pm 0.869	0.973 \pm 0.743
<i>Eubacterium xylanophilum</i>	0.367 \pm 0.193	0.834 \pm 0.871
<i>Lactobacillus</i>	2.179 \pm 6.920	0.733 \pm 0.886
<i>Bacteroides</i>	1.115 \pm 0.461	0.705 \pm 0.151

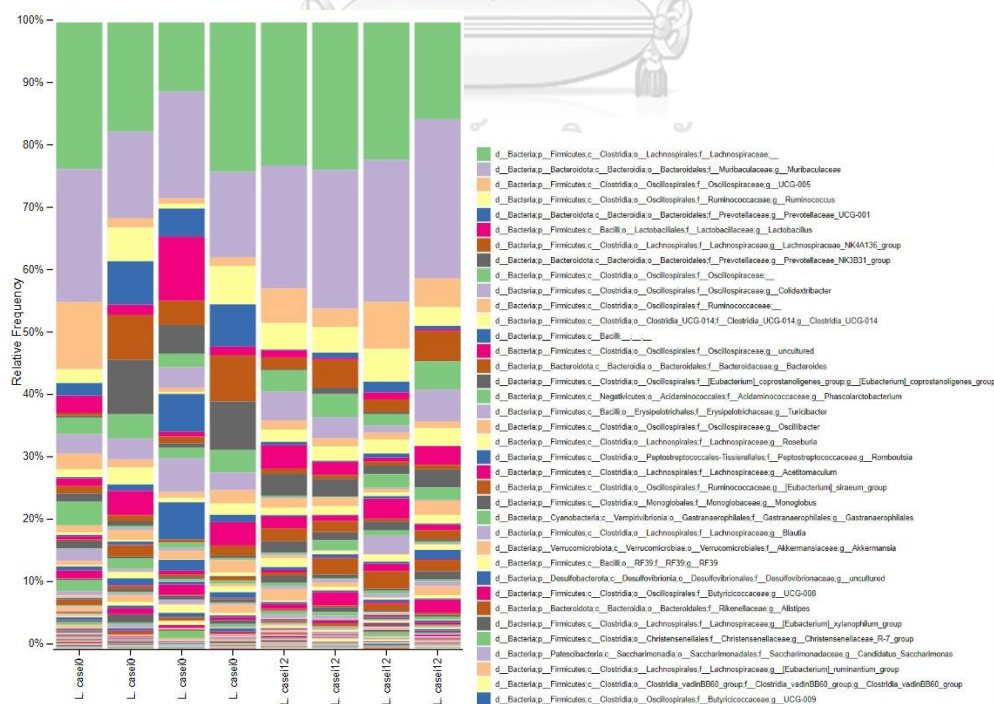


Table 22. Top 20 of relative abundance (%) from week 12 of the bacterial Genera in Synbiotic 1 group (median ± IQR) showing on week 0 and week 12.

Synbiotic 1	Week 0	Week 12
Genus		
Muribaculaceae	14.984 ± 2.609	11.277 ± 9.008
UCG_005	2.181 ± 2.475	9.741 ± 9.088
<i>Ruminococcus</i>	2.792 ± 3.096	5.883 ± 3.540
<i>Bacteroides</i>	0.888 ± 0.753	3.259 ± 4.048
<i>Colidextribacter</i>	2.723 ± 1.123	2.846 ± 1.583
<i>Phascolarctobacterium</i>	0.916 ± 0.557	2.529 ± 2.130
<i>Eubacterium_coprostanoligenes</i>	0.759 ± 0.702	2.392 ± 1.349
<i>Clostridia_UCG_014</i>	2.137 ± 0.830	2.388 ± 2.447
<i>Acetitomaculum</i>	0.175 ± 0.146	1.742 ± 2.134
<i>Monoglobus</i>	0.296 ± 0.308	1.422 ± 1.489
<i>Oscillibacter</i>	1.625 ± 0.701	1.349 ± 0.983
<i>Lactobacillus</i>	3.754 ± 2.645	1.078 ± 2.671
<i>Candidatus_saccharimonas</i>	0.341 ± 0.354	0.996 ± 1.027
Lachnospiraceae_NK4A136	4.893 ± 2.300	0.888 ± 2.501
Prevotellaceae_UCG_001	5.598 ± 2.812	0.867 ± 2.237
<i>Blautia</i>	0.588 ± 0.604	0.735 ± 1.145
<i>Roseburia</i>	2.684 ± 1.447	0.722 ± 0.387
<i>Eubacterium_ruminantium</i>	0.000 ± 0.222	0.700 ± 0.816
Christensenellaceae_R_7	0.257 ± 0.269	0.642 ± 0.564
RF39	0.577 ± 0.828	0.640 ± 0.424

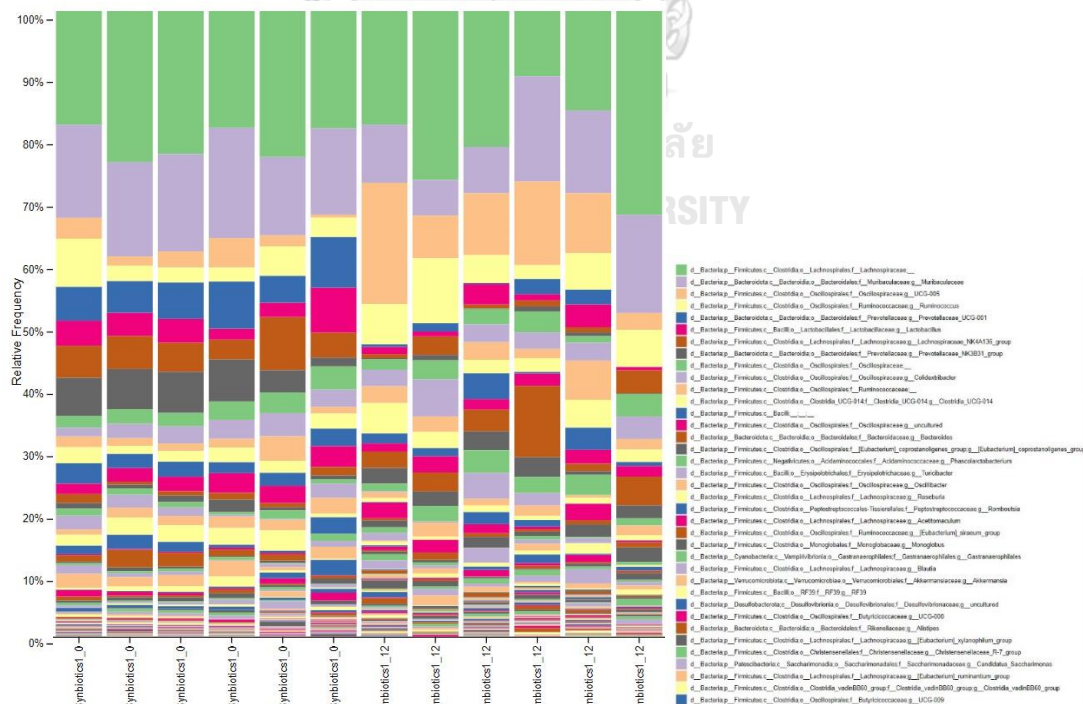


Table 23. Top 20 of relative abundance (%) from week 12 of the bacterial Genera in Synbiotics 2 group (median \pm IQR) showing on week 0 and week 12.

Synbiotic 2	Week 0	Week 12
Genus		
Muribaculaceae	16.914 \pm 12.313	13.387 \pm 4.850
UCG_005	2.848 \pm 5.920	12.457 \pm 10.810
<i>Ruminococcus</i>	1.686 \pm 4.074	5.014 \pm 0.832
<i>Clostridia_UCG_014</i>	0.938 \pm 1.340	3.116 \pm 2.166
<i>Colidextribacter</i>	1.794 \pm 3.114	3.013 \pm 2.027
<i>Phascolarctobacterium</i>	1.578 \pm 2.351	2.840 \pm 2.697
<i>Lactobacillus</i>	4.850 \pm 1.878	2.438 \pm 4.093
<i>Acetitomaculum</i>	0.000 \pm 1.254	2.356 \pm 0.651
<i>Eubacterium coprostanoligenes</i>	0.579 \pm 0.906	1.586 \pm 1.487
<i>Oscillibacter</i>	0.795 \pm 0.733	1.435 \pm 1.245
RF39	0.346 \pm 0.730	1.413 \pm 0.709
Prevotellaceae_UCG_001	6.544 \pm 5.464	1.115 \pm 5.027
Lachnospiraceae_NK4A136	4.119 \pm 6.285	1.076 \pm 3.836
<i>Bacteroides</i>	1.016 \pm 2.196	0.921 \pm 0.590
<i>Turicibacter</i>	1.820 \pm 3.635	0.912 \pm 1.632
<i>Candidatus saccharimonas</i>	0.450 \pm 0.357	0.843 \pm 0.988
<i>Gastranaerophilales</i>	0.584 \pm 0.612	0.735 \pm 0.936
<i>Monoglobus</i>	0.000 \pm 0.465	0.605 \pm 1.686
<i>Roseburia</i>	1.331 \pm 1.800	0.540 \pm 1.496
<i>Elusimicrobium</i>	0.000 \pm 0.045	0.536 \pm 0.612

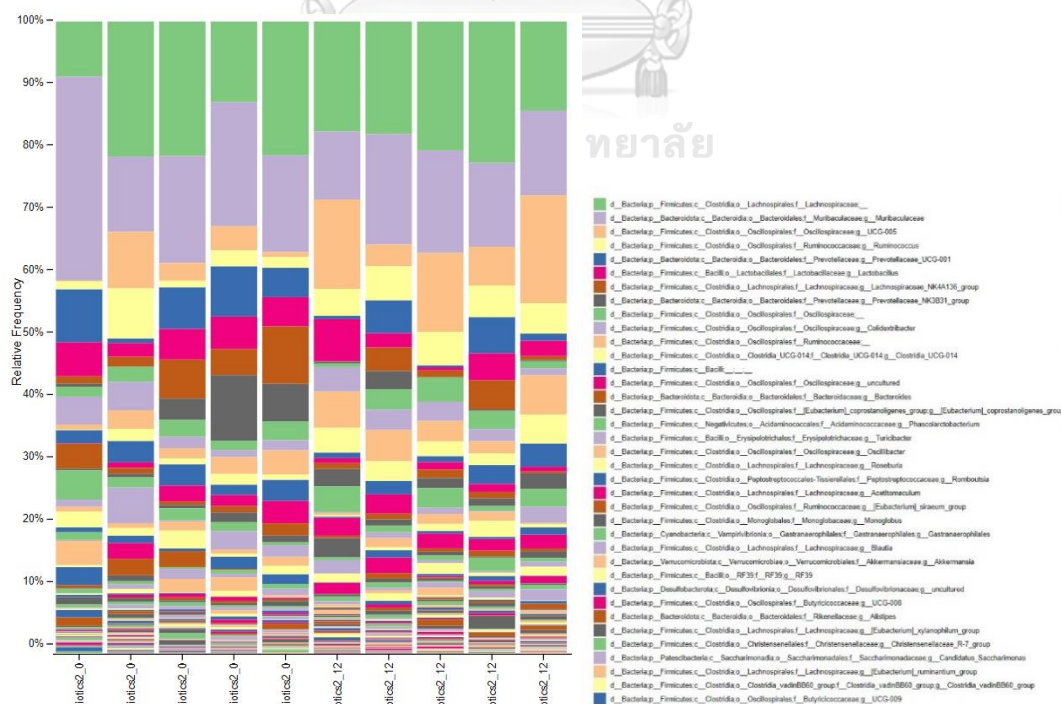


Table 24. Median and IQR of the difference of relative abundance between week 12 and week 0 in synbiotic 1 group.

Synbiotic 1	Median	IQR	p-value	Change
Genus				
Prevotellaceae_NK3B31_group	-5.736 ± 3.494		0.028	Depletion
Prevotellaceae_UCG-001	-5.051 ± 2.978		0.028	Depletion
Lachnospiraceae_NK4A136_group	-3.155 ± 3.537		0.028	Depletion
<i>Roseburia</i>	-1.820 ± 1.484		0.046	Depletion
<i>Akkermansia</i>	-1.580 ± 1.339		0.028	Depletion
<i>Lachnoclostridium</i>	-0.400 ± 0.371		0.028	Depletion
UCG-009	-0.318 ± 0.291		0.028	Depletion
<i>Clostridium sensu stricto</i> _1	-0.292 ± 0.401		0.028	Depletion
GCA-900066575	-0.078 ± 0.108		0.046	Depletion
Lachnospiraceae_FCS020_group	-0.032 ± 0.052		0.043	Depletion
Lachnospiraceae_UCG-006	-0.019 ± 0.207		0.027	Depletion
UCG-007	0.000 ± 0.006		0.028	Enrichment
<i>Anaerovorax</i>	0.035 ± 0.063		0.042	Enrichment
<i>Muribaculum</i>	0.035 ± 0.039		0.026	Enrichment
[<i>Eubacterium</i>] <i>_fissicatena_group</i>	0.104 ± 0.279		0.028	Enrichment
<i>Negativibacillus</i>	0.108 ± 0.225		0.046	Enrichment
<i>Oscillospira</i>	0.112 ± 0.346		0.046	Enrichment
<i>Butyricimonas</i>	0.164 ± 0.186		0.028	Enrichment
<i>Sellimonas</i>	0.238 ± 0.136		0.042	Enrichment
<i>Allobaculum</i>	0.320 ± 0.331		0.028	Enrichment
<i>Elusimicrobium</i>	0.350 ± 0.548		0.028	Enrichment
Christensenellaceae_R-7_group	0.421 ± 0.495		0.046	Enrichment
<i>Alloprevotella</i>	0.450 ± 0.551		0.028	Enrichment
<i>Candidatus saccharimonas</i>	0.521 ± 1.152		0.028	Enrichment
<i>Monoglobus</i>	1.126 ± 1.486		0.046	Enrichment
[<i>Eubacterium</i>] <i>_coprostanoligenes_group</i>	1.517 ± 0.906		0.028	Enrichment
<i>Acetitomaculum</i>	1.580 ± 2.107		0.028	Enrichment
<i>Phascolarctobacterium</i>	1.666 ± 1.981		0.028	Enrichment
<i>Bacteroides</i>	2.671 ± 4.000		0.028	Enrichment
UCG-005	7.560 ± 5.924		0.028	Enrichment

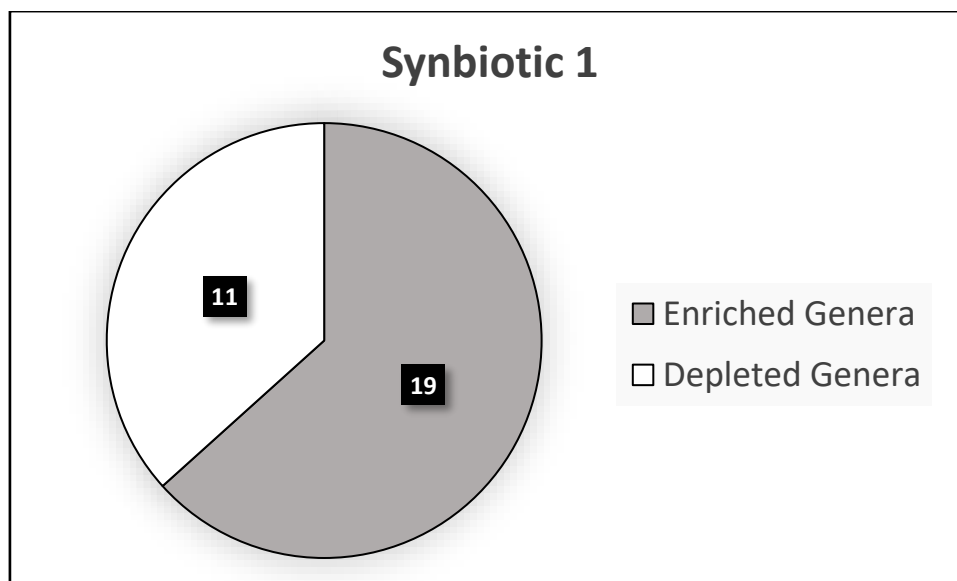


Figure 68. Proportion of the significant change in relative abundance of bacteria genus in Synbiotic 1 group.

Table 25. Median and IQR of the difference of relative abundance between week 12 and week 0 in synbiotic 2 group.

Synbiotic 2	Median	IQR	p-value	Change
Genus				
Clostridia_UCG-014	1.426 ±	3.129	0.043	Enrichment
NK4A214_group	0.134 ±	0.132	0.028	Enrichment
Angelakisella	0.048 ±	0.102	0.042	Enrichment
Frisingicoccus	0.026 ±	0.056	0.042	Enrichment

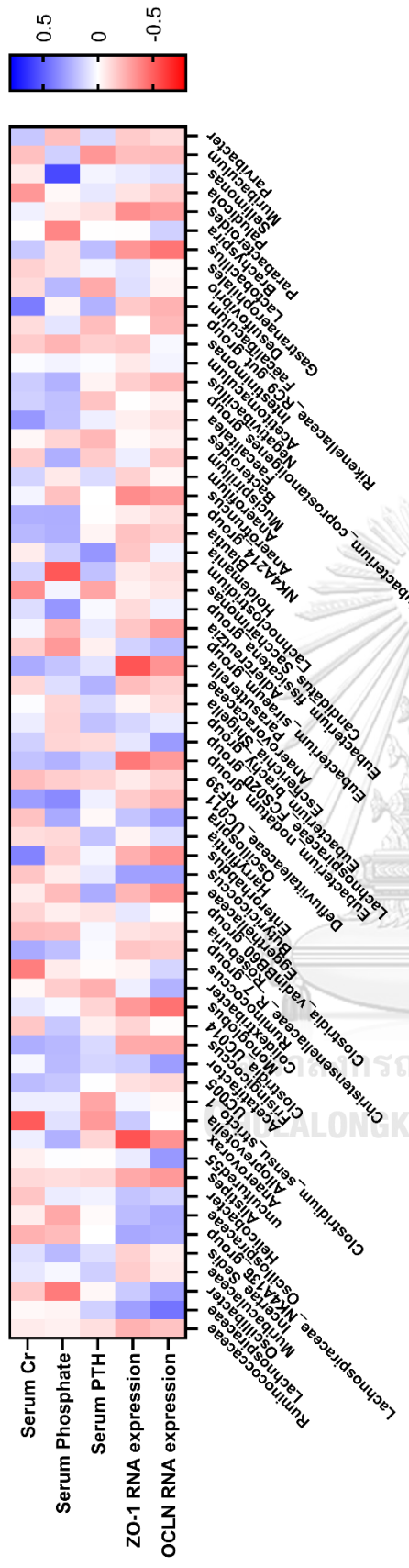


Figure 69. Heat map representing correlation between relative abundance of intestinal bacteria and blood parameters and RNA expression of tight junctions.

Colors represent the Pearson correlation. Red represents negative correlation and blue represents positive correlation.

Chapter 5

Discussion

5.1 Screening of probiotic candidates

The feces were collected from nine healthy participants who had not consumed any medications or commercial probiotic products, such as (148) yogurt or probiotic supplements, for four weeks to minimize intervention. Following this, hundreds of bacterial isolates were tested for transepithelial electrical resistance (TEER) in order to evaluate the integrity of the epithelial barrier.

The bacterial isolates were selected based on their ability promote gut integrity, determined by TEER measurement and tight junction gene expression, and anti-inflammation. Desired bacterial isolates showed an increase in TEER value, indicating an improvement in gut barrier integrity. Inflammation of the epithelial cell is known to reduce the integrity of the epithelial barrier. Therefore, anti-inflammatory properties of the bacterial isolates were also considered, in addition to their ability to improve gut barrier integrity. *Bifidobacterium longum* BFS3-09 and *Lactobacillus salivarius* LBR2-28 (temporary name) were selected as they contained the desirable properties including anti-inflammation and TEER-enhancing. In addition, both species was approved to be used as the food probiotic based on the regulation of the Thai Ministry of Public Health.

5.2 *In vitro* study on prebiotics

From the *in vitro* studies, MTT-cell viability assay revealed the adverse effect on cell viability of Caco2 cells at different concentrations. At the concentration of 1000 µg/mL, all the tested prebiotic substances resulted in less than 10% cell viability compared to the control (cells treated by phosphate buffer saline, PBS). While COS

and inulin at the concentration of 500 $\mu\text{g}/\text{mL}$ did not affect the viability of cells, maltodextrin had an adverse effect.

High concentrations of oligosaccharides may affect intestinal epithelial cells, depending on several factors such as the type of oligosaccharide, duration of exposure, and other conditions. Excessive absorption of oligosaccharides by cells may disrupt normal cellular functions, including the initiation of cellular inflammation and the inhibition of enzyme functions. Moreover, an osmotic stress may occur when there is a difference in the concentration of solutes on either side of a cell membrane, resulting in the movement of water across the membrane to balance the concentration. The effect is inversely proportional to the molecular weight, with lower molecular weight compounds exhibiting a greater effect (170).

Chitosan oligosaccharides (COS) are known to have beneficial effects on intestinal epithelial cells, including promoting cell proliferation and differentiation, enhancing barrier function, and reducing inflammation. However, high concentrations of COS can induce adverse effects on intestinal epithelial cells, including cell death or disruption of tight junctions. Wang *et al.* (2021) conducted an experiment to test the viability of COS on Caco2 cells and reported results similar to ours. They found that treatment with 1000 $\mu\text{g}/\text{mL}$ of high-molecular-weight COS significantly decreased cell viability compared to the vehicle, with a p-value of <0.05 . However, they also observed a significant reduction in cell viability in the 500 $\mu\text{g}/\text{mL}$ treatment group compared to the control (171), which contradicts our findings that demonstrated only a slight decrease in viability that was not significantly different. It is worth noting that Wang and his team treated the prebiotic for only four hours, while we administered it for a 24-hour period. This discrepancy may indicate that the cells in our study had time to acclimate to the treatment and that viability was restored overnight. To clarify this suggestion, the cell viability may be evaluated at sequential time point to determine the cell response to the treatments. To clarify this suggestion, it may be beneficial to evaluate cell viability at sequential time points to determine the response of the cells to the treatments. This will help determine if the cells undergo a transient decrease in viability followed by recovery.

According to Uerlings *et al.* (2020), the viability of IPEC-J2 cells (pig intestinal epithelial cells) was reduced to 50% by 750 $\mu\text{g/mL}$ of inulin, while 500 $\mu\text{g/mL}$ of inulin did not show any such reduction at the 12 hours of the treatment (172). However, there is no report on the viability of cells treated with a high concentration of maltodextrin. Nagaraju *et al.* (2020) only reported that 200 $\mu\text{g/mL}$ of maltodextrin had no adverse effects on HIEC-6 (Human intestinal epithelial cell line) (173). These results are consistent with the findings in this report.

Prebiotics are believed to promote human health by providing nutrients for beneficial bacteria and stimulating the production of short-chain fatty acids (SCFAs) by these bacteria. However, recent studies have suggested that prebiotics might also promote intestinal health independently of the probiotic bacteria. For instance, Wang *et al.* (2021) reported that 200 $\mu\text{g/mL}$ of COS increased the expression of occludin, a tight junction protein, in Caco2 cells which the cells' barrier integrity being disrupted by 2% DDS (dextran sulfate sodium-induced colitis cell) after 24 hours of treatment. (171). The results in our finding showed that 100 $\mu\text{g/mL}$ of COS could promote the expression of tight junction protein, ZO-1 and occludin, though the effect on claudin-1 remained unclear. Although inulin is known to be a dietary fiber that selectively stimulates the growth and activity of beneficial gut bacteria, leading to improvements in gut health and overall wellbeing (174, 175), our results showed that COS and maltodextrin had a greater effect on promoting the expression of tight junction proteins compared to inulin.

Prebiotics have been suggested to enhance gut barrier integrity, as demonstrated by their effects on TEER values in various studies. For instance, Mehmood *et al.* (2022) reported that 100 $\mu\text{g/mL}$ of COS significantly increases TEER value in T84 cells, human colonic epithelial cell, that had disrupted barrier integrity due to Afatinib treatment, at both 24 and 48 hours post-treatment (176). Similarly, Akbari *et al.* (2017) found that treatment with inulin led to a significant increase in TEER values in Caco-2 cells (177). However, our results demonstrated that only TGF- β treatment led to a significant increase in %TEER. Although inulin and maltodextrin showed a promising trend in promoting TEER value, the increase was not statistically significant in our study. In our study, we also induced

inflammation in Caco-2 cells, resulting in disrupted barrier integrity as indicated by a significant decrease in %TEER compared to healthy cells. Interestingly, treatment with 100 µg/mL inulin and maltodextrin resulted in the recovery of %TEER, which was significantly higher than that of inflamed cells treated by vehicle. These results suggest that they may have beneficial effects on gut barrier integrity, under inflammatory conditions. However, unlike a previous study using a different type of cell (176), our study did not find a significant increase in %TEER in cells treated with COS compared to inflamed cells treated by vehicles.

5.3 Animal experiments

a. Treatment formulae

Our *in vitro* studies have demonstrated the promising potential benefits of prebiotics on the promotion of gut barrier integrity. We further investigated the effect of each prebiotic individually in animal models. However, the combination of prebiotics and probiotics, known as synbiotics, has gained increasing attention in recent years for their potential to enhance gut microbiota and improve health outcomes. Synbiotics are believed to provide a more effective means of modulating the gut microbiota compared to prebiotics or probiotics alone. Despite their promising potential benefits, more research is needed to fully understand the mechanisms of action and optimal usage of synbiotics. To this end, we developed a synbiotic formula that combined two bacterial isolates with two prebiotics, inulin, and COS. In addition, we also included maltodextrin in another formula, which has fewer studies investigating its effects as a synbiotic.

b. Animal wellbeing

The results of this study suggest that chronic kidney disease (CKD) has a negative impact on the weight of rats. The weight of CKD rats in all groups was significantly lower than that of the control group throughout the 12 weeks of treatment. As it is common that CKD can lead to poor appetite, malnutrition, and weight loss. None of the treatment groups were able to completely restore the body weight of CKD rats to that of the healthy control group, indicating that the treatments

did not fully mitigate the effects of CKD on body weight. Although the weight differences were not statistically significant between the treatment groups and the CKD group, some treatment groups, COS and synbiotic 1, did show a trend towards higher body weights, suggesting that they may have a beneficial effect on weight in CKD rats. The weight-gaining observed in CKD rats across all treatment groups may be attributed to the potential of the prebiotics to elevate short-chain fatty acid (SCFA) production. SCFAs are known to have beneficial effects on weight regulation and metabolism (175). It is suggested that the elevated SCFA levels may contribute to increased energy extraction from the diet and promote weight gain.

c. Serum creatinine

The serum creatinine levels in the cisplatin-induced CKD rats were significantly elevated, indicating renal dysfunction and damage. However, at the beginning of the treatment (week 0), we observed a recovery of serum creatinine level in all treatment groups, indicating renal recovery. A single dose of 10 mg/kg of cisplatin was used in our pilot study which caused high mortality. In this experiment, the intraperitoneal injections of cisplatin were split in 2 doses of 5 mg/kg each, with a 3-day interval. Although the CKD group exhibited significantly higher serum creatinine levels than the control group, the values did not exceed 2 to 3 times that of the control group, indicating a mild degree kidney injury. Similar results were reported by Shi *et al.* (2018) which reported a significant increase in serum creatinine levels of approximately 0.4 mg/dL after 8 weeks of administering 10 mg/kg cisplatin. (178). The higher serum creatinine level in our results compared to those reported by Shi may be attributed to the 1% phosphoric acid added to the drinking water. After 12 weeks of the treatments, there was no significant difference in serum creatinine in any treatment group compared to CKD. Our result suggested that prebiotics or probiotics could not restore kidney function, similar to previous studies that showed no evidence of prebiotics or probiotics could cure the kidney impairment and restore the serum creatinine level.

Even though cisplatin-induced nephrotoxicity is a well-established method to induce CKD in animal models, the effect of the administration was inconsistent. One

alternative method that has levels of oxidative stress and inflammation is adenine-induced CKD model. This method has advantages over cisplatin-induced CKD in terms of lower mortality rates and more consistent induction of CKD. In addition, adenine-induced CKD more closely mimics the chronic and progressive nature of human CKD. However, adenine-induced CKD requires longer induction periods and continuous administration during the whole experiment to yield the stable CKD status. This model can be considered for use in future studies.

d. Serum phosphate

The serum phosphate level in normal rats is influenced by various factors such as phosphate intake, renal excretion, bone absorption and resorption, and fecal excretion. In our study, high phosphorus intake was induced by adding 1% of phosphoric acid, then the serum phosphate level of the rats in the normal group was approximately 12 mg/dL, which is twice as high as that of a healthy normal rat (approximately 6 mg/dL). We hypothesized that this was due to normal rats had normal appetite and drank more water than rats with CKD, although we could not verify this assumption since we did not record daily water intake. However, the serum phosphate in the normal group gradually decreased in week 8 and returned to normal by week 12.

In contrast, the serum phosphate level in the CKD group remained high at approximately 10 mg/dL throughout the 12-week experiment. Interestingly, in week 4 of the experiment, the rats treated with *L. casei* and both synbiotic formulae showed a significant lower in serum phosphate level compared to the CKD group, suggesting that probiotics may have a beneficial effect on regulating phosphate absorption. However, by week 8 of the experiment, the serum phosphate level in the *L. casei* group increased to a level that was not significantly different from the CKD group, suggesting that the phosphate-regulating effect of *L. casei* was temporary.

The mechanism of lower serum phosphate level in rats treated with probiotic (*L. casei*) and synbiotics could be due to their effect on gut microbiota. Theoretically, improvement of gut dysbiosis should ameliorate abnormal paracellular phosphate

absorption. However, our study showed that prebiotics supplementation alone could not exhibit those beneficial effects. It is also important to note that the use of maltodextrin as a prebiotic in Synbiotic 2 formula may have altered the gut microbiota in a way that compromised the long-term beneficial effects of the synbiotic formula. It might change the gut environment and may lead to the alteration of growth and function of beneficial bacteria that are important for gut health.

e. Serum parathyroid hormone and calcium and phosphate excretion

The lower serum PTH levels observed in the Synbiotic 1 group compared to the CKD group on week 12 seem to correspond with the serum phosphate results. The reduction in serum phosphate level mainly contributed to the reduction in PTH secretion and improvement of hyperparathyroidism. In CKD rats with hyperphosphatemia, hyperparathyroidism was observed which was similar to the study of Slatopolsky *et. al.* (1996) who reported that the elevation of serum phosphate at 10 to 12 mg/dL contributed to the elevation of the PTH of 300 to 400 pg/dL (179). PTH functions in an increase in calcium and decrease in phosphate reabsorption of the nephrons. The rats in the CKD group showed significantly higher excreted phosphate and lower excreted calcium, consistent with elevated PTH level.

The results of this study demonstrate that the Synbiotic 1 formula was effective in decreasing serum phosphate and PTH levels in rats with CKD but not significantly altering serum creatinine level. Low serum phosphate in CKD rats treated with synbiotics was unlikely due to the increased renal phosphate excretion, since our results showed no difference in phosphate excretion rate in these experimental rats compared to control CKD rats. We try to evaluate the fecal phosphate content in feces, but the result is uninterpretable since the phosphate intake of each rats cannot precisely measured.

f. Intestinal barrier integrity

We hypothesized that synbiotics should increase intestinal tight junction protein expression, like the observed result *in vitro* study. Unfortunately, the immunohistochemical studies were inconclusive. We assume that

immunohistochemistry might not be sensitive to detect the specimen from our experiment. Given that transcriptional expression is dynamic, qRT-PCR, which provides a snapshot of gene expression at a specific time point (in this case, the day the rats were sacrificed), may not accurately reflect the true extent of intestinal barrier integrity. To obtain more precise results, additional investigation using immunoblot analysis could be conducted in the further experiment. Additionally, it might be useful to measure the protein expression in different parts of the intestine to determine if the treatment had a differential effect on specific regions.

Our study did not directly measure the intestinal paracellular phosphate, as radioactive phosphate was required in the processes, but the animal center was not support for radioactive experiment. However, an alternative method to estimate the paracellular transport and gut leakage is the absorption of FITC-dextran assay. Thus, we considered that dextran has a different molecular size and mechanism of absorption compared with phosphate, making the results difficult to interpret. In the next study, we decided to use zonulin, a new biomarker for gut leakage, to evaluate gut leakage in CKD rats (180)

g. Bone density

The results of bone density present an unexpected outcome, as the CKD rats would develop mineral and bone disorder (MBD) according to the rat model used in this study did not progress to the severe stages of kidney disease. In addition, the duration of the study might not be enough to observe the manifestation of MBD in the rat model. CKD is a progressive disease, and the severity of MBD often corresponds to the duration and extent of kidney dysfunction. In this case, if the CKD rats were not in the advanced stages of the disease, it is plausible that the expected MBD-related changes did not have sufficient time to manifest. Moe *et.al.* (2009) reported that bone changes and mineralization defect were observed in the 34-week and 38-week CKD animal in polycystic kidney disease rat model (181). For further study, alternative CKD model may be considered together with a prolong experimental period to demonstrated an obvious CKD-MBD model. Moreover, computational analyses, such as ImageJ, would be conducted incorporating additional pathological parameters such

as bone formation rate, osteoclast surface, and mineralizing surface, thereby strengthening the evidence with greater concreteness.

h. Gut microbiota

The diversity and evenness of fecal bacteria increased over the course of the experiment, but this change was not significant within each treatment group individually. It may suggest that the small sample size has limited the ability to detect significant differences in diversity and evenness within each treatment group or the synbiotic dosage was not sufficient to alter the gut dysbiosis. We observed that some treatments such as *L. casei* and both Synbiotic formula have shown the trend of increasing diversity and evenness, a larger sample size may be necessary to detect more subtle changes in the microbiome composition that may have been missed.

The results showed significant changes in the relative abundance of different bacterial phyla before and after treatment. Specifically, the phylum Bacteroidota showed a significant decrease in relative abundance, while the phyla Elusimicrobacteria, Patescibacteria, and Spirochaetota showed a significant increase. The decrease in relative abundance of the phylum Bacteroidota observed in this study may be beneficial for gut health. While Bacteroidota are known to be abundant in the human gut and play an important role in the metabolism of dietary fiber, they are also opportunistic and can sometimes be pathogenic. Some studies have suggested that decreased Bacteroidetes abundance may be associated with a reduced risk of certain diseases, such as obesity and metabolic disorders. Therefore, the observed decrease in relative abundance of Bacteroidetes may be a positive outcome of the treatment and may have potential health benefits.

The Firmicutes/Bacteroidota (F/B) ratio has been linked to the maintenance of homeostasis, and alterations in this ratio can result in various pathological conditions. One instance is the development of obesity with increased abundance of certain Firmicutes species, while an increase in Bacteroidota species may lead to bowel inflammation (182, 183). In our results, the increased in F/B ratio with the significant decreased Bacteroidota may indicate the reduced the inflammation in rats treated with

synbiotic 1. Even though, the results showed the depletion in some beneficial genera, including *Roseburia* and *Akkermansia*, in rats treated with Synbiotic 1, many genera were found enriched, including *Anaerovorax*, *Muribaculum*, *Negativibacillus*, *Oscillospira*, *Butyricimonas*, *Sellimonas*, *Allobaculum*, *Elusimicrobium*, *Alloprevotella*, *Monoglobus*, *Acetitomaculum*, *Phascolarctobacterium*, and *Bacteroides*. Some of the genera were reported beneficial to gut health by reducing inflammation and involved in SCFA production such as *Oscillospira*, *Butyricimonas*, *Allobaculum*, *Phascolarctobacterium* (184-187). *Bacteroides* species which are associated with various inflammatory bowel diseases, including Crohn's disease and ulcerative colitis were found significantly increased. The reason for this increase is unclear and warrants further investigation. It is possible that the synbiotic treatment may have promoted the growth of *Bacteroides* indirectly by creating a more favorable environment for these bacteria to thrive. Even though bacterial enrichment also observed in Synbiotic 2 group, *Angelakisella* and *Frisingicoccus* are not well-studied in their effects on the intestinal health.

The Pearson correlation between the relative abundance of intestinal bacteria and five parameters: serum creatinine, serum phosphate, serum PTH, and the expression of tight junction proteins were studied to reveal the role in maintaining gut homeostasis. Beneficial bacteria are known to contribute to gut integrity and reduce phosphate absorption. We hypothesized that an increase in the relative abundance of beneficial bacteria would be associated with lower serum phosphate and PTH levels, indicative of enhanced gut integrity and reduced phosphate absorption. Interestingly, our results revealed a moderate positive correlation between serum phosphate and the genus *Sellimonas*, *NK4A214* group, and *Blautia*. This finding suggests that these bacteria may be involved in enhancing phosphate absorption within the gut. While this observation may appear contradictory to the previous study which reported that *Sellimonas intestinalis* might be an indicator of gut homeostasis recovery (188) and *Blautia* might be beneficial and function as probiotic (189).

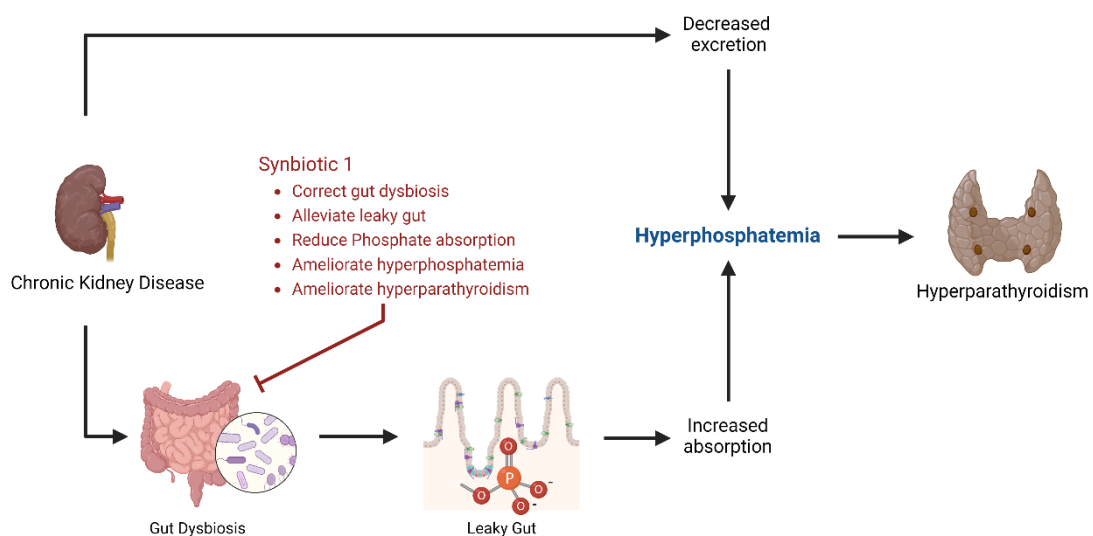
Our finding also reveals moderate negative correlation between the expression of tight junction proteins and several bacterial genera, including *Alistipes*, *Anaerovorax*, *Anaerotrunchus*, *Mucispirillum*, *Parabacteroides*, and *Muribaculum*.

These results suggest a potential association between these genera and the regulation of gut barrier function. Tight junction proteins play a crucial role in maintaining the integrity of the intestinal epithelial barrier, preventing the passage of harmful substances and pathogens from the gut lumen into the bloodstream. A decrease in the expression of tight junction proteins can compromise the integrity of the gut barrier, leading to increased intestinal permeability and potential translocation of bacteria or bacterial products into systemic circulation. Among the genera showing a negative correlation with tight junction expression, *Alistipes* (Phylum Bacteroidota) has been extensively studied in the context of gut health. Bacteroidota are frequently linked to chronic intestinal inflammation. Parker *et. al.* (2020) also reviewed that 13 species of *Alistipes* genus are highly relevant in dysbiosis and diseases (190). Therefore, the negative correlation observed with *Alistipes* in our study may suggest a potential detrimental role of certain species within this genus in relation to gut barrier function. *Mucispirillum* (Phylum Deferribacterota), *Parabacteroides* (Phylum Bacteroidota), and *Muribaculum* (Phylum Bacteroidota) are other genera that exhibited a negative correlation with tight junction expression in our study. *Mucispirillum* has been associated with intestinal inflammation, and its overgrowth has been observed in various models of colitis (191). *Parabacteroides* species have been reported as potential pathogens in certain contexts, with some strains being implicated in gut dysbiosis and inflammatory bowel diseases (192). *Muribaculum*, on the other hand, has been less extensively studied, but its negative correlation with tight junction expression suggests a potential association with compromised gut barrier function.

Chapter 6

Conclusion

The results of this study demonstrate that the synbiotic 1 formula, composed of COS, inulin, *Lactobacillus salivarius* LBR2-28, and *Bifidobacterium longum* BFS3-09 was effective in reduction of serum phosphate and PTH levels in rats with CKD without significantly altering serum creatinine and calcium levels. The decreased serum phosphate levels observed may be attributed to the modulation of gut microbiota and the increased gut integrity by tight junction protein promotion. We could not demonstrate the benefit in the reduction of mineral bone disease due to the unyielding of the advanced stage of chronic kidney disease. According to these results, synbiotic 1 exerts high potential for developing a synbiotic to alleviate hyperphosphatemia and hyperparathyroidism in CKD patients, However, further study to innovate the appropriate formulation and dosage, and test in animal with advanced stage CKD are necessary to elucidate the clinical use of this hyperphosphatemia-target synbiotic.



REFERENCES

1. Levey AS, Becker C, Inker LA. Glomerular filtration rate and albuminuria for detection and staging of acute and chronic kidney disease in adults: a systematic review. *JAMA*. 2015;313(8):837-46.
2. Jha V, Garcia-Garcia G, Iseki K, Li Z, Naicker S, Plattner B, et al. Chronic kidney disease: global dimension and perspectives. *The Lancet*. 2013;382(9888):260-72.
3. Wang H, Naghavi M, Allen C, Barber RM, Bhutta ZA, Carter A, et al. Global, regional, and national life expectancy, all-cause mortality, and cause-specific mortality for 249 causes of death, 1980–2015: a systematic analysis for the Global Burden of Disease Study 2015. *The Lancet*. 2016;388(10053):1459-544.
4. Kanda H, Hirasaki Y, Iida T, Kanao-Kanda M, Toyama Y, Chiba T, et al. Perioperative Management of Patients With End-Stage Renal Disease. *J Cardiothorac Vasc Anesth*. 2017;31(6):2251-67.
5. Wikoff WR, Anfora AT, Liu J, Schultz PG, Lesley SA, Peters EC, et al. Metabolomics analysis reveals large effects of gut microflora on mammalian blood metabolites. *Proc Natl Acad Sci U S A*. 2009;106(10):3698-703.
6. Pizzorno J. Toxins From the Gut. *Integr Med (Encinitas)*. 2014;13(6):8-11.
7. Bover J, Bailone L, Lopez-Baez V, Benito S, Ciceri P, Galassi A, et al. Osteoporosis, bone mineral density and CKD-MBD: treatment considerations. *J Nephrol*. 2017;30(5):677-87.
8. Ramezani A, Raj DS. The gut microbiome, kidney disease, and targeted interventions. *J Am Soc Nephrol*. 2014;25(4):657-70.
9. Ewaschuk JB, Diaz H, Meddings L, Diederichs B, Dmytrash A, Backer J, et al. Secreted bioactive factors from *Bifidobacterium infantis* enhance epithelial cell barrier function. *Am J Physiol Gastrointest Liver Physiol*. 2008;295(5):G1025-34.
10. Wing MR, Patel SS, Ramezani A, Raj DS. Gut microbiome in chronic kidney disease. *Exp Physiol*. 2016;101(4):471-7.
11. Martens EC, Kelly AG, Tausin AS, Brumer H. The devil lies in the details: how variations in polysaccharide fine-structure impact the physiology and evolution of gut microbes. *J Mol Biol*. 2014;426(23):3851-65.
12. Sonnenburg JL, Backhed F. Diet-microbiota interactions as moderators of human metabolism. *Nature*. 2016;535(7610):56-64.
13. Gibson GR, Probert HM, Loo JV, Rastall RA, Roberfroid MB. Dietary modulation of the human colonic microbiota: updating the concept of prebiotics. *Nutr*

Res Rev. 2004;17(2):259-75.

14. Wang IK, Wu YY, Yang YF, Ting IW, Lin CC, Yen TH, et al. The effect of probiotics on serum levels of cytokine and endotoxin in peritoneal dialysis patients: a randomised, double-blind, placebo-controlled trial. *Benef Microbes*. 2015;6(4):423-30.
15. McFarlane C, Ramos CI, Johnson DW, Campbell KL. Prebiotic, Probiotic, and Synbiotic Supplementation in Chronic Kidney Disease: A Systematic Review and Meta-analysis. *J Ren Nutr*. 2019;29(3):209-20.
16. Muanprasat C, Chatsudthipong V. Chitosan oligosaccharide: Biological activities and potential therapeutic applications. *Pharmacol Ther*. 2017;170:80-97.
17. Kunanusornchai W, Witoonpanich B, Tawonsawatruk T, Pichyangkura R, Chatsudthipong V, Muanprasat C. Chitosan oligosaccharide suppresses synovial inflammation via AMPK activation: An in vitro and in vivo study. *Pharmacol Res*. 2016;113(Pt A):458-67.
18. Muanprasat C, Wongkrasant P, Satitsri S, Moonwiriyaakit A, Pongkorpsakol P, Mattaveewong T, et al. Activation of AMPK by chitosan oligosaccharide in intestinal epithelial cells: Mechanism of action and potential applications in intestinal disorders. *Biochem Pharmacol*. 2015;96(3):225-36.
19. Yousef M, Pichyangkura R, Soodvilai S, Chatsudthipong V, Muanprasat C. Chitosan oligosaccharide as potential therapy of inflammatory bowel disease: therapeutic efficacy and possible mechanisms of action. *Pharmacol Res*. 2012;66(1):66-79.
20. Raj D, Tomar B, Lahiri A, Mulay SR. The gut-liver-kidney axis: Novel regulator of fatty liver associated chronic kidney disease. *Pharmacol Res*. 2020;152:104617.
21. Ammirati AL. Chronic Kidney Disease. *Rev Assoc Med Bras* (1992). 2020;66Suppl 1(Suppl 1):s03-s9.
22. Inker LA, Astor BC, Fox CH, Isakova T, Lash JP, Peralta CA, et al. KDOQI US commentary on the 2012 KDIGO clinical practice guideline for the evaluation and management of CKD. *Am J Kidney Dis*. 2014;63(5):713-35.
23. Kazancioglu R. Risk factors for chronic kidney disease: an update. *Kidney Int Suppl* (2011). 2013;3(4):368-71.
24. Roberts IS. Pathology of IgA nephropathy. *Nat Rev Nephrol*. 2014;10(8):445-54.
25. D'Agati VD, Kaskel FJ, Falk RJ. Focal segmental glomerulosclerosis. *N Engl J Med*. 2011;365(25):2398-411.
26. Denic A, Mathew J, Lerman LO, Lieske JC, Larson JJ, Alexander MP, et al. Single-Nephron Glomerular Filtration Rate in Healthy Adults. *N Engl J Med*.

2017;376(24):2349-57.

27. Kottgen A, Glazer NL, Dehghan A, Hwang SJ, Katz R, Li M, et al. Multiple loci associated with indices of renal function and chronic kidney disease. *Nat Genet.* 2009;41(6):712-7.
28. Pollak MR, Genovese G, Friedman DJ. APOL1 and kidney disease. *Curr Opin Nephrol Hypertens.* 2012;21(2):179-82.
29. Song EY, McClellan WM, McClellan A, Gadi R, Hadley AC, Krisher J, et al. Effect of community characteristics on familial clustering of end-stage renal disease. *Am J Nephrol.* 2009;30(6):499-504.
30. Nzerue CM, Demissochew H, Tucker JK. Race and kidney disease: role of social and environmental factors. *J Natl Med Assoc.* 2002;94(8 Suppl):28S-38S.
31. Lackland DT, Egan BM, Fan ZJ, Syddall HE. Low birth weight contributes to the excess prevalence of end-stage renal disease in African Americans. *J Clin Hypertens (Greenwich).* 2001;3(1):29-31.
32. Iseki K. Factors influencing the development of end-stage renal disease. *Clin Exp Nephrol.* 2005;9(1):5-14.
33. Ejerblad E, Fored CM, Lindblad P, Fryzek J, McLaughlin JK, Nyren O. Obesity and risk for chronic renal failure. *J Am Soc Nephrol.* 2006;17(6):1695-702.
34. Kwakernaak AJ, Zelle DM, Bakker SJ, Navis G. Central body fat distribution associates with unfavorable renal hemodynamics independent of body mass index. *J Am Soc Nephrol.* 2013;24(6):987-94.
35. Bleyer AJ, Shemanski LR, Burke GL, Hansen KJ, Appel RG. Tobacco, hypertension, and vascular disease: risk factors for renal functional decline in an older population. *Kidney Int.* 2000;57(5):2072-9.
36. Goldstein SL, Devarajan P. Acute kidney injury in childhood: should we be worried about progression to CKD? *Pediatr Nephrol.* 2011;26(4):509-22.
37. Perneger TV, Whelton PK, Klag MJ. Risk of kidney failure associated with the use of acetaminophen, aspirin, and nonsteroidal antiinflammatory drugs. *N Engl J Med.* 1994;331(25):1675-9.
38. Klag MJ, Whelton PK, Randall BL, Neaton JD, Brancati FL, Ford CE, et al. Blood pressure and end-stage renal disease in men. *N Engl J Med.* 1996;334(1):13-8.
39. Lea JP, Nicholas SB. Diabetes mellitus and hypertension: key risk factors for kidney disease. *J Natl Med Assoc.* 2002;94(8 Suppl):7S-15S.
40. Drawz P, Rahman M. Chronic kidney disease. *Ann Intern Med.* 2015;162(11):ITC1-16.

41. Adamczak M, Masajtis-Zagajewska A, Mazanowska O, Madziarska K, Stompor T, Wiecek A. Diagnosis and Treatment of Metabolic Acidosis in Patients with Chronic Kidney Disease - Position Statement of the Working Group of the Polish Society of Nephrology. *Kidney Blood Press Res.* 2018;43(3):959-69.
42. Chronic kidney disease. *Nature Reviews Disease Primers.* 2017;3(1).
43. Takeda E, Taketani Y, Sawada N, Sato T, Yamamoto H. The regulation and function of phosphate in the human body. *Biofactors.* 2004;21(1-4):345-55.
44. Takeda E, Taketani Y, Morita K, Tatsumi S, Katai K, Nii T, et al. Molecular mechanisms of mammalian inorganic phosphate homeostasis. *Advances in Enzyme Regulation.* 2000;40(1):285-302.
45. Kiela PR, Ghishan FK. Recent advances in the renal-skeletal-gut axis that controls phosphate homeostasis. *Lab Invest.* 2009;89(1):7-14.
46. Knopfel T, Pastor-Arroyo EM, Schnitzbauer U, Kratschmar DV, Odermatt A, Pellegrini G, et al. The intestinal phosphate transporter NaPi-IIb (Slc34a2) is required to protect bone during dietary phosphate restriction. *Sci Rep.* 2017;7(1):11018.
47. Sabbagh Y, O'Brien SP, Song W, Boulanger JH, Stockmann A, Arbeeny C, et al. Intestinal npt2b plays a major role in phosphate absorption and homeostasis. *J Am Soc Nephrol.* 2009;20(11):2348-58.
48. Saurette M, Alexander RT. Intestinal phosphate absorption: The paracellular pathway predominates? *Exp Biol Med (Maywood).* 2019;244(8):646-54.
49. Davis GR, Zerwekh, J.E., Parker, T.F., Krejs, G.J., Pak, C.Y., Fordtran, J.S. Absorption of phosphate in the jejunum of patients with chronic renal failure before and after correction of vitamin D deficiency. *Gastroenterology.* 1983;85(4):908-16.
50. Schiavi SC, Tang W, Bracken C, O'Brien SP, Song W, Boulanger J, et al. Npt2b deletion attenuates hyperphosphatemia associated with CKD. *J Am Soc Nephrol.* 2012;23(10):1691-700.
51. Larsson TE, Kameoka C, Nakajo I, Taniuchi Y, Yoshida S, Akizawa T, et al. NPT-IIb Inhibition Does Not Improve Hyperphosphatemia in CKD. *Kidney Int Rep.* 2018;3(1):73-80.
52. Knopfel T, Himmerkus N, Gunzel D, Bleich M, Hernando N, Wagner CA. Paracellular transport of phosphate along the intestine. *Am J Physiol Gastrointest Liver Physiol.* 2019;317(2):G233-G41.
53. Kalantar-Zadeh K, Gutkunst L, Mehrotra R, Kovesdy CP, Bross R, Shinaberger CS, et al. Understanding sources of dietary phosphorus in the treatment of patients with chronic kidney disease. *Clin J Am Soc Nephrol.* 2010;5(3):519-30.

54. King AJ, Siegel M, He Y, Nie B, Wang J, Koo-McCoy S, et al. Inhibition of sodium/hydrogen exchanger 3 in the gastrointestinal tract by tenapanor reduces paracellular phosphate permeability. *Science Translational Medicine*. 2018;10(456).
55. Block GA, Bleyer AJ, Silva AL, Weiner DE, Lynn RI, Yang Y, et al. Safety and Efficacy of Tenapanor for Long-term Serum Phosphate Control in Maintenance Dialysis: A 52-Week Randomized Phase 3 Trial (PHREEDOM). *Kidney360*. 2021;2(10):1600-10.
56. Collins FL, Rios-Arce ND, Atkinson S, Bierhalter H, Schoenherr D, Bazil JN, et al. Temporal and regional intestinal changes in permeability, tight junction, and cytokine gene expression following ovariectomy-induced estrogen deficiency. *Physiol Rep*. 2017;5(9).
57. Severson EA, Parkos CA. Mechanisms of outside-in signaling at the tight junction by junctional adhesion molecule A. *Ann N Y Acad Sci*. 2009;1165:10-8.
58. Vetrano S, Danese S. The role of JAM-A in inflammatory bowel disease: unrevealing the ties that bind. *Ann N Y Acad Sci*. 2009;1165:308-13.
59. Anderson JM, Van Itallie CM. Tight junctions. *Curr Biol*. 2008;18(20):R941-3.
60. Watson CJ, Hoare CJ, Garrod DR, Carlson GL, Warhurst G. Interferon-gamma selectively increases epithelial permeability to large molecules by activating different populations of paracellular pores. *J Cell Sci*. 2005;118(Pt 22):5221-30.
61. Van Spaendonk H, Ceuleers H, Witters L, Patteet E, Joossens J, Augustyns K, et al. Regulation of intestinal permeability: The role of proteases. *World Journal of Gastroenterology*. 2017;23(12).
62. Geall MG, Summerskill WH. Electric-potential difference--a neglected parameter of gut integrity and function? *Gut*. 1969;10(6):418-21.
63. Srinivasan B, Kolli AR, Esch MB, Abaci HE, Shuler ML, Hickman JJ. TEER measurement techniques for in vitro barrier model systems. *J Lab Autom*. 2015;20(2):107-26.
64. Murer H, Hernando N, Forster I, Biber J. Regulation of Na/Pi transporter in the proximal tubule. *Annu Rev Physiol*. 2003;65:531-42.
65. Segawa H, Shiozaki Y, Kaneko I, Miyamoto K. The Role of Sodium-Dependent Phosphate Transporter in Phosphate Homeostasis. *J Nutr Sci Vitaminol (Tokyo)*. 2015;61 Suppl:S119-21.
66. Blaine J, Weinman EJ, Cunningham R. The regulation of renal phosphate transport. *Adv Chronic Kidney Dis*. 2011;18(2):77-84.
67. Curthoys NP, Moe OW. Proximal tubule function and response to acidosis. *Clin*

- J Am Soc Nephrol. 2014;9(9):1627-38.
68. Blaine J, Chonchol M, Levi M. Renal control of calcium, phosphate, and magnesium homeostasis. *Clin J Am Soc Nephrol*. 2015;10(7):1257-72.
69. Cavalli L, Mazzotta C, Brandi ML. Phosphatonins: physiological role and pathological changes. *Clin Cases Miner Bone Metab*. 2012;9(1):9-12.
70. Christensen SE, Nissen PH, Vestergaard P, Heickendorff L, Rejnmark L, Brixen K, et al. Plasma 25-hydroxyvitamin D, 1,25-dihydroxyvitamin D, and parathyroid hormone in familial hypocalciuric hypercalcemia and primary hyperparathyroidism. *Eur J Endocrinol*. 2008;159(6):719-27.
71. Norman AW. From vitamin D to hormone D: fundamentals of the vitamin D endocrine system essential for good health. *Am J Clin Nutr*. 2008;88(2):491S-9S.
72. Bikle D, Christakos S. New aspects of vitamin D metabolism and action - addressing the skin as source and target. *Nat Rev Endocrinol*. 2020;16(4):234-52.
73. Gaffney-Stomberg E, MacArthur MR, McClung JP. Parathyroid Hormone (PTH) and the Relationship Between PTH and Bone Health: Structure, Physiology, Actions, and Ethnicity. In: Patel VB, Preedy VR, editors. *Biomarkers in Bone Disease*. Dordrecht: Springer Netherlands; 2017. p. 443-61.
74. Brown AJ. Vitamin D analogs for secondary hyperparathyroidism: what does the future hold? *J Steroid Biochem Mol Biol*. 2007;103(3-5):578-83.
75. Jeroen van de Peppel, Renny T. Franceschi, Yan Li, Eerden BCJvd. *Vitamin D*. 4 ed: Academic Press; 2018.
76. Krajisnik T, Bjorklund P, Marsell R, Ljunggren O, Akerstrom G, Jonsson KB, et al. Fibroblast growth factor-23 regulates parathyroid hormone and 1 α -hydroxylase expression in cultured bovine parathyroid cells. *J Endocrinol*. 2007;195(1):125-31.
77. D'Souza-Li L. The calcium-sensing receptor and related diseases. *Arquivos Brasileiros de Endocrinologia & Metabologia*. 2006;50(4):628-39.
78. Bouschet T, Henley JM. Calcium as an extracellular signalling molecule: perspectives on the Calcium Sensing Receptor in the brain. *Comptes Rendus Biologies*. 2005;328(8):691-700.
79. Estepa JC, Aguilera-Tejero E, Lopez I, Almaden Y, Rodriguez M, Felsenfeld AJ. Effect of phosphate on parathyroid hormone secretion in vivo. *J Bone Miner Res*. 1999;14(11):1848-54.
80. Chen RA, Goodman WG. Role of the calcium-sensing receptor in parathyroid gland physiology. *American Journal of Physiology-Renal Physiology*. 2004;286(6):F1005-F11.

81. Datta NS, Abou-Samra AB. PTH and PTHrP signaling in osteoblasts. *Cell Signal*. 2009;21(8):1245-54.
82. Schachter PP, Christy MD, Lobaugh B, Leight GS, Jr. Parathyroid hormone secretion and target organ response in experimental acute pancreatitis. *Arch Surg*. 1991;126(2):139-42.
83. Silva BC, Bilezikian JP. Parathyroid hormone: anabolic and catabolic actions on the skeleton. *Curr Opin Pharmacol*. 2015;22:41-50.
84. Richards JB, Zheng HF, Spector TD. Genetics of osteoporosis from genome-wide association studies: advances and challenges. *Nat Rev Genet*. 2012;13(8):576-88.
85. Lee M, Partridge NC. Parathyroid hormone signaling in bone and kidney. *Curr Opin Nephrol Hypertens*. 2009;18(4):298-302.
86. D. Murray R, D. Lederer E, J. Khundmiri S. Role of PTH in the Renal Handling of Phosphate. *AIMS Medical Science*. 2015;2(3):162-81.
87. Wasserman RH, Fullmer CS. On the molecular mechanism of intestinal calcium transport. *Adv Exp Med Biol*. 1989;249:45-65.
88. Hernando N, Pastor-Arroyo EM, Marks J, Schnitzbauer U, Knopfel T, Burki M, et al. 1,25(OH)₂ vitamin D₃ stimulates active phosphate transport but not paracellular phosphate absorption in mouse intestine. *J Physiol*. 2021;599(4):1131-50.
89. Ho BB, Bergwitz C. FGF23 signalling and physiology. *J Mol Endocrinol*. 2021;66(2):R23-R32.
90. Olauson H, Lindberg K, Amin R, Sato T, Jia T, Goetz R, et al. Parathyroid-specific deletion of Klotho unravels a novel calcineurin-dependent FGF23 signaling pathway that regulates PTH secretion. *PLoS Genet*. 2013;9(12):e1003975.
91. Kuro OM. The Klotho proteins in health and disease. *Nat Rev Nephrol*. 2019;15(1):27-44.
92. Weinman EJ, Steplock D, Shenolikar S, Biswas R. Fibroblast growth factor-23-mediated inhibition of renal phosphate transport in mice requires sodium-hydrogen exchanger regulatory factor-1 (NHERF-1) and synergizes with parathyroid hormone. *J Biol Chem*. 2011;286(43):37216-21.
93. Vervloet M. Renal and extrarenal effects of fibroblast growth factor 23. *Nat Rev Nephrol*. 2019;15(2):109-20.
94. Lien YH. Phosphorus: another devil in our diet? *Am J Med*. 2013;126(4):280-1.
95. Razzaque MS. Phosphate toxicity: new insights into an old problem. *Clin Sci (Lond)*. 2011;120(3):91-7.

96. Erratum: Kidney Disease: Improving Global Outcomes (KDIGO) CKD-MBD Update Work Group. KDIGO 2017 Clinical Practice Guideline Update for the Diagnosis, Evaluation, Prevention, and Treatment of Chronic Kidney Disease-Mineral and Bone Disorder (CKD-MBD). *Kidney Int Suppl.* 2017;7:1-59. *Kidney Int Suppl* (2011). 2017;7(3):e1.
97. Karp HJ, Vaihia KP, Karkkainen MU, Niemisto MJ, Lamberg-Allardt CJ. Acute effects of different phosphorus sources on calcium and bone metabolism in young women: a whole-foods approach. *Calcif Tissue Int.* 2007;80(4):251-8.
98. Guo Y, Li H, Liu Z, Li C, Chen Y, Jiang C, et al. Impaired intestinal barrier function in a mouse model of hyperuricemia. *Mol Med Rep.* 2019;20(4):3292-300.
99. Vaziri ND, Yuan J, Norris K. Role of urea in intestinal barrier dysfunction and disruption of epithelial tight junction in chronic kidney disease. *Am J Nephrol.* 2013;37(1):1-6.
100. Natividad JM, Verdu EF. Modulation of intestinal barrier by intestinal microbiota: pathological and therapeutic implications. *Pharmacol Res.* 2013;69(1):42-51.
101. Arumugam M, Raes J, Pelletier E, Le Paslier D, Yamada T, Mende DR, et al. Enterotypes of the human gut microbiome. *Nature.* 2011;473(7346):174-80.
102. Thursby E, Juge N. Introduction to the human gut microbiota. *Biochem J.* 2017;474(11):1823-36.
103. Belizario JE, Napolitano M. Human microbiomes and their roles in dysbiosis, common diseases, and novel therapeutic approaches. *Front Microbiol.* 2015;6:1050.
104. Donaldson GP, Lee SM, Mazmanian SK. Gut biogeography of the bacterial microbiota. *Nat Rev Microbiol.* 2016;14(1):20-32.
105. Belizario JE, Faintuch J. Microbiome and Gut Dysbiosis. *Exp Suppl.* 2018;109:459-76.
106. Hooper LV, Macpherson AJ. Immune adaptations that maintain homeostasis with the intestinal microbiota. *Nat Rev Immunol.* 2010;10(3):159-69.
107. Louis P, Flint HJ. Formation of propionate and butyrate by the human colonic microbiota. *Environ Microbiol.* 2017;19(1):29-41.
108. Correa-Oliveira R, Fachi JL, Vieira A, Sato FT, Vinolo MA. Regulation of immune cell function by short-chain fatty acids. *Clin Transl Immunology.* 2016;5(4):e73.
109. Lin L, Zhang J. Role of intestinal microbiota and metabolites on gut homeostasis and human diseases. *BMC Immunol.* 2017;18(1):2.

110. Morrison DJ, Preston T. Formation of short chain fatty acids by the gut microbiota and their impact on human metabolism. *Gut Microbes*. 2016;7(3):189-200.
111. Sender R, Fuchs S, Milo R. Revised Estimates for the Number of Human and Bacteria Cells in the Body. *PLoS Biol*. 2016;14(8):e1002533.
112. Palmer DJ, Metcalfe J, Prescott SL. Preventing disease in the 21st century: the importance of maternal and early infant diet and nutrition. *J Allergy Clin Immunol*. 2012;130(3):733-4.
113. Lepage P, Leclerc MC, Joossens M, Mondot S, Blottiere HM, Raes J, et al. A metagenomic insight into our gut's microbiome. *Gut*. 2013;62(1):146-58.
114. Sangiuliano B, Perez NM, Moreira DF, Belizario JE. Cell death-associated molecular-pattern molecules: inflammatory signaling and control. *Mediators Inflamm*. 2014;2014:821043.
115. Backhed F, Fraser CM, Ringel Y, Sanders ME, Sartor RB, Sherman PM, et al. Defining a healthy human gut microbiome: current concepts, future directions, and clinical applications. *Cell Host Microbe*. 2012;12(5):611-22.
116. Reinoso Webb C, Kobozev I, Furr KL, Grisham MB. Protective and pro-inflammatory roles of intestinal bacteria. *Pathophysiology*. 2016;23(2):67-80.
117. Baumler AJ, Sperandio V. Interactions between the microbiota and pathogenic bacteria in the gut. *Nature*. 2016;535(7610):85-93.
118. Antharam VC, Li EC, Ishmael A, Sharma A, Mai V, Rand KH, et al. Intestinal dysbiosis and depletion of butyrogenic bacteria in *Clostridium difficile* infection and nosocomial diarrhea. *J Clin Microbiol*. 2013;51(9):2884-92.
119. Harley IT, Karp CL. Obesity and the gut microbiome: Striving for causality. *Mol Metab*. 2012;1(1-2):21-31.
120. Heeney DD, Gareau MG, Marco ML. Intestinal *Lactobacillus* in health and disease, a driver or just along for the ride? *Curr Opin Biotechnol*. 2018;49:140-7.
121. Fukui H. Increased Intestinal Permeability and Decreased Barrier Function: Does It Really Influence the Risk of Inflammation? *Inflamm Intest Dis*. 2016;1(3):135-45.
122. Watanabe H, Miyamoto Y, Honda D, Tanaka H, Wu Q, Endo M, et al. p-Cresyl sulfate causes renal tubular cell damage by inducing oxidative stress by activation of NADPH oxidase. *Kidney Int*. 2013;83(4):582-92.
123. Wong J, Piceno YM, DeSantis TZ, Pahl M, Andersen GL, Vaziri ND. Expansion of urease- and uricase-containing, indole- and p-cresol-forming and contraction of short-chain fatty acid-producing intestinal microbiota in ESRD. *Am J Nephrol*.

2014;39(3):230-7.

124. Vaziri ND, Wong J, Pahl M, Piceno YM, Yuan J, DeSantis TZ, et al. Chronic kidney disease alters intestinal microbial flora. *Kidney Int.* 2013;83(2):308-15.

125. Wang IK, Lai HC, Yu CJ, Liang CC, Chang CT, Kuo HL, et al. Real-time PCR analysis of the intestinal microbiotas in peritoneal dialysis patients. *Appl Environ Microbiol.* 2012;78(4):1107-12.

126. De Angelis M, Montemurno E, Piccolo M, Vannini L, Lauriero G, Maranzano V, et al. Microbiota and metabolome associated with immunoglobulin A nephropathy (IgAN). *PLoS One.* 2014;9(6):e99006.

127. Williams NT. Probiotics. *Am J Health Syst Pharm.* 2010;67(6):449-58.

128. Sanders ME, Merenstein DJ, Reid G, Gibson GR, Rastall RA. Probiotics and prebiotics in intestinal health and disease: from biology to the clinic. *Nat Rev Gastroenterol Hepatol.* 2019;16(10):605-16.

129. Tillisch K, Labus J, Kilpatrick L, Jiang Z, Stains J, Ebrat B, et al. Consumption of fermented milk product with probiotic modulates brain activity. *Gastroenterology.* 2013;144(7):1394-401, 401 e1-4.

130. Gao C, Major A, Rendon D, Lugo M, Jackson V, Shi Z, et al. Histamine H2 Receptor-Mediated Suppression of Intestinal Inflammation by Probiotic *Lactobacillus reuteri*. *mBio.* 2015;6(6):e01358-15.

131. Bruzzese E, Raia V, Gaudiello G, Polito G, Buccigrossi V, Formicola V, et al. Intestinal inflammation is a frequent feature of cystic fibrosis and is reduced by probiotic administration. *Aliment Pharmacol Ther.* 2004;20(7):813-9.

132. Fukuda S, Toh H, Hase K, Oshima K, Nakanishi Y, Yoshimura K, et al. Bifidobacteria can protect from enteropathogenic infection through production of acetate. *Nature.* 2011;469(7331):543-7.

133. Sanders ME, Klaenhammer TR. Invited Review: The Scientific Basis of *Lactobacillus acidophilus* NCFM Functionality as a Probiotic. *Journal of Dairy Science.* 2001;84(2):319-31.

134. Barnett AM, Roy NC, Cookson AL, McNabb WC. Metabolism of Caprine Milk Carbohydrates by Probiotic Bacteria and Caco-2:HT29(-)MTX Epithelial Co-Cultures and Their Impact on Intestinal Barrier Integrity. *Nutrients.* 2018;10(7).

135. Bindels LB, Delzenne NM, Cani PD, Walter J. Towards a more comprehensive concept for prebiotics. *Nat Rev Gastroenterol Hepatol.* 2015;12(5):303-10.

136. Slavin J. Fiber and prebiotics: mechanisms and health benefits. *Nutrients.* 2013;5(4):1417-35.

137. Costabile A, Kolida S, Klinder A, Gietl E, Bauerlein M, Froberg C, et al. A double-blind, placebo-controlled, cross-over study to establish the bifidogenic effect of a very-long-chain inulin extracted from globe artichoke (*Cynara scolymus*) in healthy human subjects. *Br J Nutr.* 2010;104(7):1007-17.
138. Calame W, Weseler AR, Viebke C, Flynn C, Siemensma AD. Gum arabic establishes prebiotic functionality in healthy human volunteers in a dose-dependent manner. *Br J Nutr.* 2008;100(6):1269-75.
139. Claesson MJ, Clooney AG, O'Toole PW. A clinician's guide to microbiome analysis. *Nat Rev Gastroenterol Hepatol.* 2017;14(10):585-95.
140. Graspentner S, Loeper N, Kunzel S, Baines JF, Rupp J. Selection of validated hypervariable regions is crucial in 16S-based microbiota studies of the female genital tract. *Sci Rep.* 2018;8(1):9678.
141. Bolyen E, Rideout JR, Dillon MR, Bokulich NA, Abnet CC, Al-Ghalith GA, et al. Reproducible, interactive, scalable and extensible microbiome data science using QIIME 2. *Nat Biotechnol.* 2019;37(8):852-7.
142. Willis AD. Rarefaction, Alpha Diversity, and Statistics. *Front Microbiol.* 2019;10:2407.
143. Kim BR, Shin J, Guevarra R, Lee JH, Kim DW, Seol KH, et al. Deciphering Diversity Indices for a Better Understanding of Microbial Communities. *J Microbiol Biotechnol.* 2017;27(12):2089-93.
144. Schloss PD, Westcott SL, Ryabin T, Hall JR, Hartmann M, Hollister EB, et al. Introducing mothur: open-source, platform-independent, community-supported software for describing and comparing microbial communities. *Appl Environ Microbiol.* 2009;75(23):7537-41.
145. Lemos LN, Fulthorpe RR, Triplett EW, Roesch LF. Rethinking microbial diversity analysis in the high throughput sequencing era. *J Microbiol Methods.* 2011;86(1):42-51.
146. Pielou EC. The measurement of diversity in different types of biological collections. *Journal of Theoretical Biology.* 1966;13:131-44.
147. Sambuy Y, De Angelis I, Ranaldi G, Scarino ML, Stamatii A, Zucco F. The Caco-2 cell line as a model of the intestinal barrier: influence of cell and culture-related factors on Caco-2 cell functional characteristics. *Cell Biol Toxicol.* 2005;21(1):1-26.
148. [Available from: <https://media.biocompare.com/m/37/product/7024629-1-400x300.jpg>].
149. Guo X, Rao JN, Liu L, Zou T, Keledjian KM, Boneva D, et al. Polyamines are necessary for synthesis and stability of occludin protein in intestinal epithelial cells. *Am*

J Physiol Gastrointest Liver Physiol. 2005;288(6):G1159-69.

150. Wang Y, Kirpich I, Liu Y, Ma Z, Barve S, McClain CJ, et al. Lactobacillus rhamnosus GG treatment potentiates intestinal hypoxia-inducible factor, promotes intestinal integrity and ameliorates alcohol-induced liver injury. *Am J Pathol.* 2011;179(6):2866-75.

151. Thongpan I, Suntronwong N, Vichaiwattana P, Wanlapakorn N, Vongpunsawad S, Poovorawan Y. Respiratory syncytial virus, human metapneumovirus, and influenza virus infection in Bangkok, 2016-2017. *PeerJ.* 2019;7:e6748.

152. Roy D. *Progress in Industrial Microbiology*: Elsevier; 2003.

153. Mangin I, Suau A, Magne F, Garrido D, Gotteland M, Neut C, et al. Characterization of human intestinal bifidobacteria using competitive PCR and PCR-TTGE. *FEMS Microbiol Ecol.* 2006;55(1):28-37.

154. Arici M, Bilgin B, Sagdic O, Ozdemir C. Some characteristics of Lactobacillus isolates from infant faeces. *Food Microbiology.* 2004;21(1):19-24.

155. Berridge MV, Tan AS. Characterization of the cellular reduction of 3-(4,5-dimethylthiazol-2-yl)-2,5-diphenyltetrazolium bromide (MTT): subcellular localization, substrate dependence, and involvement of mitochondrial electron transport in MTT reduction. *Arch Biochem Biophys.* 1993;303(2):474-82.

156. Xiao K, Cao S, Jiao L, Song Z, Lu J, Hu C. TGF-beta1 protects intestinal integrity and influences Smads and MAPK signal pathways in IPEC-J2 after TNF-alpha challenge. *Innate Immun.* 2017;23(3):276-84.

157. Nair AB, Jacob S. A simple practice guide for dose conversion between animals and human. *J Basic Clin Pharm.* 2016;7(2):27-31.

158. Charan J, Kantharia ND. How to calculate sample size in animal studies? *J Pharmacol Pharmacother.* 2013;4(4):303-6.

159. Ma LJ, Fogo AB. Model of robust induction of glomerulosclerosis in mice: importance of genetic background. *Kidney Int.* 2003;64(1):350-5.

160. Meyer N, Kroger M, Thummler J, Tietze L, Palme R, Touma C. Impact of three commonly used blood sampling techniques on the welfare of laboratory mice: Taking the animal's perspective. *PLoS One.* 2020;15(9):e0238895.

161. Westgard S, Petrides V, Schneider S, Berman M, Herzogenrath J, Orzechowski A. Assessing precision, bias and sigma-metrics of 53 measurands of the Alinity ci system. *Clin Biochem.* 2017;50(18):1216-21.

162. Rossert J, Terraz C, Dupont S. Regulation of type I collagen genes expression. *Nephrol Dial Transplant.* 2000;15 Suppl 6:66-8.

163. Cohen EP, Olson JD, Tooze JA, Bourland JD, Dugan GO, Cline JM. Detection and quantification of renal fibrosis by computerized tomography. PLoS One. 2020;15(2):e0228626.
164. Rostom A, Murray JA, Kagnoff MF. American Gastroenterological Association (AGA) Institute technical review on the diagnosis and management of celiac disease. Gastroenterology. 2006;131(6):1981-2002.
165. Chen S, Li J, Peng H, Zhou J, Fang H. Administration of erythropoietin exerts protective effects against glucocorticoid-induced osteonecrosis of the femoral head in rats. Int J Mol Med. 2014;33(4):840-8.
166. WMA DECLARATION OF HELSINKI – ETHICAL PRINCIPLES FOR MEDICAL RESEARCH INVOLVING HUMAN SUBJECTS [Available from: <https://www.wma.net/policies-post/wma-declaration-of-helsinki-ethical-principles-for-medical-research-involving-human-subjects/>].
167. ข้อกำหนดจรรยาบรรณการดำเนินการต่อสัตว์เพื่องานทางวิทยาศาสตร์. 2014.
168. Utilization of Probiotic Microorganisms in Foods. Sect. 86 D (2011).
169. Miller RP, Tadagavadi RK, Ramesh G, Reeves WB. Mechanisms of Cisplatin nephrotoxicity. Toxins (Basel). 2010;2(11):2490-518.
170. Marteau P, Seksik P. Tolerance of probiotics and prebiotics. J Clin Gastroenterol. 2004;38(6 Suppl):S67-9.
171. Wang Y, Wen R, Liu D, Zhang C, Wang ZA, Du Y. Exploring Effects of Chitosan Oligosaccharides on the DSS-Induced Intestinal Barrier Impairment In Vitro and In Vivo. Molecules. 2021;26(8).
172. Uerlings J, Schroyen M, Willems E, Tanghe S, Bruggeman G, Bindelle J, et al. Differential effects of inulin or its fermentation metabolites on gut barrier and immune function of porcine intestinal epithelial cells. Journal of Functional Foods. 2020;67.
173. Nagaraju PG, P S, Dubey T, Chinnathambi S, C GP, Rao PJ. Influence of sodium caseinate, maltodextrin, pectin and their Maillard conjugate on the stability, in vitro release, anti-oxidant property and cell viability of eugenol-olive oil nanoemulsions. Int J Biol Macromol. 2021;183:158-70.
174. Bhanja A, Sutar PP, Mishra M. Inulin-A polysaccharide: Review on its functional and prebiotic efficacy. J Food Biochem. 2022;46(12):e14386.
175. Weitkunat K, Schumann S, Petzke KJ, Blaut M, Loh G, Klaus S. Effects of dietary inulin on bacterial growth, short-chain fatty acid production and hepatic lipid metabolism in gnotobiotic mice. J Nutr Biochem. 2015;26(9):929-37.
176. Mehmood T, Pichyangkura R, Muanprasat C. Chitosan Oligosaccharide

Prevents Afatinib-Induced Barrier Disruption and Chloride Secretion through Modulation of AMPK, PI3K/AKT, and ERK Signaling in T84 Cells. *Polymers (Basel)*. 2022;14(20).

177. Akbari P, Fink-Gremmels J, Willems R, Difilippo E, Schols HA, Schoterman MHC, et al. Characterizing microbiota-independent effects of oligosaccharides on intestinal epithelial cells: insight into the role of structure and size : Structure-activity relationships of non-digestible oligosaccharides. *Eur J Nutr*. 2017;56(5):1919-30.

178. Shi M, McMillan KL, Wu J, Gillings N, Flores B, Moe OW, et al. Cisplatin nephrotoxicity as a model of chronic kidney disease. *Lab Invest*. 2018;98(8):1105-21.

179. Slatopolsky E, Finch J, Denda M, Ritter C, Zhong M, Dusso A, et al. Phosphorus restriction prevents parathyroid gland growth. High phosphorus directly stimulates PTH secretion in vitro. *J Clin Invest*. 1996;97(11):2534-40.

180. Fasano A. All disease begins in the (leaky) gut: role of zonulin-mediated gut permeability in the pathogenesis of some chronic inflammatory diseases. *F1000Res*. 2020;9.

181. Moe SM, Chen NX, Seifert MF, Sinderson RM, Duan D, Chen X, et al. A rat model of chronic kidney disease-mineral bone disorder. *Kidney Int*. 2009;75(2):176-84.

182. Abenavoli L, Scarpellini E, Colica C, Boccuto L, Salehi B, Sharifi-Rad J, et al. Gut Microbiota and Obesity: A Role for Probiotics. *Nutrients*. 2019;11(11).

183. Shen ZH, Zhu CX, Quan YS, Yang ZY, Wu S, Luo WW, et al. Relationship between intestinal microbiota and ulcerative colitis: Mechanisms and clinical application of probiotics and fecal microbiota transplantation. *World J Gastroenterol*. 2018;24(1):5-14.

184. Gophna U, Konikoff T, Nielsen HB. *Oscillospira* and related bacteria - From metagenomic species to metabolic features. *Environ Microbiol*. 2017;19(3):835-41.

185. Lee H, An J, Kim J, Choi D, Song Y, Lee CK, et al. A Novel Bacterium, *Butyricimonas virosa*, Preventing HFD-Induced Diabetes and Metabolic Disorders in Mice via GLP-1 Receptor. *Front Microbiol*. 2022;13:858192.

186. Wu F, Guo X, Zhang J, Zhang M, Ou Z, Peng Y. *Phascolarctobacterium faecium* abundant colonization in human gastrointestinal tract. *Exp Ther Med*. 2017;14(4):3122-6.

187. Zheng Z, Lyu W, Ren Y, Li X, Zhao S, Yang H, et al. *Allobaculum* Involves in the Modulation of Intestinal ANGPTL4 Expression in Mice Treated by High-Fat Diet. *Front Nutr*. 2021;8:690138.

188. Muñoz M, Guerrero-Araya E, Cortés-Tapia C, Plaza-Garrido A, Lawley TD, Paredes-Sabja D. Comprehensive genome analyses of *Sellimonas intestinalis*, a potential biomarker of homeostasis gut recovery. *Microbial Genomics*. 2020;6(12).

189. Liu X, Mao B, Gu J, Wu J, Cui S, Wang G, et al. *Blautia*—a new functional genus with potential probiotic properties? *Gut Microbes*. 2021;13(1).
190. Parker BJ, Wearsch PA, Veloo ACM, Rodriguez-Palacios A. The Genus *Alistipes*: Gut Bacteria With Emerging Implications to Inflammation, Cancer, and Mental Health. *Frontiers in Immunology*. 2020;11.
191. Herp S, Durai Raj AC, Salvado Silva M, Woelfel S, Stecher B. The human symbiont *Mucispirillum schaedleri*: causality in health and disease. *Medical Microbiology and Immunology*. 2021;210(4):173-9.
192. Cui Y, Zhang L, Wang X, Yi Y, Shan Y, Liu B, et al. Roles of intestinal *Parabacteroides* in human health and diseases. *FEMS Microbiology Letters*. 2022;369(1).





จุฬาลงกรณ์มหาวิทยาลัย
CHULALONGKORN UNIVERSITY

VITA

NAME	WEERAPAT ANEGKAMOL
DATE OF BIRTH	3 AUGUST 1983
PLACE OF BIRTH	BANGKOK
INSTITUTIONS ATTENDED	B.Sc. (Biology), Faculty of Science, Mahidol University M.Sc. (Environmental Biology), Faculty of Science, Mahidol University



จุฬาลงกรณ์มหาวิทยาลัย
CHULALONGKORN UNIVERSITY